REVISTA PORTUGUESA DE QUÍMICA

Os artigos publicados são de exclusiva responsabilidade dos seus autores
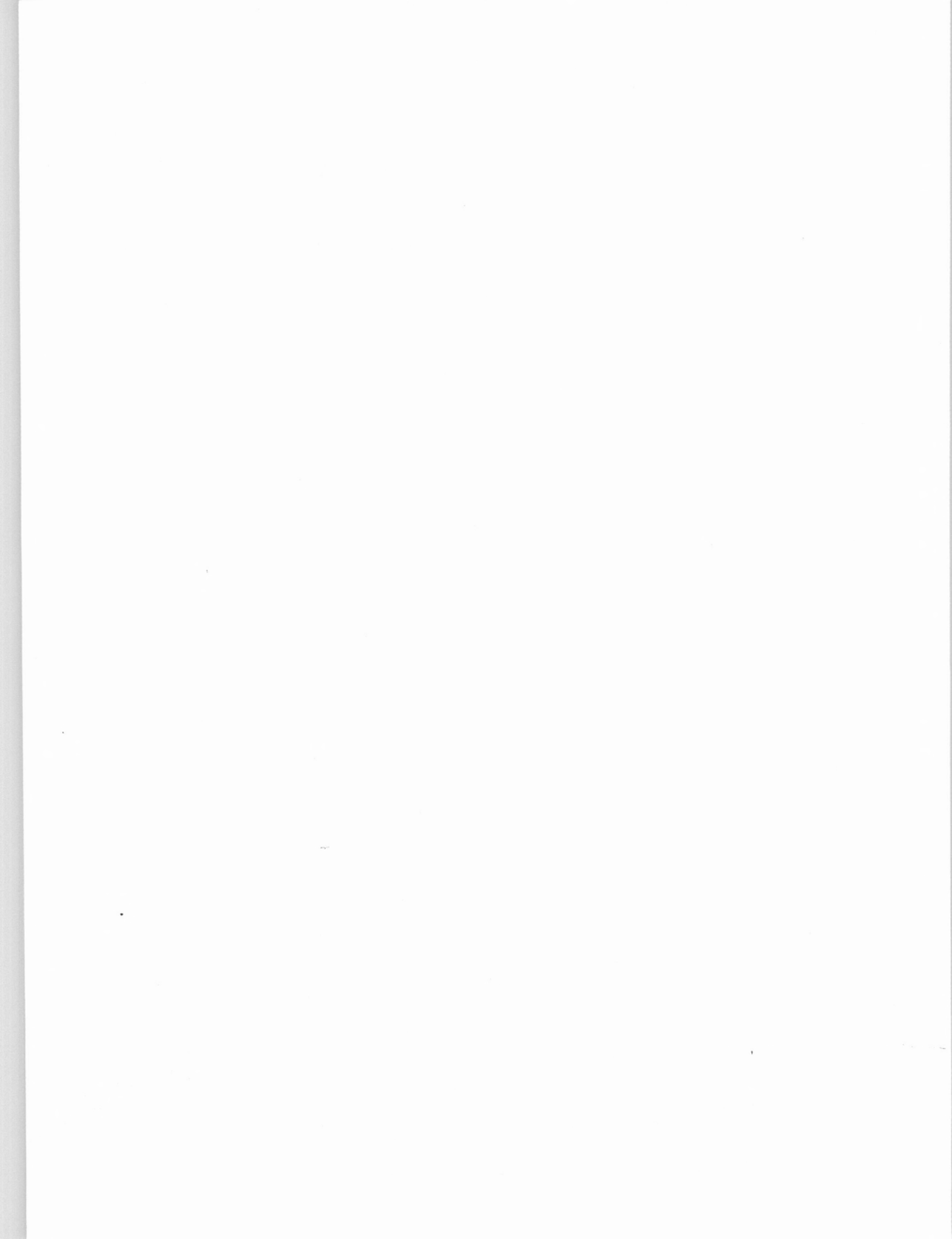
índice

JOSÉ L. ANDRÉS
AGUSTÍ LLEDÓS
MIQUEL DURAN
JUAN BERTRÁN

Departament de Química,
Universitat Autònoma de Barcelona
08193 Bellaterra, Catalonia,
SPAIN

EFFECT OF AN UNIFORM ELECTRIC FIELD ON CHARGE TRANSFER PROCESSES. A THEORETICAL STUDY (*)

The influence of an external uniform electric field on the proton transfer in the $(H_3O_2)^-$ system and on the methyl transfer in the $(FCH_3F)^-$ system is analyzed theoretically. The electric field effect is incorporated in the one-electron part of the Fock matrix. Reaction profiles are dramatically modified with the increase in intensity of the applied field. The electric field is found to intervene in the reaction coordinate. In this way, strong fields emerge as a new kind of catalysts in chemical reactions.

New techniques like Field Ionization Spectroscopy and Field Ionization Mass Spectroscopy have allowed to reach electric fields of the range 10^9–10^{11} V/m [1]. It is well known that the field-free characteristics of molecules differ dramatically from those which characterize them under such strong fields [2]. One can also think that external electric fields will influence the reactivity of chemical systems. In particular, it is obvious that charge-transfer processes will be very influenced by the presence of strong fields.

Processes like proton transfer or Walden inversion reactions allow to define clearly their reaction coordinate. That is the reason why modifications in their reaction profiles due to the presence of strong electric fields have been studied theoretically. In a number of cases the electric fields have been originated by the presence of an ion [3-8]. To our knowledge, however, only two theoretical works have introduced an uniform electric field, in both cases on proton transfer reactions. In a pioneer paper, Parker [9] studied the modifications in the tunnelling effect in the proton transfer between DNA bases, where the electric field was introduced in an empirical way. In a recent paper, Zundel [10] computed the first-order interaction between the electric field and the dipole moment, and found that double-well shapes were substantially modified with the increase in intensity of the electric field. Our ultimate goal is to study both proton-transfer and Walden inversion reactions under the influence of an uniform electric field. The latter is introduced by proper changes in the one-electron part of the Fock matrices in the Hartree-Fock SCF method.

In the $(H_3O_2)^-$ system, previous theoretical calculations with the 4-31G basis set showed a double-well minimum with a barrier height for the proton transfer of 0.20 kcal/mol [11]. When electric fields of the order 10^7 V/m were applied along the H-O-H axis, the barrier height was substantially lowered. For an intensity of $7.2 \cdot 10^7$ V/m, the barrier no longer

exists. Likewise, in the $(FCH_3F)^-$ system, use of the 3-21G basis set showed that when no field was applied, a double-well minimum is obtained with a barrier to the methyl transfer of 12.2 kcal/mol referred to the minima [8]. When electric fields of the order 10^8 V/m are applied along the F-C-F axis, the barrier heights are dramatically modified. For an intensity of $1.4 \cdot 10^9$ V/m, the barrier does not exist anymore.

Analysis of the changes occurred in electronic distribution in the minima of the above field-free processes due to the presence of an electric field may help us to understand the reasons why the systems evolve spontaneously towards the products. Presence of such electric fields causes by itself an electronic transfer in the same direction of the transfer process, that is, makes the reacion to advance. Furthermore, electron densities at the forming and breaking bond critical points are increased and diminished respectively due to the effect of the external electric field. A similar effect could be produced by a shorthening of the first bond and lengthening of the second one. These changes obviously belong to the internal reaction coordinate. Since the electric field causes similar modifications in the electronic distribution, one can say that the external electric field belongs also to the internal reaction coordinate.

To understand the reasons of the spontaneous evolution of the system towards products, one must look at the forces acting on nuclei. In the field-free minimum, no forces act obviously. When an electric field is applied, there is an electron density reorganization, so that forces are induced in the nuclei, and the system is no longer in equilibrium. Nuclei move along the forces and reach the geometry optimal under the electric field. Changes produced in electron density in the direction of the field induce the nuclei to move in this same direction. On the contrary, the electric field acts in the opposite direction on the nuclei, which are positively charged. Depending on whether the electron density around a nucleus is larger or smaller than the nuclear

charge, the force acting on it will follow the direction of the electric field or go against it. In the two processes considered, either the F^- or the OH^- are negatively charged, and either the H^+ in the $(H_3O_2)^-$ system or the methyl in the $(FCH_3F)^-$ system are positively charged. Thus, forces will appear in the direction of the field at the negatively-charged groups, whereas forces against the field will arise at the positively-charged groups, so the systems will evolve in such a way that initial bonds will break and new bonds will be formed. The proton or methyl transfer, respectively, will thus be produced.

An interesting conclusion of this work is that the mere presence of an external electric field may produce an acceleration in the reaction rate without the presence of any catalyst. Clearly, if the electric field has to help in the charge transfer, it must be oriented with respect to the reacting system. This cannot be achieved in isotropic media, but it is conceivable in anisotropic media. In particular, it can be achieved in electrode interfaces and membranes, where it is well known that presence of electric fields accelerates several chemical processes. Finally, it is worth noting that changes in enzymatic conformations previous to enzymatic reactions allow the reaction field to be oriented adequately with respect to the chemical process in such a way that enzymatic catalysis may be explained in some cases by a suitable orientation of the electric field.

REFERENCES

[1] H. D. BECKEY, «Field Ionization Mass Spectroscopy», Akademie-Verlag: Berlin, 1971.
[2] H. NAKATSUJI, T. HAYAKAWA, T. YONEZAWA, *J. Am. Chem. Soc.*, 1981, **103**, 7426.

[3] I. CERNUSÁK, M. URBAN, *Coll. Czechoslov. Chem. Commun.*, 1978, **43**, 1956.

[4] J. E. SANHUEZA, O. TAPIA, *J. Mol. Struct.*, 1982, **89**, 131.

[5] B. M. RODE, *Theor. Chim. Acta*, 1980, **56**, 245.

[6] S. SCHEINER, P. REDFERN, M. M. SZCZESNIAK, *J. Phys. Chem.*, 1985, **89**, 262.

[7] M. M. SZCZESNIAK, S. SCHEINER, *J. Phys. Chem.*, 1985, **89**, 1835.

[8] E. CARBONELL, J. L. ANDRÉS, M. DURAN, A. LLEDÓS, J. BERTRÁN, *J. Am. Chem. Soc.*, 1988, **110**, 996.

[9] B. R. PARKER, *Chem. Phys. Lett.*, 1974, **24**, 22.

[10] G. ZUNDEL, M. ECKERT, *J. Phys. Chem.*, 1987, **91**, 5170.

[11] J. L. ANDRÉS, M. DURAN, A. LLEDÓS, J. BERTRÁN, *Chem. Phys. Lett.*, 1986, **124**, 177.

RESUMO

Efeito de um campo eléctrico uniforme em processos de transferência de carga. Um estudo teórico.

Faz-se o estudo teórico da influência de um campo eléctrico externo sobre a transferência do protão no sistema $(H_3O_2)^-$ e a transferência do metilo no sistema $(FCH_3F)^-$. O efeito do campo eléctrico é incorporado na parte mono-electrónica da matriz de Fock. Os perfis de reacção são modificados dramaticamente com o aumento de intensidade do campo aplicado. Verifica-se que o campo eléctrico intervém na coordenação de reacção. Desta maneira, os campos intensos aparecem como um novo tipo de catalisador de reacções químicas.

PAOLO GRIGOLINI (*)
Institute for Nonlinear Science, R-002
University of California, San Diego
La Jolla, CA 92093
U.S.A.

THE «REDUCED» MODEL THEORY: A SUITABLE APPROACH FOR STUDYING COMPLEX SYSTEMS OF CHEMICAL AND BIOLOGICAL INTEREST (**)

With intuitive yet rigorous arguments it is shown that the «redu-ced» model theory (RMT) can be successfully applied to studying classical systems fulfilling the constraint of canonical equilibrium. In this case the RMT results in a unique form coincident with the derivations from a rigorous microscopi picture. Complex systems of biological interest, without the constraint of canonical equilibrium, are characterized by a gamut of different expressions. The RMT sheds light on the «microscopic» reasons for the ubiquitous nature of these systems.

1. Introduction

The «reduced» model theory (RMT) has been developed ten years ago [1] with the basic purpose in mind of providing a simplified description of complex systems in the field of radiationless decay processes in large molecules [2, 3]. This approach has been subsequently extended to studying the molecular dynamics at the liquid state [4-6], solid state physics [7, 8] and complex processes of biological interest [9].

We shall illustrate hereby the basic tenets of the RMT by referring ourselves to physics. However, it must be remarked that similar arguments apply also to chemistry and biology. Physics affords mathematical models of the world: The Newton equations, for instance, are a mathematical model of the dynamics of macroscopic and microcospic bodies (the latter ones usually termed particles). This simple mathematical model becomes very complicated when a large number of particles is considered. Let us consider, for instance, the simplest as possible model of liquid: The liquid argon. The mathematical model provided by classical mechanics is, in this case, a set of virtually infinite number of Newton equations, describing the reciprocal inteaction among the argon atoms via Lennard-Jones potentials. It is evident that the analytical treatment of this system is beyond the capabilities of human beings, thereby affording a relevant example of a complex model.

Since the particles of this ensemble are identical, we can focus our attention only on one of them, the tagged particle, and we wonder if a drastically reduced picture for the dynamics of the tagged particle is possible. This reduced picture should make it possible to obtain analytical results and should also turn out to be equivalent, in a statistical sense, to the original complex model. If the tagged particle were characterized by a mass much larger than that of the other particles, the answer to that fundamental question would be positive. The pioneer work of Einstein and Langevin shows indeed that the statistical properties of the

Brownian particle can be accounted for in terms of a simple analytical descriprion. This is so because in this case only the degrees of freedom of the tagged particle must be considered, the infinite number of the remainders being simulated by a friction term and a stochastic force. Under these conditions the velocity auto-correlation function of the Brownian particle turns out to be exponential.

Unfortunately, Nature frequently challenges us with cases where this simple picture does not hold. In the above mentioned case of liquid argon, for instance, the autocorrelation function of velocity is far from being exponential. This is so because the time scale of the system of interest, i.e. the tagged particle, is the same as that of the other particles, whereas it is well known [1] that the standard Langevin and Fokker-Planck equations rely on the assumptions of a wide time scale separation between system and bath.

The original purpose of the RMT was that of building up a «reduced» model, statistically equivalent to the complex one, so as to extend to these critical conditions the basic ideas of Einstein and Langevin. Actually, within the quantum-mechanical context used to develop the theory of radiationless decays in large molecules, the RMT relies [2] on replacing a dense set of states, acting as a quantum- -mechanical reservoir, with a single state (or a few states) undergoing a decay process of exponential nature. This method was shown to provide a complete description of the whole excitation-decay process thereby making it possible to relate the behavior of the decay process to the actual way used to prepare the excited state with experimental techniques.

The main purpose of this paper is to show that even the field of stochastic physics can draw significant benefits from the ideas of the RMT. When modelling a complex system via the theoretical tools of stochastic physics, the assumption of a wide time scale separation between «system» and «bath» is currently done. According to van Kampen [11] this assumption is a major source of ambiguities but in the standard, and completely settled,

case of Brownian motion. Instead of using the alternative method of master equation, as suggested by van Kampen [11], thereby losing the appealing flavor of intuitive understanding, by using the RMT we can successfully face these difficulties within the framework of an intuitive and phenomenological approach of Langevin kind.

In the special case where the phenomenological description must be compatible with a hamiltonian origin and the important constraint of canonical equilibrium must be fulfilled, the RMT produces a unique result, wich is proven to coincide with that obtained, with a much more elaborated calculation, from a rigorous microscopic picture [12]. Our point of view on this issue coincides with that of Ramshaw [13] and Ramshaw and Lindenberg [14], who used the extended Langevin approach [13] to recover at a phenomenological level the rigorous Fokker-Planck equation derived by Green and Zwanzig [15] and Grabert et al. [16] from a genuine microscopic picture.

To illustrate this basic aspect of the RMT we shall use the model of reactant system of ref. [17], consisting of a reaction coordinate in interaction with non-reacting modes. As an element of novelty of this paper, we rederive the same result of ref. [17] with simple intuitive arguments only based on the Langevin picture, whereas ref. [17] relies on a complicated, albeit rigorous, projection method applied to the Fokker-Planck level of description.

When the canonical constraint does not apply, as it is usually the case when modeling biological processes, a purely phenomenological approach is not bounded to end up in a unique result (remember the van Kampen criticism [11]). The RMT, however, has the capability of relating the macroscopic behavior of the system with some peculiar aspects of the «microscopic» (or, it would be better to say, mesoscopic [11]) level of description behind the phenomenological picture.

Section II is devoted to illustrating the general strategy of the RMT. In Section III we discuss the case of a reacting system interac-

ting with non-reactive modes. Section IV is devoted to studying a model for a population increase in a fluctuating environment.

II. **The basic tenets of the RMT**

Let us consider the system described by

$$\dot{X} = A(X) + G(X, \Xi(t)), \qquad (II.1)$$

where X denotes a set of variables of interest and Ξ simulates the stochastic influence of environment. In many cases an equation of this kind has a phenomenological foundation and one would be tempted to adopt the simplifying assumption that the Ξ's are mutually uncorrelated white and Gaussian noises, with vanishing mean value, defined by

$$<\Xi_i(o)\Xi_j(t)> = 2\delta_{ij} Q_i \delta(t). \qquad (II.2)$$

According to van Kampen [11] this road is fraught with unsettled difficulties: The only safe case where the Langevin approach can be applied without meeting the basic flaw mentioned by van Kampen [11] is the standard Brownian motion,

$$\dot{v} = -\gamma v + f(t), \qquad (II.3)$$

where v is the velocity of the Brownian particle, γ the friction affecting its motion and f(t) is a Gaussian white noise, with vanishing mean value, defined by

$$<f(o)f(t)> = 2Q\delta(t). \qquad (II.4)$$

The intensity of noise, Q, is related to the friction γ by the fluctuation-dissipation relationship (m is the mass of the particle)

$$Q = \gamma <v^2> = \gamma \frac{k_B T}{m} \qquad (II.5)$$

It is also well known that eq. (II.3) is associated with the Fokker-Planck equation:

$$(\delta/\delta t)\rho(v;t) = \{\gamma(\delta/\delta v)v + \gamma k_B T(\delta^2/\delta v^2)\}\rho(v;t). \quad (II.6)$$

By using a rigorous projection approach [18] it is possible to show that eqs. (II.3) and (II.6) are a good approximation of physical reality provided that the «bath» of the Brownian particle is characterized by a time scale τ fulfilling the condition $\tau << 1/\gamma$. In the special case where the system of interest is coupled to the «bath» via a linear interaction, the condition $\tau << 1/\gamma$ makes eqs. (II.3) and (II.6) to be an exact description of physical reality.

The RMT consists of replacing eq. (II.1) with the much safer set of equations

$$\dot{X} = A(X) + G(X, \Xi(t)) \qquad (II.7)$$

$$\dot{\Xi}_i = -\gamma_i \Xi_i + f_i(t) + \psi_i(X, \Xi) \ (i = 1, 2, ...). \qquad (II.8)$$

Each variable Ξ_i is assumed to be coupled to its own thermal bath in the same safe way as that leading to the standard Brownian motion of eqs. (II.3) and (II.6) with the proper fluctuation-dissipation relations

$$<f_i(o)f_j(t)> = 2\gamma_i <\Xi_i^2> \delta(t) \delta_{ij}. \qquad (II.9)$$

This leads us to associate eqs. (II.7) and (II.8) with a unambiguous multidimensional Fokker-Planck equation, from which via a rigorous projection approach [18] the reduced equation of motion for X can be derived. In the next Section we shall derive rigorous results on the dynamics of X without having recourse to that rigorous (but technically involved) projection approach.

III. First example: A chemical reaction process driven by a fluctuating potential

Let us consider the case where the chemical reaction process is described by

$$\dot{x} = v$$
$$\dot{v} = - \frac{\delta V}{\delta x} - \gamma v(t) + q(x)\xi(t) + f(t). \tag{III.1}$$

$f(t)$ is the standard white noise associated to the dissipative term $-\gamma v$ (see eqs. II.3 to II.5). With eq. (III.1) we mean that in addition to this standard fluctuation-dissipation process the reacting system undergoes also the influence of the fluctuating potential

$$V_T(x,t) = V(x) + \psi(x)\,\xi(t), \tag{III.1'}$$

$\psi(x)$ being related to $q(x)$ of eq. (III.1) by

$$\psi'(x) = -q(x). \tag{III.1''}$$

Actually, $q(x)\xi(t)$ is a state-dependent stochastic force $(q'(x) \neq o)$ and according to the RMT ξ must be regarded as being driven by both a heat reservoir (in the same way as v of eq. (II.3) is led by its own thermal bath) and by the interaction with x.

If the canonical constraint is to hold, the interaction of ξ with x must be defined in a proper way. To do that, instead of using formal arguments we look at x as being a space coordinate of another oscillator the velocity of which is driven by both a standard fluctuation-dissipation process and a conservative interaction with the oscillator of interest. We thus obtain

$$\dot{x} = v$$
$$\dot{v} = - \frac{\delta V}{\delta x} - \gamma v(t) + f(t) - \psi'(x)\xi(t)$$
$$\dot{\xi} = w \tag{III.2}$$
$$\dot{w} = -\Delta w - w^2_R \xi + f_w(t) - \psi(x),$$

where

$$\langle f_w(o)f_w(t)\rangle = 2\,Q_w\delta(t) = 2\Delta\langle w^2\rangle\delta(t). \tag{III.3}$$

The introduction of w has been made necessary to properly define the interaction potential $\psi(x)\xi$. This variable can be made to disappear by using the Smoluchowsky approximation [18], $\dot{w} = O$, which leads us to express w in terms of Δ, $-\omega^2_R\xi$, $f_w(t)$ and $-\psi(x)$ (see the last equation of the set of eq. (III.2)). By replacing the result on the r.h.s. of the third equation of the set of eq. (III.2), we obtain

$$\dot{x} = v$$
$$\dot{x} = - \frac{\delta V}{\delta x} - \gamma\,v(t) + f(t) - \psi'(x)\xi \tag{III.4}$$
$$\dot{\xi} = -\Gamma\xi - \psi(x)/\Delta + F(t),$$

where $F(t)$ is a Gaussian white noise, with vanishing mean value, defined by $(\Gamma\Delta = \omega^2_R)$

$$\langle F(o)F(t)\rangle = 2\Gamma\langle\xi^2\rangle\delta(t). \tag{III.5}$$

Eq. (III.4) is the simplest picture of a multiplicative (or state-dependent) fluctuation, compatible with the requirement of canonical equilibrium.

From eq. (III.2) we see that the space coordinates (x,ξ) must reach the canonical equilibrium distribution $\exp[-(V + \psi\xi + \omega^2_R\xi/2)/k_BT]$. Via contraction over ξ we find that x must be canonically distributed within the effective potential

$$\Phi_{eff} \equiv V - \psi^2/(\Delta\Gamma) = V - \psi^2/\omega^2_R. \tag{III.6}$$

The easiest way of making the effective potential Φ_{eff} apear within the Langevin picture is to make the following change of variable,

$$\tilde{\xi} = \xi + \Psi/(\Delta\Gamma). \tag{III.7}$$

We thus obtain from eq. (III.4)

$$\dot{x} = v$$

$$\dot{v} = -\frac{\delta V}{\delta x} - \gamma v - \psi'(x)\{\xi - \psi(x)/(\Delta\Gamma)\} + f(t) \quad \text{(III.8)}$$

$$\dot{\tilde{\xi}} = -\Gamma\xi + F(t) + \psi'(x)v/(\Delta\Gamma).$$

Eq. (III.8) can also be written as follows

$$\dot{x} = v$$

$$\dot{v} = -\frac{\delta}{\delta x}\Phi_{eff} - \gamma v - \psi'(x)\tilde{\xi} + f(t) \quad \text{(III.9)}$$

$$\dot{\tilde{\xi}} = -\Gamma\tilde{\xi} + F(t) + \psi'(x)v/(\Delta\Gamma),$$

which indeed involves the effective potential Φ_{eff}.

This is the first remarkable effect of a multiplicative fluctuation fulfilling the constraint of canonical equilibrium. To stress how this effect is important, let us consider the case where the bare potential is given the harmonic form.

$$V = \omega_o^2 x^2/2. \quad \text{(III.10)}$$

Let us give the interaction potential $\psi(x)\xi$ the simplest as possible non-linear structure by assuming

$$\psi(x) = \alpha\, x^2/2. \quad \text{(III.10')}$$

From eq. (III.6) we then obtain

$$\Phi_{eff}(x) = \omega_o^2 x^2/2 - \alpha^2 x^4/(4\omega_R^4). \quad \text{(III.11)}$$

The process of escape via thermal fluctuation from the bare potential (the chemical reaction process, according to the Kràmers picture [19]) would be impossible, whereas the «truncated harmonic potential» of eq. (III.11) makes it possible.

If we assume that Γ is so large as to make valid the Smoluchowsky approximation on ξ, $\dot{\tilde{\xi}} = 0$, we get from et. (III.9)

$$\dot{x} = v$$
$$\dot{v} = -\frac{\delta}{\delta x}\Phi_{eff} - \gamma\, v - \psi'^2 v/(\Delta\Gamma^2) - \psi'(x)\xi + f(t). \quad \text{(III.12)}$$

Eq. (III.12) illustrates the second remarkable result obtained with the simple arguments of this paper (and made possible by the use of the basic indications of the RMT). If $\psi'(x)$ were independent of x, the friction $\gamma + \psi'^2/(\Delta\Gamma)$ would be connected to the white stochastic force f(t) $-\psi'(x)\xi$ by a standard fluctuation-dissipation relationship. In the non linear case, on the contrary, i.e. when $\psi''\neq 0$, we see that the friction term turns out to depend on the state of the system of interest. The intensity of the damping can be defined via the mean-field approximation

$$\gamma_{eff} = \gamma + <\psi'^2(x)>/(\Delta\Gamma^2). \quad \text{(III.13)}$$

According to eq. (III.13) an increase in temperature produces an increase of the effective friction so as to provoke, in some cases [20], a transition from the underdamped to the overdamped regime.

The result of eq. (III.13) coincides with that derived by Ramshaw and Lindenberg [14] by using the augmented Langevin approach [13]. These authors showed that it is possible to recover within the context of a phenomenological picture the same formal result as that derived from a rigorous microscopic treatment. In the limiting case of ξ being a white noise this result does not depend on the detailed dynamics of ξ.

To shed light into this aspect, let us consider the equation of motion of the probability distribution $\sigma(x,v;t)$. This is shown [21] to read

$$\frac{\delta}{\delta t}\sigma(x, v; t) = L_a\, \sigma(x, v; t) +$$

$$+ \int_0^t ds <\xi(o)\xi(s)>\psi'(x)\frac{\delta}{\delta v} e^{L_a s}$$

$$\otimes(\frac{\delta}{\delta v} + v/(k_B T)) e^{-L_a s}\, \psi'(x)\, \sigma(x, v; t), \quad \text{(III.14)}$$

where (III.15)

$$L_a \equiv -v\frac{\delta}{\delta x} + \Phi'_{eff}\frac{\delta}{\delta v} + \gamma\left(\frac{\delta}{\delta v}v + k_B T\frac{\delta^2}{\delta v^2}\right).$$

Whitin this picture the decay of the correlation function $<x(o)x(s)>$ is not bounded to be an exponential function of time. The actual behavior of the system is in general dependent on the detailed form of the decay of x. However, when the dynamics of x is much faster than that associated with the operator L_a of eq. (III.15), the upper limit of time integration, t, on the r.h.s. of eq. (III.14) can be replaced by ∞ and eq. (III.14) turns out to coincide with the Fokker-Planck equation associated with eq. (III.12), with Γ defined by

$$1/\Gamma \equiv \int <\xi(o)\xi(s)>/<\xi> \, ds. \qquad (III.16)$$

Regardless the details of the dynamics of ξ, if both $1/\Gamma$ and $1/\gamma$ are very short, we obtain for the probability distribution of x, $\phi(x,t)$, the following equation of motion [20].

$$\frac{\delta}{\delta t} \phi(x; t) = \frac{\delta}{\delta x} \{k_B T/(\gamma + \psi'^2(x)/(\omega_R \Gamma^2))\} [\frac{\delta}{\delta x} +$$

$$+ \Phi'_{eff}/(k_B T)]\phi(x; t) \qquad (III.17)$$

The unique charater of this structure is pointed out by noticing that the form of eq. (III.17) does not depend on whether $1/\Gamma$ is much smaller than $1/\gamma$, or viceversa. In the case dealt with in the next Section, on the contrary, the form of the resulting Fokker-Planck equation is closely dependent on the ratio of the internal relaxation to the lifetime of the external noise.

The modelling of complex systems relying on a hamiltonian microscopic description and not necessarily fulfilling the constraint of canonical equilibrium, requires much more caution, since, as shown in the next Section, the white noise assumption on the environmental fluctuations does not make it possible to reach a unique form of diffusion equation.

IV. RMT without canonical constraints

Let us consider the prototype for the increase of a population in a random environment, the number of individuals of this population being denoted by n,

$$\dot{n} = (k_o + k(t))n(t). \qquad (IV.1)$$

k(t) is assumed to be a Gaussian white noise, with vanishing mean value, defined by the correlation function.

$$<k(o)k(t) = 2Q\delta(t). \qquad (IV.2)$$

According to the Ito [2] and Stratonovich [23] algorithm, the Fokker-Planck equation associated with eq. (IV.1) should read ($\sigma(n;t)$ denotes the probability distribution of n at the time t)

$$\frac{\delta}{\delta t} \sigma(n; t) = \{-k_o \frac{\delta}{\delta n} n + Q \frac{\delta}{\delta n} n \frac{\delta}{\delta n} n\} \sigma(n; t) \quad (IV.3)$$

$$\frac{\delta}{\delta t} \sigma(n; t) = \{-k_o \frac{\delta}{\delta n} n + Q \frac{\delta^2}{\delta n^2} n^2\} \sigma(n; t), \quad (IV.3')$$

respectively.

We immediately obtain from eq. (IV.3) and eq. (IV.3')

$$\frac{\delta}{\delta t} <n(t)> = (k_o + Q) <n(t)> \qquad (IV.4)$$

$$\frac{\delta}{\delta t} <n(t)> = k_o <n(t)>, \qquad (IV.4')$$

respectively. Quite surprisingly, the algorithms lead us to two different predictions: According to the former the environmental fluctuations should make the rate of population increase larger, whereas the latter predicts no effect on the process of population increase.

The first comment we must make on eq. (IV.1), supplemented by eq. (IV.2). is that this is precisely the kind of picture which, according to the prescriptions of the RMT, should be avoided. The general strategy outlined in Section II leads us, indeed, to regard k(t) as being a colored noise. This would make the Stratonovich form of diffusion operator correct, thereby obliging us to reject the Ito form of diffusion operator. We want to add some

further remarks to this. The phenomenological equation $\dot{n} = k\,n$ (i.e. eq. (IV.2)) is based on the assumption that the time scale of the dynamics concerning such processes as the search for food, competition among the members of the population under study, and so on, infinitely short. This is certainly a good assumption when dealing with the deterministic motion $\dot{n} = k_o\,n$. When a white noise is introduced, however, this means a motion so fast as to become competitive with even the fastest «microscopic» process. In other words, the macroscopic dynamics of the system is no more independent of the details of the microscopic dynamics.

To emphasize this relevant property, let us consider the model, recently proposed [24] to provide a more exhaustive picture of the problem of population increase under the influence of a random environment. This model reads

$$\dot{n} = r(t) - k_D n(t)$$
$$\dot{r} = -\gamma r(t) + \beta n(t). \qquad (IV.5)$$

Where r denotes the amount of resources (wich are supposed to be virtually infinite) changed into eatable food, and β expresses the capability of this population of changing resources into food (by hunt, for instance). γ is a decay parameter, which might either mean that the food is a perishable good or that the prey (in the case where this population gets food by hunt) tends to escape the predator. k_D is the death rate of the population under study. If we assume the «microscopic» time scale $1/\gamma$ to be so short as to make the Smoluchowsky approximation $(\dot{r} = o)$ valid, we obtain from the second of the equations of the set of eq. (IV.5), $r = \beta n/\gamma$, which, when replaced into the first equantion of the same set, results in

$$\dot{n} = (\beta/\gamma - k_D)n. \qquad (IV.6)$$

We identify $\beta/\gamma - k_D$ with k_o of eq. (IV. 1). We would like to remark that for the phenomenological model $\dot{n} = k\,n$ to hold, a time much larger than the microscopic time $\tau = 1/\gamma$ has to elapse.

Thus the model of eq. (IV. 5) is characterized by a non-vanishing «microscopic» time scale. We want now to see what the consequences of that property are when this model is made undergo the influence of a fast external fluctuation. For the reasons illustrated in section II even this fluctuation must be regarded as being characterized by a finite lifetime. Let assume, furthermore, that the environmental fluctuation influences the hunter capability of the population. This means

$$\dot{n} = r - k_D\,n$$
$$\dot{r} = -\gamma r + (\beta + \xi)n \qquad (IV.7)$$
$$\dot{\xi} = -\Gamma\xi + f_\xi(t),$$

where, of course, $f_\xi(t)$ is a white gaussian noise, with vanishing mean value, defined by

$$<f_\xi(o)f_\xi(t)> = 2\Gamma<\xi^2> d(t). \qquad (IV.8)$$

By making the naïve Smoluchowský approximations $\dot{r} = o$ and $\dot{\xi} = o$, eq. (IV.7) can be immediately written in the form of eq. (IV.1) with

$$k_o = \beta/\gamma - k_D \qquad (IV.9)$$

$$k(t) = f_\xi(t)/(\Gamma\gamma). \qquad (IV.10)$$

The noise $k(t)$ is defined by the correlation function of eq. (IV.2) with

$$Q = <\xi^2>/\Gamma\gamma^2). \qquad (IV.11)$$

The three-dimensional Fokker-Planck equation associated with the three-dimensional Langevin equation of eq. (IV.7), leading the time evolution of the probability distribution $\delta(n,r,\xi;t)$, can be written in a unambigous way. By adopting the contraction procedure, whose application to a system equivalent to that of eq. (IV.7) has been already illustrated in a detailed way in ref. 25, we obtain for the reduced distribution,

$$\sigma(n;t) = \int dr d\xi \delta(n, r; t), \qquad (IV.12)$$

the following equation of motion

$$\frac{\delta}{\delta t} \sigma(n; t) = \{-k_o \frac{\delta}{\delta n} n + Q \frac{R}{1+R} \frac{\delta}{\delta n} n + $$
$$+ \frac{Q}{1+R} \frac{\delta^2}{\delta n^2} n^2\} \sigma(n; t), \qquad (IV.13)$$

where

$$R = \frac{\gamma}{\Gamma} = \frac{\frac{1}{\Gamma}}{\frac{1}{\gamma}} \qquad (IV.14)$$

We thus see that when the speed of the external fluctuation is much larger than the internal relaxation of the system ($R \ll 1$) we recover the Ito form of eq. (IV.3'), whereas when the «microscopic» lifetime $1/\gamma$ is much shorter than the lifetime of external fluctuation ($R \gg 1$) the Stratonovich form of eq. (IV.3) is derived. The latter result supports the afore expressed statement that a colored noise acting in the totally inertialess system of eq. (IV.1) must result in the Stratonovich algorithm. The ubiquitous character of eq. (IV.13) must contrasted with the unique possible form of the canonical case (eq. (III.17).

We conclude this paper by saying that in the absence of canonical constraints it is not possible to obtain unique results. A range of different results is in general allowed. This ubiquitous character of nonlinear stochastic processes (non supplemented by the constraint of canonical equilibrium) nevertheless, is related via the RMT to basic properties of the «microscopic» dynamics behind the purely phenomenological description. The competition between a very fast external noise and a very fast relaxation process has the surprising effect of influencing the macroscopic motion of our system (long time dynamics). This is extremely interesting indeed because it means that an external noise very fast could be used as an efficient probe of the hidden microscopic dynamics. In principle, by arbitrarily changing the color of the external noise, it should be possible to draw information on the «microscopic» system, simply by monitoring the dependence of the rate of population increase on the lifetime of the external noise.

REFERENCES

[1] P. GRIGOLINI, Chem. Phys. Letters, 46, 483 (1977)
[2] P. GRIGOLINI, Il Nuovo Cimento, 63-B, 17 (1981)
[3] This former version of the RMT has deep analogy with the work of Rhodes and co-workers. See, for instance, A. R. ZIV and W. RHODES, J. Chem. Phys. 65, 4895, and references therein.
[4] M. W. EVANS, Adv. Chem. Phys., 62, 183 (1985)
[5] M. FERRARIO, P. GRIGOLINI, A. TANI, R. VALLAURI and B. ZAMBON, Adv. Chem. Phys., 62, 225 (1985)
[6] D. BERTOLINI, M. CASSETTARI, M. FERRARIO, P. GRIGOLINI, and G. SALVETTI, Adv. Chem. Phys., 62, 277 (1985)
[7] G. GROSSO and G. PASTORI PARRAVICINI, Adv. Chem. Phys., 62, 81 (1985)
[8] G. GROSSO and G. PASTORI PARRAVICINI, Adv. Chem. Phys., 62, 133 (1985)
[9] P. GRIGOLINI, F. MARCHESONI and PRESCIUTTINI, Adv. Chem. Phys., 62, 477 (1985)
[10] P. GRIGOLINI, Adv. Chem. Phys., 62, 1 (1985)
[11] N. G. van Kampen, Stochastic Processes in Physics and Chemistry, Amsterdam (1981)
[12] K. Lindenberg and V. Seshadri, Physica, 109-A, 483 (1981)
[13] J.D. RAMSHAW, J. Stat. Phys., 38, 669 (1985)
[14] J.D. RAMSHAW, K. LINDENBERG, J. Stat. Phys., 45, 295 (1986)
[15] M. S. GREEN, J. Chem. Phys., 20, 1281 (1952); R. ZWANZIG, Phys. Rev. 124, 983 (1961)
[16] M. GRABERT, R,. GRAHAM, and M. S. GREEN, Phys. Rev., 21-A, 2136 (1980)
[17] T. FONSECA, P. GRIGOLINI, D. PAREO, J. Chem. Phys., 83, 1039 (1985)
[18] P. GRIGOLINI, F. MARCHESONI, Adv. Chem. Phys., 62, 29 (1985)
[19] H. A. KRAMERS, Physica (Utrecht), 7, 284 (1984)
[20] S. FAETTI, L. FRONZONI, P. GRIGOLINI, Phys. Rev. 32-A, 1150 (1985)
[21] P. GRIGOLINI, work in progress
[22] K. ITO, Mem. Am. math. Soc. 4, 1 (1951)
[23] R. L. STRATONOVICH, Topics in the Theory of Random Noise (Gordon and Breach, New York, 1963), Vols. 1 and 2.
[24] P. GRIGOLINI and PRESCIUTTINI, work in progress
[25] S. FAETTI, C. FESTA. L. FRONZONI, P. GRIGOLINI, Adv. Chem Phys., 62, 445 (1985)

RESUMO

A teoria do modelo «reduzido»: Um método para estudar sistemas complexos de interesse químico e biológico.

Com argumentos intuitivos mas rigorosos, mostra-se que a teoria do modelo «reduzido» (TMR) pode ser aplicada ao estudo de sistemas clássicos satisfazendo a constrição de equilíbrio canónico. Neste caso, a TMR origina uma forma única coincidente com as derivações a partir de uma imagem microscópica rigorosa. Sistemas complexos de interesse biológico, sem a constrição de equilíbrio canónico, são caracterizadas por uma variedade de expressões diferentes. A TMR esclarece as razões «microscópicas» da diversidade destes sistemas.

JOSÉ M. LLUCH
JUAN BERTRÁN
Departament de Química
Universitat Autònona de Barcelona,
08193 Bellaterra,
Barcelona,
SPAIN

SOLVATION EFFECTS ON CHEMICAL REATIONS: FROM QUANTUM CHEMISTRY TO STATISTICAL MECHANICAL SIMULATIONS [*]

In this brief review the S_N2 reaction is taken as an example to show how the solvation effects on chemical reactions may be included into sucessive steps, by using Quantum Chemistry and Statistical Mechanics. Furthermore, some special features of the treatment of proteins in solution are discussed.

1. INTRODUCTION

Although reactions in the gas phase are simpler to deal with theoretically, the fact remains that most chemical reactions encountered in practice occur in liquid (especially aqueous) solutions. In contrast to the gas phase, where reactants follow their route to products in isolation, in solution the solvent molecules continually perturb the reactants in their course. Thus, because of these increased interactions in condensed media, the mechanism and the kinetics of a wide variety of reactions are changed appreciably on going from the gaseous state to solution.

In the last few years the application of Monte Carlo and Molecular Dynamics computer simulation techniques allowed a notorious progress in the theoretical study of solution reactions. So, the aim of this brief review is to show how the solvation effects on chemical reactions may be included into successive steps, by attempting to connect Quantum Mechanics with Statistical Mechanics. We will divide this work into two sections. In the first, we will take the S_N2 reaction as an illustrative example. In the second section, we will consider the special features and problems which appear in the treatment of proteins in solution.

2. A STRIKING EXAMPLE: S_N2 REACTION

2.1. *Experimental data*

The bimolecular nucleophile substitution S_N2 reaction,

$$X^- + RY \rightarrow XR + Y^-$$

is one of the most fundamental of organic reactions. This reaction has been extensively studied and it is well known to be experimentally sensitive to solvent polarity [1-3]. Recent gas phase experiments in the total absence of solvent have revealed that the reaction pro-

ceeds up to 20 orders of magnitude faster in the gas phase than in solution [4]. Even the qualitative nature of the reaction appears to be altered through solvation. The gas phase reaction takes place via a three-step mechanism [2,5]: formation of a stable ion-dipole complex X$^-$... RY without an activation barrier, subsequent isomerization of the complex to the dipole-ion complex XR... Y$^-$ with an activation barrier, and final dissociation of the latter complex. The resulting potential energy surface has a double-well form with a central barrier. On the contrary, the corresponding energy profile in solution is generally believed to be unimodal [6]. To bridge the gap between the gas phase and solution results, Bohme et al. [7-8] have reported the first attempt to follow the transition in the kinetics of $S_N 2$ reactions which ensues from the stepwise solvation of the nucleophile. They have measured the rate constants in the gas phase for nucleophilic $S_N 2$ displacements reactions of CH_3Cl and CH_3Br with different solvated anions $X^-(XH)_n$. Their results show that the rate constant decreases progressively from n=0 to 3, the total drop in reactivity being at least three orders of magnitude.

2.2. Quantum Chemistry results

From the theoretical point of view, the three-step mechanism proposed experimentally in gas phase without solvent molecules, has been reproduced by several authors [9-13] through the application of Quantum Mechanical methods. However the inclusion of the solvent effects is a much more difficult task. Some attempts along this line have been made [14-15]. In particular, the fluoride exchange reaction

$$F^- + CH_3F \rightarrow FCH_3 + F^-$$
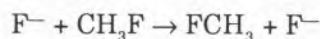
in the absence of water molecules and then solvating each fluorine atom with one water molecule, have been studied [15]. In both cases the characteristic double-well energy profile was found. The introduction of one water molecule solvating each fluorine atom stabilizes by solvation all the points of the profile. The magnitude of the stabilization diminishes as the dispersion of the negative charge increases, and therefore it decreases in the sequence reactants > intermediate > transition state. As a consequence, the depth of the intermediate potential well diminishes greatly and the energy barrier for the second step increases slightly, leading thus to an appreciable decrease of the reaction rate. An interesting fact which should be underlined is that the solvation parameters are important components of the transition vector at the transition state. Therefore, the motion of the solvent molecules themselves is an important part of the motion of the whole system along the reaction coordinate. Thus, the solvent does not adjust its position to the changing chemical system but takes part in it. Later we will return to this point.

2.3. Monte Carlo results

In spite of the simplicity of the supermolecule model used for the fluoride exchange reaction, the calculated barrier was found to be increased significantly with the introduction of only two solvent molecules, in good agreement with the experimental data. However this model is yet too much simple to describe correctly what happens in solution. The cluster reactions do not include the significant contribution of bulk solvent reorganization to the activation barrier in solution and the effects of statistical averaging. The Monte Carlo method [16-17] appears to be the most suitable theoretical technique to circumvent the mentioned limitation.

Applied to the computer simulation of solutions, the Monte Carlo technique is a numerical method in the frame of Classical Statistical Mechanics, which allows to generate a set of solution configurations with a given pro-

bability distribution function, through the realization of a Markov chain. Usually the Boltzmann distribution function is chosen:

$$\Pi\left(\vec{r}^{(N)}\right) = \frac{e^{-\,u\,(\vec{r}^{(N)})/kT}}{\int e^{-\,u\,(\vec{r}^{(N)})/kT}\,d\,\vec{r}^{(N)}}$$

where $u\,(\vec{r}^{(N)})$ is the interaction energy of the solution configuration given by the vector $\vec{r}^{(N)}$. From the obtained results, mean values of mechanical properties, values of nonmechanical properties (entropy, free energy, free enthalpy), structural analysis (radial distribution functions, solvation numbers, holes, chains of solvent molecules), significant structures, probability of fluctuations, etc., can be determined.

The first computation of a free entalphy for an S_N2 reaction in solution, by using a combined Quantum/Statistical approach, has been performed by Jorgensen et al. [18-20]. They studied the reaction of chloride ion with methyl chloride in gas phase, in aqueous solution, and in dimethylformamide (DMF):
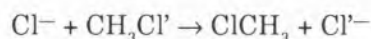
$$Cl^- + CH_3Cl' \rightarrow ClCH_3 + Cl'^-$$

where Cl' denotes the leaving group. The basic procedure in this approach involves three steps:

1) The gas-phase reaction profile is obtained using ab initio calculations by determining the energies and geometries of the $[ClCH_3Cl']^-$ cluster at a number of representative points on the potential surface. The 6-31G* basis set was employed. The typical double-well energy profile was found. The calculated energy of the ion-dipole complex relative to the reactants (−10.3 kcal/mol) as well as the energy of the transition state relative to the ion-dipole complex (13.9 kcal/mol) are in accord with the experimental complexation enthalphy (8.6 kcal/mol) [21] and intrinsic barrier (11.6 ± 1.8 kcal/mol) [19]. To build the full reaction profile a C_{3v} symmetry was imposed. The reaction coordinate was defined as

$$r_c = r_{C\,Cl'} - r_{C\,Cl}$$

which is symmetric about the transition state ($r_c = 0$). Then the calculated geometric parameters and total energies were fitted to analytical functions of r_c. So, a complete analytic discription of the energies and geometries at all points on the gas phase reaction profile was obtained.

2) Intermolecular potential functions to describe the solute-solvent interactions are developed, the pair-potential approach being assumed. Ab initio calculations were employed to obtain a large data base of energies and geometries of solute-solvent clusters at a variety of points on the potential surface. Then the parameters for the potential functions were adjusted as a function of the reaction coordinate r_c. The intermolecular potential function for the solvent-solvent interactions were taken from previous work [22-23].

3) Monte Carlo simulations are carried out to determine the free enthalphy profile for the reaction in solution. For this purpose the potential of mean force along the reaction coordinate was obtained by using importance sampling methods. A system with periodic boundary conditions was employed containing the solute cluster surrounded by 250 water molecules (or 180 DMF molecules), enough to adequatly represent bulk solvent participation in the reaction. Monte Carlo simulations were executed at standard experimental conditions of 25°C and 1 atm in the isothermal– isobaric (NPT) ensemble. An unimodal free enthalphy profile with a large central barrier was found for the reaction in aqueous solution. The calculated free energy of activation (26.3 ± 0.5 kcal/mol) is in quantitative agreement with the experimental value (26.6 kcal/mol) [24]. A significant contribution to the barrier is due to the desolvation process which occurs on going from the ion-dipole complex to the transition state. So, when the solvent is DMF, whose anion solvating ability is slower than that of water, the reaction profile is found to be intermediate between those for the reaction in the gas phase and in aqueous solution,

showing a double-well form. The calculated free enthalpy barrier in DMF is 19.3 ± 0.5 kcal/mol (the corresponding experimental value is 22.7 kcal/mol [24]). It has to be emphasized that the results obtained for both solvents correctly reproduce the several orders of magnitude rate difference for gas phase and solution S_N2 reactions.

In addition, precise information on the nature of solvation for the key points on the reaction surface (reactants, intermediates and transition state) can be provided by simulations in which the solute cluster is frozen at the appropriate geometry [19,15,26].

2.4. *Dynamical effects*

An important critical remark must be made with regard to the Monte Carlo equilibrium simulation described above. While the enthalpy profile is the larger determinant of rates for this kind of reactions in solution, an accurate theory of reactions rates certainly cannot ignore the dynamical effects. The free enthalpy description treats the solvent as a system which is always equilibrated to the reaction system at all points along the reaction coordinate, in such a way that simple Transition State Theory (TST) is a good model for the reaction. However TST breaks down as recrossings of the transition state surface are observed. Moreover, it has already been mentioned that the solvent coordinates participate in the reaction coordinate [15]. In this point Molecular Dynamics computational simulation is required.

Molecular Dynamics calculations have shown [27] that the reaction dynamics in solution can be understood in terms of a simple picture which consist of three stages: Activation of reactants, barrier crossing and deactivation of products. For the S_N2 reaction of chloride ion with methyl chloride in water, significant deviations from the simple picture of passage over a free entalphy barrier in the reaction coordinate have been found [28-29]. Thus a marked departure from TST occurs in the form of barrier recrossing. This recrossing effect can be accounted for by the so-called transmission coefficient κ correction to TST. As is well known, the actual rate constant k is then written in terms of the simple TST rate constant k^{TST} as

$$k = \kappa \, k^{TST}$$

where κ adjust the TST result to correct for the solvent induced recrossing. The value of the κ is obtained [28] generating trajectories which are initialized from an equilibrium distribution on the transition state surface. These trajectories are run both forward and backward in time to determine the ensemble of them which lead to successful reactions.

2.5 *Conclusion*

In summary, in this section we have shown how the Quantum Chemistry, Monte Carlo method and Molecular Dynamics may be combined to provide both qualitative and quantitative useful information regarding chemical reactions in solution. Unfortunately a global calculation, like the one described here for the S_N2 reaction, requires an enormous amount of computer time and hence it is not an easily available task. However, the fast development of new computers with very high performance allows us to expect that, in the near future, this kind of treatment can be applied to a wide variety of chemical processes.

3. SOME SPECIAL FEATURES OF MOLECULAR DYNAMICS SIMULATIONS OF PROTEINS IN SOLUTION

The classic view of proteins has been static in character, primarily because of the dominant role of the information provided by high-resolution X-ray crystallography for these very complex systems. Nowadays the static view of protein structure is being replaced by a dynamic picture. The atoms of which the protein is

composed are recognized to be in a state of constant motion at ordinary temperatures. From the X-ray structure of a protein, the average atomic positions are obtained, but the atoms exhibit fluidlike motions of sizable amplitudes around these average positions. Any attempt to understand the function of proteins requires an investigation of the dynamics of the structural fluctuations and their relation to activity and conformational change. So, Molecular Dynamics is by far the most promising theoretical tool to study the behaviour of proteins in vacuo and in solution. When Molecular Dynamics is used to model large molecular systems, like proteins [30-31], several practical limitations appear. Main sources of problems are related to the number of degrees of freedom and the length of the time step. Given the size of the macromolecular systems, the number of degrees of freedom should be reduced as much as possible, while retaining a truthful simulation of the physical characteristics of interest. Moreover the length of the time step Δt in the numerical integration of the equations of motion is limited by the highest frequency (ν_{max}) in the system ($\Delta t << \nu_{max}^{-1}$), which typically corresponds to a bond stretch involving a hydrogen atom. Thus, for proteins with hydrogens a time step of $5 . 10^{-16}$ s is appropriate. If Δt can be lengthened by eliminating degrees of freedom, the computer time required for a Molecular Dynamics run of a specific length will decrease.

There are several ways to achieve a reduction of degrees of freedom:

1) Extended-atom representation [31]: Some or all hydrogen atoms are incorporated in the heavy atoms to which they are bound. The main disadvantages of this procedure are that it is difficult to represent accurately hydrogen bonding, dipole and quadrupole moments, and steric effects to hydrogens, and that hydrogen coordinates are necessary for some types of analysis.

2) Constraint Dynamics [32-35]: Hard degrees of freedom, that is, those corresponding to high-frequency normal modes, can be treated as if they were completely constrained and thus be eliminated from the system. The introduction of constraints in a dynamical calculation is only allowed if: a) the frequency components of the motion along the frozen degrees of freedom are well separated from the other frequencies occurring in the system, and b) the coupling between both types of motion is weak. It has been found [34] that the combined use of bond length and bond angle constraints in molecules with other internal degrees of freedom is not physically justified. In contrast, constraining bond lengths only is both physically allowed and computationally efficient, leading to an increase of a factor 4 in the allowed time step. Molecular constraints belong to the class of scleronomous (i.e., time independent) holonomic constraints of the form

$$\sigma_k(\vec{r_1},..., \vec{r_N}) = 0 \quad , \quad k = 1 \div l$$

for the case of l internal constraints in a N-atom molecule.
For instance,

$$r^2_{ij} - d^2_{ij} = 0$$

is a distance constraint. In a system of N atoms the problem is to solve 3N Newton's equation of motion while satisfying l constraints

$$m_i \ddot{\vec{r_i}} = -\vec{\nabla}_i \ (V(\vec{r_1},..., \vec{r_N}) + \Sigma^l_{k=1} \ \lambda_k \sigma_k), \ i=1 \div N$$

where $\vec{r_i}$ is the cartesian position vector of atom i, m_i is the masse of i, $V(\vec{r_1},..., \vec{r_N})$ is the potential energy, λ_k are time dependent multipliers, $\vec{F_i} = -\vec{\nabla}_i V(\vec{r_1},..., \vec{r_N})$ is the total uncons-

trained force on atom i as if no constraints were present and $\vec{G}_i = -\Sigma^l_{k=1} \lambda_k \vec{\nabla}_i \sigma_k$ is the total constraint force on atom i which compensates the components of $\vec{F}_i$ that act along the directions of the constraints.

There are several methods to solve the equations of motion subject to constraints. Perphaps, the so-called SHAKE and a generalization of this are the best procedures [33,35].

3) Stochastic dynamics [36-37]: Less relevant degrees of freedom can be ignored and their influence approximated by a combination of mean force interactions, stochastic forces and frictional forces. When simulating a protein in solution, this approach is specially suitable to represent the effect of the solvent molecules. Its main problem is that the solvent molecules are not explicitly considered.

The simulation method of Stochastic Dynamics consists on integrating the Langevin equation of motion

$$m_i \ddot{\vec{r}}_i = -\vec{\nabla}_i V + \vec{R}_i - \gamma_i \dot{\vec{r}}_i$$

where V is the potential of mean force, $\vec{R}_i$ is the stochastic force on atom i and $-\gamma_i \dot{\vec{r}}_i$ is the frictional force on atom i. This stochastic simulation technique may reduce the computing effort by an order of magnitude.

Finally it is necessary to emphasize that the simulation of biological macromolecules is only just starting its development. A wide range of biological problems involving nucleic acids, enzymes, membrane lipids, drug design, and many others related to the Biotechnology, are ready for study and exciting new results can be expected as dynamical methods are applied to them. In the coming years, the improvement of the theoretical methods and algorithms, and the increasing computer power will allow that a very significant progress can be accomplished in this field.

REFERENCES

[1] A. J. PARKER, Chem. Rev., 69, 1 (1969).

[2] W. M. OLMSTEAD and J. I. BRAUMAN, J. Am. Chem. Soc., 99, 4219 (1977).

[3] W. J. ALBERY and M. M. KREEVOY, Adv. Phys. Org. Chem., 16, 87 (1978).

[4] K. TANAKA, G. I. MACKAY, J. D. PAYZANT, D. K. BOHME, Can. J. Chem., 54, 1643 (1976).

[5] M. J. PELLERITE and J. I. BRAUMAN, J. Am. Chem. Soc., 102, 5993 (1980).

[6] C. H. INGOLD, «Structure and Mechanism in Organic Chemistry», 2nd ed. Cornell University Press, Ithaca, NY, 1969.

[7] D. K. BOHME and G. I. MACKAY, J. Am. Chem. Soc., 103, 978 (1981).

[8] D. K. BOHME and A. B. RAKSIT, J. Am. Chem. Soc., 106, 3447 (1984).

[9] A. J. DUKE and R. W. F. BADER, Chem. Phys. Lett., 10, 631 (1971).

[10] A. DEDIEU and A. VEILLARD, in «Quantum Theory of Chemical Reactions», Vol. 1, ed. R. Daudel, A. Pullman, L. Salem and A. Veillard, Reidel, Dordrecht, 1980, p. 69.

[11] F. KEIL and R. AHLRICHS, J. Am. Chem. Soc., 98, 4787 (1976).

[12] S. WOLFE, D. J. MITCHELL and H. B. SCHLEGEL, J. Am. Chem. Soc., 103, 7692, 7694 (1981).

[13] F. CARRION and M. J. S. DEWAR, J. Am. Chem. Soc., 106, 3531 (1984).

[14] K. MOROKUMA, J. Am. Chem. Soc., 104, 3733 (1982).

[15] J. JAUME, J. M. LLUCH, A. OLIVA and J. BERTRAN, Chem. Phys. Lett., 106, 232 (1984).

[16] W. W. WOOD, in «Physics of Simple Liquids», ed. H. N. V. TEMPERLEY, J. S. ROWLINSON and G. S. RUSHBROOKE, North-Holland, Amsterdam, 1968.

[17] J. P. VALLEAU and S. G. WHITTINGTON, «A guide to Monte Carlo for Statistical Mechanics: 1. Highways», in «Statistical Mechanics. Part A: Equilibrium Techniques». ed. B. J. Berne, Plenum Press, New York, 1977.

[18] J. CHANDRASEKHAR, S. F. SMITH and W. L. JORGENSEN, J. Am. Chem. Soc., 106, 3049 (1984).

[19] J. CHANDRASEKHAR, S. F. SMITH and W. L. JORGENSEN, J. Am. Chem. Soc., 107, 154 (1985).

[20] J. CHANDRASEKHAR and W. L. JORGENSEN, J. Am. Chem. Soc., 107, 2974 (1985).

[21] R. C. DOUGHERTY and J. D. ROBERTS, Org. Mass. Spectrom., 8, 77 (1974).

[22] W. L. JORGENSEN, J. CHANDRASEKHAR, J. D. MADURA, R. W. IMPEY and M. L. KLEIN, J. Chem. Phys., 79, 926 (1983).

[23] W. L. JORGENSEN and C. J. SWENSON, J. Am. Chem. Soc., 107, 569 (1985).

[24] D. J. McLENNAN, Aust. J. Chem., 31, 1897 (1978).

[25] I. CERNUSAK and M. URBAN, Coll. Czech. Chem. Comm., 49, 1854 (1984).

[26] O. Tapia and J. M. Lluch, *J. Chem. Phys.*, **83**, 3970 (1985).

[27] J. P. Bergsma, J. R. Reimers, K. R. Wilson and J. T. Hynes, *J. Chem. Phys.*, **85**, 5625 (1986).

[28] J. P. Bergsma, B. J. Gertner, K. R. Wilson and J. T. Hynes, *J. Chem. Phys.*, **86**, 1356 (1987).

[29] B. J. Gertner, J. P. Bergsma, K. R. Wilson, S. Lee and J. T. Hynes, *J. Chem. Phys.*, **86**, 1377 (1987).

[30] M. Karplus and J. A. McCammon, *Ann. Rev. Biochem.*, **53**, 263 (1983).

[31] B. R. Brooks, R. E. Bruccoleri, B. D. Olafson, D. J. States, S. Swaminathan and M. Karplus, *J. Comp. Chem.*, **4**, 187 (1983).

[32] W. F. van Gunsteren and H. J. C. Berendsen, *Mol. Phys.*, **34**, 1311 (1977).

[33] J. P. Ryckaert, G. Ciccotti and H. J. C. Berendsen, *J. Comp. Phys.*, **23**, 327 (1977).

[34] H. J. C. Berendsen and W. F. van Gunsteren, in «Molecular Liquids- Dynamics and Interactions», ed. A. J. Barnes et al., Reidel, Dordrecht, 1984, p. 475.

[35] J. P. Ryckaert, *Mol. Phys.*, **55**, 549 (1985).

[36] W. F. van Gunsteren, H. J. C. Berendsen and J. A. C. Rullmann, *Mol. Phys.*, **44**, 69 (1981).

[37] T. Akesson and B. Jonsson, *Mol. Phys.*, **54**, 369 (1985).

RESUMO

Efeitos de solvatação em reacções químicas: Da química quântica as simulações de mecânica estatística.

Nesta breve revisão, a reacção S_N2 é tomada como exemplo para mostrar como os efeitos de solvatação nas reacções químicas podem ser incluídos em etapas sucessivas, usando química quântica e mecânica estatística. São ainda discutidas algumas características especiais do tratamento das proteínas em solução.

SEBASTIÃO J. FORMOSINHO
Departamento de Química,
Universidade de Coimbra,
3049 Coimbra Codex,
PORTUGAL

TRANSITION STATE BOND ORDER AS A SOURCE OF MECHANISTIC VERSATILITY IN ENZYME CATALYSIS [*]

The intersecting-state model (ISM) is. applied to the study of enzyme catalysis. It is shown that enzymes tend to maximize the transition state bond order, n. Such fact leads to quite fast and selective reaction processes. The ambident behaviour of some enzyme catalyses is discussed in terms of the control of reactivity by n* and the reaction energy, ∆G°, which have opposite variations on ∆G* as a function of the polarity of the reaction sites. The intramolecular character of enzyme reactions has been found to be dominated by bond lengths and n* parameters of the reactive bonds.*

INTRODUCTION

We have recently examined the origin of the catalytic power of enzymes [1], in terms of the intersecting-state model (ISM) [2]. This work has been aimed at developing a view of these catalyses that can be understood, at least in the first approximation, in relatively elementary terms, without resorting to elaborate quantum mechanical calculations. The main conclusion is that such a power is due to the concerted effect of several molecular factors, namely free-energy effects in the enzyme-substrate complexes, decrease in force constants and bond lengths of the reactive bonds and enhancements of the so called «transition state bond order».

ISM provides a minimum set of molecular parameters to interpret chemical reactivity for an unidimensional potential-energy model. The energy barrier is estimated through the intersection of two potencial energy curves: one for the reactants and the other for the products. For a prototype reaction

$$A + B-C \rightarrow A-B + C \qquad (1)$$

the horizontal separation of the potential energy curves, d, corresponds to the sum of the bond extensions of BC and AB up to the transition state, as long as one can neglect the interaction between the electronic states at the crossing point of the potential energy curves. We have shown [2] that the sum of the bond extensions is given by

$$d = [(a' \ln2/n^*) + (a'/2) \ (\Delta G^o/\lambda)^2 \ 1 \qquad (2)$$

where n^* is the transition state bond order, ΔG^o is the reaction energy, $1 = 1_{AB} + 1_{BC}$ the sum of the equilibrium bond lengths of reactant and product, and λ is a measure of the capacity of the transition states to accommodate energy; a' is a constant ($a' = 0.156$).

In general, one uses harmonic potential energy curves, characterized by the corresponding force constants, f_i. Under this approximation the molecular parameters which control che-

mical reactivity can be classified into: i) reagent-product parameters: reaction energy (ΔG^o), force constants (f) and bond lengths (l); ii) transition-state parameters: transition state bond order (n^*) and configuration mixing parameter (λ). Although such a distinction is useful, one must realize that n^* is not independent of the electronic nature of reactants and products [2-5].

Since it generally takes more energy to stretch a bond than to change a bond angle, the emphasis on the control of chemical reactivity by the extensions of bonds rather than angles should arise no surprise. Even some rotational isomerizations have been interpreted within ISM [6] and only in some unimolecular isomerizations of small cyclic systems, together with bond extensions, there are significant contributions of the bending motions and bond angles changes along the reaction coordinate [7]. For the enzyme reactions we will only consider the bond extensions.

In terms of the current models of chemical reactivity, the concept of a variable bond order along the reaction coordinate is the least well known. Furthermore, n^* is the parameter which can produce the largest acceleration rate and one which is associated with the greatest number of mechanistic features. In view of these facts, in the present paper we intend to investigate further the importance of n^* in enzyme catalysis, for the hypothetical reaction

$$E + S \underset{K_M}{\overset{k_{cat}}{\rightleftharpoons}} S \longrightarrow E + \text{products} \qquad (3)$$
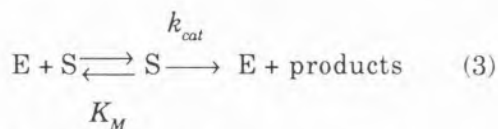
where k_{cat} is related to the reaction energy barrier by the Transition State equation

$$k_{cat} = (k_B T/h) \exp(-\Delta G^*_{cat}/RT) \qquad (4)$$

Eq (2) shows that d is small when λ is high. This suggests that lower energy barriers are provided by floppy and disordered transition states (ΔS^* high). Therefore, throughout the paper we will take $\lambda >> |\Delta G^o|$.

INTRAMOLECULARITY

Intramolecular reactions often proceed much faster than their intermolecular counterparts and this has been considered a source of catalytic activity [8]. Menger [9] has discussed in detail the origin of intramolecular acceleration, which can often amount to several powers of ten in magnitude, and has eliminated concentration effects, misalignment of reactants and entropic factors as the main source of such large rate enhancements. For example, entropies of activation correlate poorly with intramolecular efficiencies and this agrees with other findings on other chemical reactions; the intersecting-state model can reproduce well the experimental ΔG^* values of several electron exchange reactions, but not the variations of ΔH^* and $T\Delta S^*$ [10].

ISM provides a good estimation of ΔE^* for vapour phase reactions involving the breaking of one bond and the making of another one. However, for gas phase reactions of complex molecules or reactions in solution there are many other degrees of freedom than one stretching in reactants and in products. To keep the model unidimensional, one has to treat such degrees of freedom on a statistical basis by employing free-energies (G) rather than internal energies (E). Under such conditions ISM provides a good estimation of ΔG^* for several types of reactions. In consequence, ΔS^* does not show as an additional contribution for the reaction energy barrier *, but is essentially a measure of the distribution of the internal energy in complex reacting systems.

Menger has suggested that the great source of the intramolecular rate acceleration is the «critical distance» of the reactants [9]. For example, for proton transfer reactions from H_3O^+ to H_2O Schneider [11] finds by quantum mechanical calculation that decreasing the

---

* When $\Delta G^o \neq 0$, ΔS^* can have an indirect effect on the energy barrier via the mixing entropy parameter when $\lambda \ll |\Delta G^o|$.

O-O distance from 2.95 A° to 2.55 A° increases the rates 10^{11}-fold; the decrease from 2.75 A° to 2.55 A° increases the rates 10^4 times. Such decreases in distances between reactants are present in several intramolecular processes [9]. In enzyme reactions such effects have been invoked, for example, on the hydrolysis of thionoesters which are far less reactive than normal esters. This is attributed to the fact that the C=S bond length and the optimal S... HN= bond distances for the thionoesters are longer than the ester counterparts [12].

Within ISM such «distance effects» can be associated with bond lengths, l, due to changes in the the equilibrium bond lengths of the bond-forming process in the products. For proton transfer reactions, with typical values of force constants $f_r = f_p = f = 4 \times 10^3$ kJ mol^{-1} A$^{\circ -2}$ and bond lengths $l = 2.0$ A° [4], one can verify the effect of the increase in l by ca. 0.4 A°, at a constant f. Virtually independent of ΔG^o ($\lambda >> |\Delta G^o|$), the decrease in the rate constants is 10^7 times with $n^* = 0.5$ and ca. 30 times with $n^* = 1.0$. This is the range of the transition state bond order values for the normal acids; n^* is close to 0.5 for carbon acids and to unity for HF (oxygen and nitrogen acids have $n^* \simeq 0.75$–0.85) [4]. Although the «distance effects» can produce large rate accelerations, particularly for the slow reactions (n^* low), the calculation suggests that other molecular factors are involved in the rate acceleration effect of 11 orders of magnitude; the most important is n^*.

EVIDENCE FOR THE IMPORTANCE OF n^*

Although changes in l, f and ΔG^o are all important in enzyme catalysis [1], changes in the transition state bond order are also certainly quite significant in some reactions. In principle n^* can be viewed as an empirical parameter of chemical reactivity, free from the effects of l, f, ΔG^o and λ. However, for the majority of chemical reactions n^* has a simple physical meaning, given by counting the number of bonding, nonbonding and antibonding electrons of the reactive bonds in the activated complexes.

For hydrogen transfer in hydride reactions, in the vapour phase, since one is dealing with the breaking and the forming of single bonds, the chemical bond order can be conserved along the reaction coordinate, $n_{AB} + n_{BC} = 1$. In consequence, for the transition states at the thermoneutral situation $n_{AB}^\# = n_{BC}^\# = 1/2$. This situation is found when reagents and products do not possess nonbonding or antibonding electrons [2]. However, if there are occupied nonbonding or antibonding electrons in reactants and products, one of such pairs can acquire a bonding character when the transition states have a bent geometry [3-5]. This electronic siphoning increases n^* ($n^* = 1$ or 3/2), decreases d and, in consequence, diminishes ΔG^*.

Solvents can also affect n^* through an interaction with the nonbonding pairs of electrons of reactants. For example, nucleophilic substitutions on methyl,

$$X^- + CH_3Y \rightarrow XCH_3 + Y^- \qquad (5)$$

where X and Y are halogens, have $n^* = 1$ in the gas phase, independently of the nature of X and Y, due the conversion of a nonbonding pair of electrons from the reactants to a bonding pair in the transition state [13]. However, in liquid solutions $n^* < 1$, approaching the limiting value of $n^* = 0.5$ for X=Y=F, in water. This limiting value implies that the total bond order is conserved along the reaction coordinate, because the nonbonding pair of electrons of the fluorine atom cannot acquire a bonding character at the transition state because of a strong interaction with the H_2O molecules. For other systems n^* depends on the nature of the solvent and of the nucleophile: i) n^* is higher with poor acceptor solvents (nonpolar) and lower with good acceptor solvents (polar); ii) n^* increases with the increase of the softness of the nucleophiles measured by their Mulliken electronegativities, $I+A$ (I ionization energy, A affinity), and, in general, n^* is the

sum of the individual contributions of X and Y ($n^* = C_n \#(X) + C_n \#(Y)$) [14].

Whereas reactions (5) are faster in nonpolar solvents, because their reactivities are dominated by n^*, the Menschutkin reaction

$$Et_3N + EtI \longrightarrow Et_4N^+ + I^- \qquad (6)$$
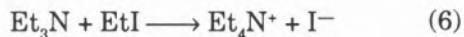
is faster in polar solvents, because its reactivity is controlled by the changes in ΔG^o rather than n^* [13]. The development of charges favours a large decrease in ΔG^o in the more polar media.

The transition state bond order can also be increased through the participation of electron-rich bonds ($n=2$ or 3) in the reaction coordinate [7-15] and, in a less significant manner, through electronic siphoning of electron-rich substituents [7-16]. In contrast, n^* can be decreased through the loss of the synchronicity of the reactions, namely due to steric or solvent viscosity effects [16-18].

A strong evidence of the role of n^* in enzyme catalysis comes from mutagenesis studies, where mutant enzymes are prepared with changed aminoacid residues. Tyrosyl-tRNA synthetase catalyses the aminoacylation of tRNA; a change of histidine-45 by asparagine-45, which is positioned to form a hydrogen bond with the γ-phosphoryl group of ATP, does not affect the binding of ATP but increases the reaction barrier by ca. 19 kJ mol^{-1} [19-20]. Since for such enzyme reactions we do not expect a significant change in the force constants and equilibrium bond lengths of the reactive bonds, such variation in k_{cat} must be attributed to changes in n^* in the mutant enzyme.

There are also other enzyme reactions where changes in subsites increase k_{cat}, but do not change K_M. A good example is the structure of the active site of papain; the specificity for large hydrophobic residues in the S_2 subsite is manifested in increased values of k_{cat} rather than in a tighter binding [20]. Within ISM such feature can be interpreted in terms of an increase of n^* in a less polar environment, at a constant ΔG^o. The «charge relay system» [21] invoked in many enzyme reactions is a mechanism of siphoning electronic density into the transition states and, consequently, to increase n^*.

CALCULATIONS FOR SELECTED ENZYME REACTIONS

One role for metals in metalloenzymes is that of a electrophilic catalyst, by «siphoning» electronic density into the transition states. This type of mechanism has been mimicked in model compounds; for example, the base catalyzed hydrolysis of glycine ethyl ether is increased more than 6 orders of magnitude when the compound is coordinated to Co^{3+} [22]

$$k = 1.5 \times 10^6 \ M^{-1} \ s^{-1} \ (n^* = 1.0)$$

$$k' = 0.6 \ M^{-1} \ s^{-1} \ (n^* = 0.78)$$

$$H_2NCH_2CO_2Et \qquad (7)$$
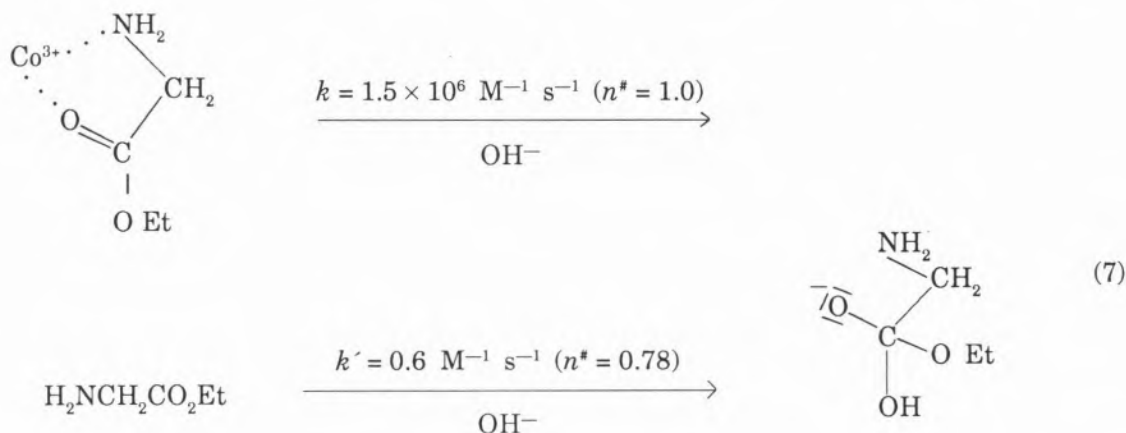
For the formation of the tetrahedral intermediate shown in reaction (7), the reactive bonds are C=O in reactants and two C–O bonds in the products (for two bonds $f_p = \sqrt{2f_{C-O}}$). With the f, l and bond strength data reported by Gordon and Ford [23], the relevant parameters are: $f_r=7.3\times10^3$ kJ mol^{-1} A^{-2}, $f_p=4.3\times10^3$ kJ mol^{-1} A^{-2}, $l=l_{C=O}+l_{C-O}=2.64$ Å and ΔG^o=-30 kJ mol^{-1}. This allows one to estimate the transition state bond orders presented above, as described elsewhere [1-5].

Apparently the metal ion siphons electronic density into the transition state, but the mechanism is possibly more subtle. If one of the oxygen lone pairs of the CO$^-$ group becomes bonding in the transition state then n^*=1.0. For the reaction in solution such pair interacts with the polar solvent molecules and $n^*<1.0$ (n^*=0.78). When the reagent is coordinated to Co^{3+}, the interaction of the CO$^-$ group with the solvent molecules is prevented and the metal ion, behaving as a hard group, allows the CO$^-$ lone pairs to become completely free to siphon electronic density into the transition state.

An interesting case of a very efficient metalloenzyme is carbonic anhydrase which catalyzes the reaction

$$O=C=O + H_2O \longrightarrow O=C \Big\langle {O^- \atop OH}$$

$$\text{(8)}$$

$$+ H^+ \qquad \Delta G^o\text{=36 kJ mol}^{-1}$$
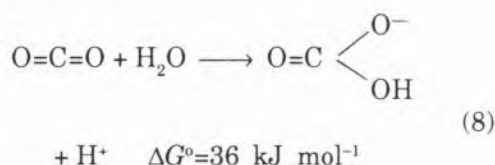
The O enzyme is the most efficient, with k_{cat}=10^6 s^{-1} and ΔG^*=40 kJ mol^{-1} at room temperature. We will assume that the force constants and bond lengths of the reactive bonds have typical values [23]: reagents C=O, $f_r=7.3\times10^3$ kJ mol^{-1} Å^{-2} and l_r=1.215 Å, and products (two C–O and one O–H bonds) $f_p = \sqrt{\Sigma f_i^2}=6\times10^3$ kJ mol^{-1} Å^{-2} and $l_p=(2_{C-O}+l_{OH})/3$=1.269 Å. With this set of data the estimated transition state bond order is very high, n^*=2.0. Not only does a lone pair of the CO$^-$ group become bonding at the transition state, but electronic density is siphoned through a resonance mechanism *via* the C=O

bond. If the lone pair of the CO$^-$ group was completely unable to become bonding at the transition state, then n^*=1 and ΔG^*=79.5 kJ mol^{-1}. This would correspond to a decrease in the reaction rate of ca. 7 orders of magnitude. Warshel and Sussman [24] have recently reported a calculation of the effect of a site-directed mutagenesis of rat trypsin, employing a simulation method based on a combination of the empirical valence bond (EVB) method and a free-energy perturbation method [25]. Here we would like to address the same problem within the much simpler ISM formalism. Craik *et al.* [26] have shown that the replacement of Gly-216 and Gly-226 by alanine produces a ca. 2000 fold reduction in the catalytic rate constant for amide hydrolysis, but a negligible change in K_M (<20). For the calculations we will assume a single kinetic step, which is probably not the real situation. This assumption implies a synchronous and concerted character for the reaction

$$\text{(9)}$$
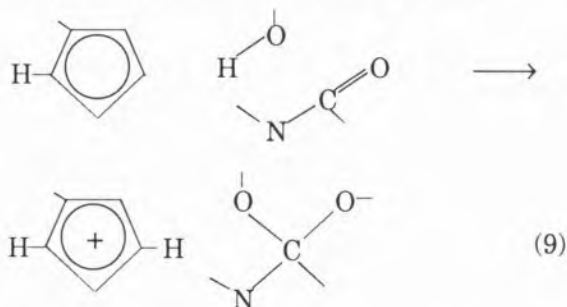
In consequence the absolute n^* values should be smaller than the ones calculated. However, for comparative purposes such an effect can be neglected.

For reaction (9) the reactive bonds are: reactants, C=O and O–H, and products 2 C–O and a C–H bonds. Using the f and l data of ref. 23, one calculates $f_r=8.4\times10^3$ kJ mol^{-1} Å^{-2}, $f_p=5.3\times10^3$ kJ mol^{-1} Å^{-2} and $l=2.4$ Å; the reaction energy is ΔG^O=46 kJ mol^{-1} [24]. To assess the effect of mutagenesis we will consider the effective n^* value as an weighted average of n_a# of a carbon acid (n^*=0.56 [4]) and the n_h^* values for the hydrolysis reaction ($n^*=(n_a^*+2 n_h^*)/3$). The maximum n_h^* is 1.0 and we will consider that mutagenesis causes geometric

changes that deform the oxyanion site in such a way that interaction of the CO⁻ lone pair with water molecules of the hydrogen network can occur. Obviously in simple terms it is not possible to translate the geometrical changes into changes of $n_h^{\#}$. However, if one assumes that such value ranges between the values estimated previously for the hydrolysis of glycine ethyl ether in a polar environment and that coordinated to Co^{3+}, $n_h^{\#}$ should range somewhere between 0.78 and 1.0. The effective $n^{\#}$ values will range between 0.85 ($\Delta G^{\#}$=104 kJ mol⁻¹) and 0.71 ($\Delta G^{\#}$=136 kJ mol⁻¹), i.e. mutagenesis should decrease k_{cat} by a factor smaller than 4×10^5. For a value of $n_n^{\#}$=(1+0.78)/2, $n^{\#}$=0.78 the estimated decrease is 300 times which is in the range of the experimental effect, taking also into account the small variation of K_M.

Although the present explanation gives effects in fair agreement with experiment, we must point out that we have neglected any variation in the free-energy at the reaction site. However, since the reaction creates electrical charges, ΔG can decrease strongly with an increase in the polarity of the reaction site. In consequence, if ΔG^O dominates the effect of $n^{\#}$, then a more polar environment would make the catalytic reaction faster, in contrast with the predictions based on the effect of $n^{\#}$. Warshel appears to favour this last mechanism for the reactions under study [24,27].

SELECTIVITY

When one compares similar chemical reactions, the changes in reactivity are, in general, dominated by two structural factors: $n^{\#}$ and ΔG^O. Under special circumstances one of those factors is the ruling one and interesting features of chemical reactivity can be observed. One of those features is ambient reactivity such as found in

$$O=N-O \underset{BuCl}{\overset{MeI}{\longrightarrow}} \begin{array}{ll} MeNO_2 + I^- & n^{\#} \text{ control} \\ BuONO+Cl^- & \Delta G^o \text{ control} \end{array} \qquad (10)$$
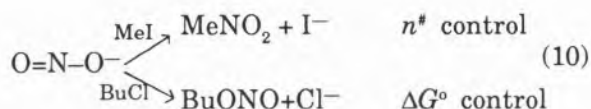
The transition state bond order dominates the reactivity of one of the reactions and the reaction energy the other [28].

A similar situation can be present in the mechanism for editing in protein synthesis, as described by Fersht [29]. In the absence of an editing mechanism the errors in the aminoacid selection would be considerably larger than observed, for example, the isoleucyl-tRNA should favour isoleucine over valine by a factor of ca. 150, which combined with the higher concentration of valine *in vivo* systems would give an error rate ca. 1 in 30. Due to an editing mechanism the error is only 1 in 3000. The addition of tRNA[Ile] to the correct enzyme substrate complex gives Ile-tRNA[Ile]; the addition of tRNA[Ile] to the incorrect complex of valyl adenylate leads to hydrolysis in quantitative yields to valine and tRNA[Ile].

The overall mechanism involves high energy intermediates EI along the reaction path, which are then partitioned between further synthesis and destruction by hydrolytic editing.

$$E + S \rightleftharpoons ES \longrightarrow EI \overset{\text{synthesis}}{\underset{\text{destruction}}{\diagdown}} \qquad (11)$$
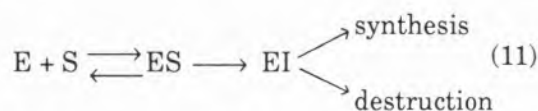
The enzyme can operate such ambient behaviour in distinct and separate reaction sites [29], one more hydrophobic that enhances the $n^{\#}$-control and diminishes the ΔG^O effect, the other more hydrophilic that enhances the ΔG^O-effect and diminishes the value of $n^{\#}$. Synthesis is favoured in the correct intermediate by $n^{\#}$-control in the hydrophobic site, and destruction via hydrolysis is favoured for the incorrect intermediate by ΔG^O-control in the hydrophilic site. The enhancement of the ambient behaviour in proper sites allows a large ratio in the rate constants for the adequate reactions, k(synthesis)EI[corr]/k(destruction)EI[corr] and k(destr.)EI[incorr]/k(synt.)EI[incorr] which can amount typically to factors of 10^2–10^3 [28].

Such behaviour conforms well with the qualitative features of enzyme analogue catalysis

by encapsulation of an organic substrate in the cavity of a macrocyclic compound. For example, the reaction of bromomethylnaphthalene with the ambident anion NO_2^-

$$(12)$$
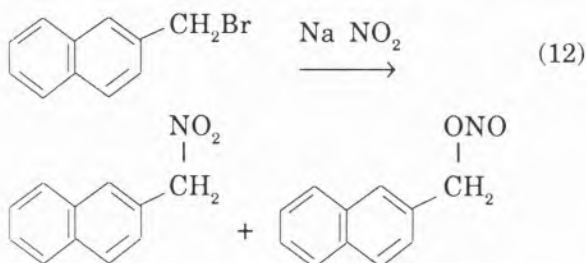
is catalysed by a macrocyclic-azacyclophane. The most remarkable feature of the reaction is the increase in the product ratio $R–NO_2/R–ONO$ which corresponds exactly to the observed overall rate constant increase as a function of the catalyst-to-substrate concentration ratio [30]. The encapsulation of the reagents in a less polar environment allows the increase of $n^{\#}$ and increaes the $n^{\#}$-control product ($R-NO_2$) ca. 4-5 times. In contrast, the opposite effect is observed upon the addition of open-chain alkylammonium salts during the substitution reactions [30]. The interaction of the lone pairs of NO_2^- with the added cation in a polar medium decreases $n^{\#}$ and ΔG^O and favours the ΔG^O-control product R-ONO.

A final word must be said about reaction selectivity in enzyme catalysis. There is an old principle in physical organic chemistry, the Reactivity-Selectivity Principle (RSP) [31], which states that the more reactive species tend to be less selective in their reactivity than the less reactive ones. Although enzymes have a substrate protection their optimization, which has been accomplished by nature over many million of years, should provide mechanisms for fast and selective catalysed reactions rather than fast and unselective processes. We have shown [5] that RSP is obeyed when the changes in reactivity are controlled by the changes in ΔG^O; in contrast an anti-RSP behaviour is found when the changes in reactivity are dominated by the

changes in $n^{\#}$. This argument leads us to suggest a great importance of $n^{\#}$ in enzyme catalysis, because it ensures that the fastest reactions are also the most selective ones. Further, it appears that natural enzymes have evolved in the sense to attain the maximum $n^{\#}$ compatible with the molecular structure of the reacting partners.

REFERENCES

[1] S. J. FORMOSINHO and J. J. C. TEIXEIRA-DIAS, *J. Mol. Catal.*, **42**, 127 (1987).

[2] A. J. C. VARANDAS and S. J. FORMOSINHO, *J. Chem. Soc. Faraday Trans. 2*, **82**, 953 (1987).

[3] S. J. FORMOSINHO, *Rev. Port. Quim.*, **27**, 427 (1985).

[4] S. J. FORMOSINHO, *J. Chem. Soc. Perkin Trans. 2*, **61**, 427 (1987).

[5] S. J. FORMOSINHO, *J. Chem. Soc. Perkin Trans. 2*, in press.

[6] J. SEITA and S. J. FORMOSINHO, *Tetrahedron*, 839 (1988).

[7] S. J. FORMOSINHO and A. J. C. VARANDAS, *Rev. Port. Quim.*, **28**, 33 (1986).

[8] W. P. JENCKS, «Catalysis in Chemistry and Enzymology», MCGRAW-HILL, New York, 1969, chap. 1; T. C. Bruice, *Annu. Rev. Biochem.*, **45**, 331 (1976).

[9] F. M. MENGER, *Tetrahedron*, **39**, 1013 (1983); *Acc. Chem. Res.*, **18**, 128 (1985); in «Nucleophilicity», J. M. HARRIS and S. P. McMANUS, eds., ACS, **215**, 209 (1987). For an alternative explanation see, for example, M. I. PAGE and W. P. JENCKS, *Gazz. Chim. Italiana*, **117**, 455 (1987).

[10] S. J. FORMOSINHO, *Rev. Port. Quim.*, **28**, 38 (1986).

[11] S. SCHEINER, *J. Am. Chem. Soc.*, **103**, 315 (1981).

[12] P. CAMPBELL, N. T. NASHED, B. A. LAPINSKAS and J. GURRIERI. *J. Biol. Chem.*, **258**, 59 (1983); B. ASBOTH and L. POLGAR, *Biochemistry*, **22**, 117 (1983).

[13] S. J. FORMOSINHO, *Tetrahedron*, **43**, 1116 (1987).

[14] S. J. FORMOSINHO, *J. Phys. Org. Chem.*, submitted for publication.

[15] S. J. FORMOSINHO, and V. M. S. GIL, *J. Chem. Soc. Perkin Trans. 2*, 1655 (1987).

[16] S. J. FORMOSINHO, *Tetrahedron*, **42**, 4557 (1986).

[17] H. D. BURROWS and S. J. FORMOSINHO, *J. Chem. Soc. Faraday Trans, 1*, **83**, 431 (1987).

[18] S. J. FORMOSINHO, S. M. B. COSTA and A. L. MAÇANITA, to be published.

[19] G. Winter, A. R. Fresht, A. J. Wilkinson. M. Zoller and M. Smith, *Nature*, **299**, 956 (1982).

[20] A. Fersht, «Enzyme Structure and Mechanism», 2nd ed., Freeman, New York, 1985, pp. 323, 324 and 318, 411, 415. ⁻

[21] D. M. Blow, J. J. Birktoft and B. S. Hartley, *Nature*, **221**, 337 (1970).

[22] Ref. 20, p. 68.

[23] A. J. Gordon and R. A. Ford, «The Chemist's Companion», Wiley, New York, 1972, pp. 107, 113, 114.

[24] A. Warshel and F. Sussman, *Proc. Natl. Acad. Sci. USA*, **83**, 3806 (1986).

[25] A. Warshel and R. M. Weiss, *J. Am. Chem. Soc.*, **102**, 6218 (1980).

[26] C. S. Craik, C. Largman, T. Fletcher, S. Roczanick, P. J. Barr, R. Fletterick and W. J. Rutter, *Sicence*, **228**, 291 (1985).

[27] A. Warshel and S. Russell, *J. Am. Chem. Soc.*, **108**, 6569 (1986).

[28] S. J. Formosinho, L. G. Arnaut and A. M. A. R. Gonçalves, to be published.

[29] Ref. 20, pp. 354-358.

[30] H.-J. Schneider, R. Busch, R. Kramer, U. Schneider and I. Theis, in «Nucleophilicity» (ref. 9), p. 457.

[31] C. D. Johnson, *Chem. Rev.*, **75**, 755 (1975); *Tetrahedron*, **36**, 3461 (1980).

RESUMO

O papel da ordem de ligação no estado de transição na selectividade da catálise enzimática

O modelo de intersecção de estados (ISM) é aplicado ao estudo da catálise enzimática. Mostra-se que as enzimas tendem a maximizar a ordem de ligação do estado de transição, n', o que assegura a existência de reacções muito rápidas e selectivas. O carácter ambivalente de certas catálises é interpretado em termos do controlo da reactividade por n' e pela energia da reacção, ΔG°, que conduzem a variações opostas na barreira de energia das reacções, em função da polaridade do meio. O efeito da intramolecularidade nas reacções enzimáticas é bem interpretado em termos dos parâmetros n' e de comprimentos de ligação das ligações reactivas.

FERNANDO M. S. SILVA FERNANDES
BENEDITO J. COSTA CABRAL
Departamento de Química & CECUL (INIC)
Rua Ernesto de Vasconcelos, Bloco C1-Piso 5
1700 Lisboa,
PORTUGAL

MOLECULAR DYNAMICS BY COMPUTER SIMULATION [*]

The purpose of this paper is to present a short survey of molecular dynamics methods by computer simulation with incidence on general aspects rather than on technicalities.

1. INTRODUCTION

In the present context, molecular dynamics (MD) and Monte Carlo (MC) methods are understood as computer simulation techniques for studying thermodynamic and structural properties of solids and fluids.

MD methods [1-2] produce trajectories in phase space by numerically solving Newton's equations of motion for the molecules in the sample. Time averages are then calculated over those trajectories.

MC methods [3-4] generate statistical ensembles by giving random displacements to the molecules and accepting, or rejecting, the resulting configurations with a probability proportional to appropriate Boltzmann factors. Ensemble averages are then calculated over the generated configurations.

According to statistical mechanics [5] time and ensemble averages are equal. Therefore MD and MC methods should be equivalent as far as equilibrium properties are concerned. In fact, MC methods can not deal with dynamic phenomena. On the contrary, MD is able to probe both equilibrium and dynamic properties.

MC methods are easier to implement in a computer program for they only require the calculation of the total energy of each configuration while MD also requires the forces on each particle. The computer effort for a comparable statistical accuracy is, however, of the same order of magnitude for MD and MC.

The purpose of this paper is to present a short survey of molecular dynamics methods with greater incidence on general aspects rather than on technicalities.

2. BOUNDARY CONDITIONS

Due to memory and computer time requirements the number, N, of molecules that is possible to follow in time with the present generation of computers is of order 10^2-10^4

depending on the complexity of the molecules and the type of computer.

This is a rather small number for the simulation of bulk systems where the number of molecules is of order 10^{23}. Therefore, the use of boundary conditions is inevitable in order to eliminate surface effects.

and the bulk system is approximated by a periodically repeated sample. This is illustrated in Figure 1.

The potential energy and the force on each molecule are calculated by taking into account the periodicity of the system as we shall see.
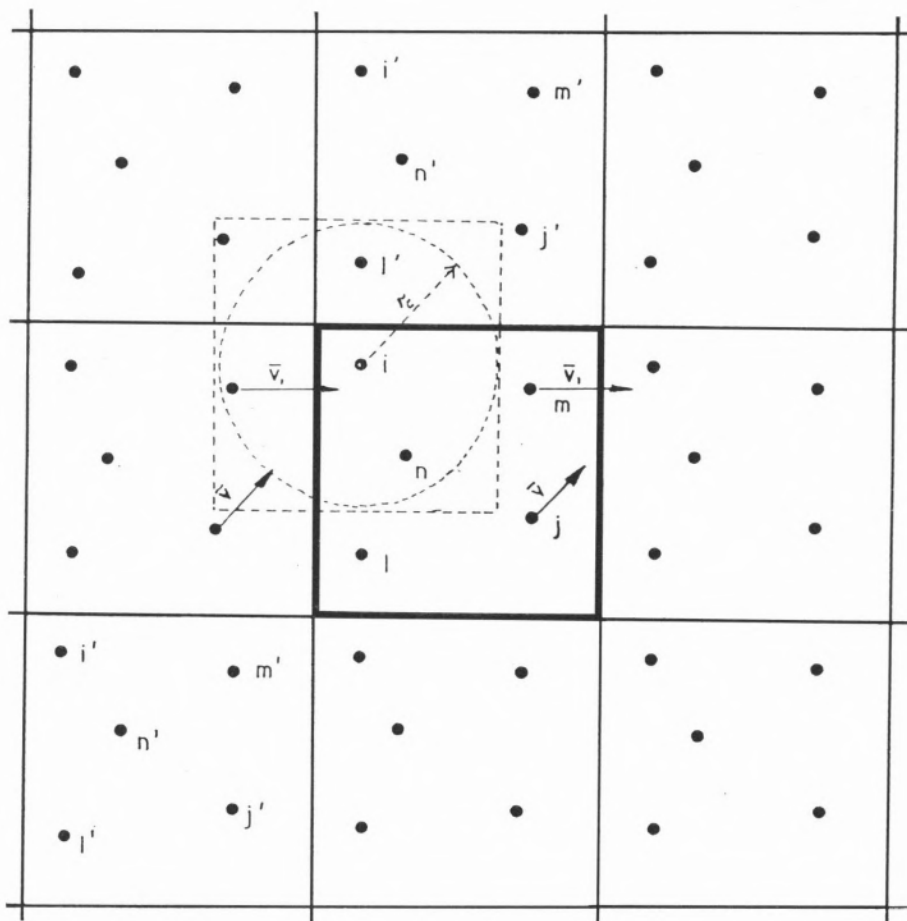

Figure 1

MD box, its translation and boundary conditions in two dimensions.
(For clarity, only five molecules are shown in each square).

Cubic boundary conditions are common in most of the calculations: N molecules are enclosed in a cubic box (MD box) whose volume, V, is chosen according to a pre-defined density. The MD box is made to behave as though it were part of an infinite system by surrounding it by periodically repeated images of itself. Thus, all surfaces are eliminated

The density is maintained by assuming that when a molecule leaves the MD box through a wall, an image enters the box, through the opposite wall, with the same velocity.

There are a variety of boundary conditions [6-7]. However, apart from the cube, the most suitable shape seems to be the truncated octhedron.

3. MOLECULAR DYNAMICS AT CONSTANT ENERGY

The following steps are involved in a conventional molecular dynamics program:

a) Assign initial positions, $\mathbf{r}_i(o)$, to the molecules in the MD box.
The positions of a lattice are generally chosen. Alternatively, the positions of a previous run can be taken.
b) Assign initial molecular velocities $\mathbf{v}_i(o)$, such that the total momentum is zero.
It is common practice to assign initial velocities from a Maxwell-Boltzmann distribution [8], but there are other alternatives [9].
c) Calculate the intermolecular potential energy, $U(\mathbf{r}^N)$, and derive the force on each molecule:

$$\mathbf{F}_i = -\nabla_i U(\mathbf{r}^N) \qquad (1)$$

The potential energy is usually assumed to be pairwise additive:

$$U(\mathbf{r}^N) = \sum_{i<j} u(r_{ij}) \qquad (2)$$

where $u(r_{ij})$ i an effective pair potential [10] and $r_{ij} = |\mathbf{r}_i - \mathbf{r}_j|$.
The calculation of forces and potential energy take into account the boundary conditions. We shall return to that in the next paragraph.
d) Integrate Newton equations of motion for each of the N molecules taking into account the boundary conditions.
There are a variety of numerical algorithms to carry out the integrations, but a very simple and stable one is the Verlet algorithm [11] which may be written [12] in the so-called leapfrog version:

$$\mathbf{v}_i(t+\delta t/2) = \mathbf{v}_i(t-\delta t/2) + \mathbf{F}_i(t)\delta t/m_i$$
$$\mathbf{r}_i(t+\delta t) = \mathbf{r}_i(t) + \mathbf{v}_i(t+\delta t/2) \cdot \delta t \qquad (3)$$
$$\mathbf{v}_i(t) = [\mathbf{v}_i(t+\delta t/2) + \mathbf{v}_i(t-\delta t/2)]/2$$

where

$$\mathbf{v}_i(t-\delta t/2) = [\mathbf{r}_i(t) - \mathbf{r}_i(t-\delta t)]/2$$

m_i is the molecular mass and t the integration time-step.
The time-step must be less than the molecular relaxation times and is of order $10^{-16} - 10^{-14}$ seconds depending on the type of molecules.
e) Let the system evolve in time for n_e time-steps where n_e is the number needed to reach equilibrium.
f) Let the system evolve in time for the next n_p time-steps where n_p is the number appropriate to obtain a good statistical accuracy.
g) Calculate time averages over the n_p steps.

The above procedure keeps the volume and the number of molecules constant. Furthermore, once the initial positions and velocities are assigned, the initial total energy of the system is defined:

$$E(o) = 1/2 \sum_i^N m_i v_i^2(o) + U(\mathbf{r}^N(o)) \qquad (4)$$

As the system evolves in time without external interferences, then $E(t)=E(o)$. Thus the total energy is conserved along the trajectory in phase space. According to statistical mechanics the time average of any property over that trajectory should be equivalent to the microcanonical ensemble average. In other words, microcanonical ensemble averages can be obtained from the molecular dynamics trajectory.
As the total energy, volume and number of particles are kept constant, the temperature and pressure, for example, fluctuate along the trajectory. The system will reach equilibrium when the averages of fluctuating instantaneous properties are constant in time.
The instantaneous temperature is defined from equipartition theorem [5]:

$$T = \sum_i^N m_i v_i^2/3Nk \qquad (5)$$

where k is the Boltzmann constant.
The instantaneous pressure is defined from virial theorem [5]:

$$P = (1/3V)(\sum_i^N m_i v_i^2 + \sum_i^N \sum_{j>i}^N r_{ij} \cdot F_{ij}) \qquad (6)$$

The algorithm (3) is only appropriate for the molecular centre of mass motion. For polyatomic molecules, rotational and vibrational degrees of freedom mus be considered. In many systems of importance, namely hydrocarbons melts, polymers and lipid bilayers, internal rotation and vibration are important in determining equilibrium and dynamical properties.

The inclusion of vibration directly in simulations is not an easy matter. It is essentially a quantum mechanical phenomenon which can not be tackled using classical equations of motion. Herman and Berne [13] described a method of including quantum vibration. On the other hand, the simulation of quantum systems is now possible by means of molecular dynamics of wave packets [14-15] and path integral Monte Carlo methods [16].

The motion of rigid models, or models with internal rotations, may be treated classically. There are a variety of algorithms to describe rotation [17-18]. A standard one is the SHAKE algorithm [19] and its more recent version RATLE [18]. They are based on the Verlet algorithms and allow the integrations to be carried out in cartesian coordinates.

3.1 Calculation of Potential Energy and Forces

The evaluation of potential energy and forces must consider not only the particles in MD box but also their images in order to eliminate surface effects and to approach a bulk system. When the interactions between molecules are short-ranged, that is to say, when they can be neglected after ≈ 3 molecular diameters (the so-called cut-off distance, r_c) the calculation is carried out using the minimum image approximation: given a particle i, the MD box is translated so that is centred on i (see Figure 1). Then, the particle i only interacts explicitly with the particles or images within the sphere of radius r_C centred on particle i. The distance r_C must be less than (or equal to) half of the MD box side lenght. After the cut-off distance, it is assumed an uniform

distribution of particles and long range corrections are analitically calculated [11].

The minimum image approximation with truncation is largely used in the study of non-polar systems, in particular, of noble gases.

Such an approximation is however unsuitable for ionic or highly polar systems where the electrostatic interactions extend over many molecular diameters. All images have then to be accounted for. The classical method for calculating the electrostatic potential of a system of charges in a periodic cell is the Ewald sum method [20]. However the expression and the computer code [21] are rather involved. Recently Adams and Dubey [22] derived a modified expression for the Ewald sum in terms of an effective pair potential. This enables the calculation to be performed in a very simple and efficient way. The modified Ewald sum is straightforwardly introduced in a conventional program because the calculations are also carried out with the minimum image convention, but now without truncation. Recently Fernandes and Cabral [23] have applied the method to a simulation of molten salts.

3.2 Other Properties

Kinetic and potential energies, temperature and pressure referred to above are first order thermodynamic properties and primary output data from a simulation.

Given an instantaneous property X, its time average over the MD trajectory is denoted by <X>. For example, the time average of the temperature is:

$$<T> = <\sum_i^N m_i v_i^2/3Nk> \qquad (7)$$

Second order properties, such as specific heats and thermal-pressure coefficients, can be calculated from the fluctuations in first order thermodynamic properties. For example, the heat capacity at constant volume is given by:

$$C_V/Nk = 3/2 \, [\, 1-2N \, (\, <EK^2>-<EK>^2 \,)/3k^2T^2 \,]^{-1} \qquad (8)$$

where EK is the kinetic energy. They have been thoroughly reviewed by Cheung [24] and by Haile and Graben [25].

Chemical potential, and related properties, can be evaluated by Widom method [26-27]. It basically involves establishing a m x m x m grid within the MD cell (m 10). At each time step, the potential energy u_t of a test particle is calculated on each of the grid points. Then the chemical potential is give by:

$$\mu = -k<T>\ln[\exp(-\beta u_t)>] \qquad (9)$$

where $\beta = (kT)^{-1}$.

The pair radial distribution function, g(r), a structural property, is calculated by dividing the configuration space around each molecule into concentric spherical shells of thickness δr. If the average number of neighbours in a shell is n(r) then:

$$g(r) = (V/N)n(r)/4\pi r^2 \delta r \qquad (10)$$

The radial distribution function is related to the static structure factor through a Fourier transform [4]. The structure factor, in turn, is obtained from X-ray and neutron scattering. Thus, it is possible to compare the simulated functions with experimental results. On the other hand, the radial distribution function forms the underlying structural basis for first-order thermodynamic properties [28].

Time correlation functions [4] can also be obtained by MD. For instance, the velocity auto-correlation function defined as

$$Z(t) = <\mathbf{v}(t) . \mathbf{v}(o)> \qquad (11)$$

is an important quantity. It elucidates the diffusive processes in liquids [29]. The Fourier transform of (11) gives the frequency spectrum and the integration gives the self-diffusion coefficient:

$$D = 1/3 \int_o^\infty Z(t) \, dt \qquad (12)$$

Other transport coefficients, spectroscopic and scattering properties are directly related to time correlation functions [4,30]. Therefore, they may be quantitavely predicted from MD. Dynamic structure of liquids, which is related to inelastic neutron scattering, is obtained through the space-time van Hove correlation function [4]. Moreover the study of current fluctuations [4], inevitable in order to get a full understanding of the collective modes of a liquid, can also be realized by MD.

4. MOLECULAR DYNAMICS AT CONSTANT TEMPERATURE AND PRESSURE

MD at constant energy has limitations from an experimental standpoint. In fact, as far as experiments are concerned, it is desirable to perform simulations at a constant pre-defined temperature and/or pressure, which is not possible with MD at constant energy.

One way to carry out simulations at these conditions is to integrate the equations of motion subjected to constraints such that the trajectories in phase space correspond to (N, V, T), (N, P, H) or (N, P, T) statistical ensembles.

There are a variety of methods to maintain temperature at a constant pre-defined value [12,31]. The method we generally follow is the damped force method of Hoover [32] and Evans [33]. It is theoretically founded and easily incorporated into the leapfrog algorithm.

The basic assumption of the method is that each molecule is subjected to the total force.

$$\mathbf{F}_t = \mathbf{F}_i - \alpha \mathbf{p}_i/m_i \qquad (13)$$

where $\mathbf{F}_i$ is the force due to the other molecules and $\alpha p_i/m_i$ is a damping force whose parameter α is calculated by the condition of constant instantaneous temperature dT/dt = 0. The motion equations are:

$$\mathbf{p}_i = \mathbf{F}_i - \alpha \mathbf{p}_i/m_i \qquad (14)$$

where $\mathbf{p}_i$ is the linear momentum.

The leapfrog algorithm (3) is easily modified to introduce this constraint. The formulae is given by Brown and Clark [12] in a readily implementable form.

To maintain the pressure at a pre-defined value there also are some methods [17,34]. A standard one is the Andersen method [35,36]. Both volume and pressure are allowed to fluctuate, in the later case about a fixed mean. The MD box volume is expanded if the instantaneous internal pressure, P_i, is greater than the desired value P_e and constracted if P_i is less than P_e.

The volume equation of motion is:

$$\ddot{V} = [P_i - P_E]/M \qquad (15)$$

where M is the so-called «piston mass».

The motion equations for the particles are:

$$\ddot{R}_i = F_i/m + R_i/3V [\ddot{V} - (2/3) (\dot{V}/V)^2] \qquad (16)$$

and

$$\dot{r}_i = \dot{R}_i - R_i \dot{V}/3V) \qquad (17)$$

$\dot{R}_i$ is the actual velocity of particle i and $\dot{r}_i$ its «thermodynamic velocity», that is to say, the velocity related to internal forces and that contribute to thermodynamic properties.

The above equations are also easily incorporated in the leapfrog algorithm. The formulae is given by Brown and Clark [12] and Fincham and Heyes [17].

The piston mass is an ajustable parameter and is chosen so that the fluctuations in the volume do not reach an unphysical frequency or the system does not undergo a catastrophic irreversible expansion or contraction.

5. NONEQUILIBRIUM MOLECULAR DYNAMICS

The MD methods described so far are equilibrium methods. They assume that the system is not subjected to external perturbations (such as shear forces, temperature gradients, electric fields, etc.) and that it attains equilibrium before the calculation of any properties. Even the calculation of transport coefficients by means of time correlation functions referred to in 3.1., assume the system to be in equilibrium when the correlation functions are evaluated. This is justified by linear response theory [4] which establishes the relation between the linear response of a system to an external perturbation and the properties of the system in equilibrium.

Apart from the self-diffusion coefficient, it is not efficient to calculate transport coefficients by equilibrium MD. The corresponding time correlation functions are difficult to obtain with good accuracy and the computer time involved is often prohibitive [37]. However, it is possible to perform molecular dynamics with the system subjected to external perturbations and to study directly the response of the system. The theory shows [17] that the ratio of the response to the external field gives the transport coefficient of interest. Such methods are known as nonequilibrium molecular dynamics (NEMD) or non-standard molecular dynamics [38-40].

One way of performing NEMD has been devised by Cicotti and Jacucci [41] and is based on the calculation of two trajectories: one with and one without the applied perturbation. The net effect of the perturbation is then obtained by subtraction of the zero-perturbation trajectory from that with the applied perturbation. The method allows the applied perturbations to be sufficiently small so that there is no problem with nonlinear effects. Good statistics are obtained from averaging over a few hundred pairs of trajectories. An important feature of the method is that it produces not merely the steady-state response to an applied perturbation but the average time-dependent response, so that it becomes possible to obtain such properties as the frequency-dependent shear viscosity.

NEMD techniques are not restricted to use for the calculation of transport coefficients but

also can successfully be used to obtain second-order thermodynamic quantities [17] as an alternative to the fluctuation method referred to in 3.1.

New NEMD techniques which have proved to be useful in exploring molecular systems far from equilibrium are presently being investigated [42].

6. FINAL COMMENTS

Computer simulation is a powerful technique to clarify and even to provide new insights into the molecular dynamics of condensed states of matter. It can be used to study either relatively simple problems like the thermodynamic properties of simple systems or complex problems like proteins [43] or rotation-translation coupling [44]. The latter is important, for example, to explain why the physical properties of enantiomers and of their racemic mixture are different. For instance, at room temperature, a racemic mixture of lactic acid is a liquid whereas the individual enantiomers are solid.

The sizes of molecules and the ensembles that may be studied will grow as computer power grows [45]. Intermolecular potentials will be improved and some approximations like the assumption of pairwise additivity will be better understood.

Computer simulation of the molecular dynamics is an invaluable tool for the development of analytical theories and to overcome their inherent mathematical problems.

Our group in Lisbon is involved in the study of simple systems, alcohols, surfaces, and transport properties by MD and MC methods. We welcome the portuguese biochemists and biotechnologists.

ACKNOWLEDGMENTS

REFERENCES

[1] J. B. ALDER, and WAINRIGHT, *J. Chem. Phys.*, **31**, 459 (1959).

[2] A. RAHMAN, *Phys. Rev.*, **136A**, 405 (1964).

[3] N. METROPOLIS, A. W. ROSENBLUTH, M. N. ROSENBLUTH, and A. J. TELLER, *J. Chem. Phys.*, **21**, 1087 (1953).

[4] J. P. HANSEN and I. R. McDONALD, «Theory of Simple Liquids», Academic Press (1976).

[5] T. L. HILL, «Statistical Mechanics», McGraw Hill (1956).

[6] D. J. ADAMS, *Information Quarterly*, CCP5, **10**, 30 (1983).

[7] W. SMITH, *Information Quarterly*, CCP5, **10**, 37 (1983).

[8] D. W. HEERMANN, «Computer Simulation Methods in Theoretical Physics», Springer-Verlag (1986).

[9] F. M. S. S. FERNANDES, Ph. Thesis, University of Southampton (1977).

[10] G. MAITLAND, M. RIGBY, B. SMITH and W. WAKEHAM, «Intermolecular Forces. Their Origin and Determination», Claredon Press (1981).

[11] L. VERLET, *Phys. Rev.*, **159**, 98 (1967).

[12] D. BROWN and J. H. R. CLARKE, *Mol. Phys.*, **51**, 1243 (1984).

[13] M. F. HERMAN and B. BERNE, *J. Chem. Phys.*, **78**, 4103 (1983).

[14] W. SMITH and K. SINGER, *Information Quarterly*, CCP5, **13**, 38 (1984).

[15] W. SMITH and K. SINGER, *Information Quarterly*, CCP5, **17**, 53 (1985).

[16] W. SMITH and K. SINGER *Information Quarterly*, CCP5, **25**, 18 (1987).

[17] D. FINCHAM and D. M. HEYES, *Adv. Chem. Phys.*, **63**, 493 (1985).

[18] H. ANDERSEN *J. Comp. Phys.*, **52**, 24 (1983).

[19] J. P. RYCHAERT, G. CICOTTI and H. J. C. BERENDSEN, *J. Comp. Phys.*, **23**, 327 (1977).

[20] P. P. EWALD, *Ann. Physyk (Leipzig)*, **64**, 253 (1921).

[21] W. SMITH, *Information Quarterly*, CCP5, **21**, 37 (1986).

[22] D. ADAMS and G. DUBEY, *Information Quarterly*, CCP5, **22**, 39 (1986).

[23] F. M. S. S. FERNANDES, and J. B. CABRAL, *Portugal. Phys.*, **18**, 39 (1987).

[24] P. S. Y. CHEUNG, *Mol. Phys.*, **33**, 519 (1977).

[25] J. M. HAILE and H. W. GRABEN, *Mol. Phys.*, **40**, 1433 (1980).

[26] K. S. SHING and K. E. GUBBINS, *Mol. Phys.*, **46**, 1109 (1982).

[27] J. G. POWLES, *Chem. Phys. Lett.*, **86**, 335 (1982).

[28] H. J. M. HANLEY and D. J. EVANS, *Mol Phys.*, **39**, 1039 (1980).

[29] A. RAHMAN, *J. Chem. Phys.*, **45**, 2585 (1966).

[30] D. J. TILDESLEY, Proc. of Nato Advanced Study Institute of Molecular Liquids Dynamics and Interactions, Italy (1983), p. 519.

[31] D. M. HEYES, *Chem. Phys.*, **82**, 285 (1983).

[32] W. G. HOOVER, *Physica*, **A118**, 111 (1983).

[33] D. J. EVANS, *J. Chem. Phys.*, **78**, 3279 (1983).

[34] H. J. C. BERENDSEN, J. P. M. POSTMA, W. F. VAN GUNSTEREN, A. DINOLA and J. R. HAAK, *J. Chem. Phys.*, **81**, 3684 (1984).

[35] H. C. Andersen, *J. Chem. Phys.*, **72**, 2384 (1980).

[36] J. Haile and H. Graben, *J. Chem. Phys.*, **73**, 2412 (1980).

[37] E. M. Gosling, I. R. McDonald and K. Singer, *Mol. Phys.*, **26**, 1475 (1973).

[38] W. G. Hoover, *Ann. Rev. Phys. Chem.*, **34**, 103 (1983).

[39] W. G. Hoover *Phys. Today*, **37**, 44 (1984).

[40] D. J. Evans, J. M. Howard and H. Siegfried, *Phys. Today*, **37**, 26 (1984).

[41] Cicotti and Jacucci, *Phys. Rev. Lett.*, **35**, 789 (1975).

[42] W. G. Hoover, H. A. Posch, B. L. Holian, M. J. Gillian, M. Mareschal and C. Massobrio, *Molecular Simulation*, **1**, 79 (1987).

[43] W. van Gunsteren and H. Berendsen, *J. Mol. Biol.*, **176**, 559 (1984).

[44] M. Evans and G. Evans, *Adv. Chem. Phys.*, **63**, 377 (1985).

[45] D. Fincham, *Molecular Simulation*, **1**, 1 (1987).

RESUMO

Dinâmica Molecular por Simulação Computacional

O objectivo deste artigo é o de apresentar uma breve revisão dos métodos de dinâmica molecular por simulação computacional com mais ênfase em aspectos genéricos do que em detalhes técnicos.

M. L. S. L. COSTA
Centro de Espectrometria de Massa da Universidade de Lisboa,
Complexo I,
Av.ª Rovisco Pais
1000 Lisboa,
PORTUGAL

PHOTOELECTRON SPECTRA AND AB INITIO CALCULATIONS (*)

Ultraviolet Photoelectron Spectroscopy (UVPES) is the most powerful experimental method for studing valence orbital structure of molecules and ions. The outstanding feature of UVPES is its ability to eject electrons from any of the occupied energy levels in a molecule and, since each of these levels has a different ionization energy, only those particular electrons for study are selected. According to Koopmans'theorem, each ionization energy is simply equal in magnitude to an orbital energy. Through use of this approximation, UVPES provides an experimental determination of a molecular orbital diagram. The rapid advances of this technique have stimulated developments and applications of quantum chemical methods of computing vertical ionization energies. Interpretation of the photoelectron spectrum of ethyl azide with the aid of ab initio calculations is mentioned.

Ultraviolet Photoelectron Spectroscopy (UVPES) is the most powerful experimental method for measuring ionization energies and ionic vibration frequencies and of investigating molecular electronic structure.

This technique is a modern application of the photoelectric effect. When photons of energy hν fall onto a sample, a given electron in a particular energy level of the sample with characteristic binding energy, less than hν, can in general, be photoejected.

The basic photoionization process which occurs in a photoelectron spectrometer can be written:

$$M + h\nu \longrightarrow M^+ + e^- \qquad (1)$$

This process will in general result in the formation of a number of rotational and vibrational states for a given electronic state of ion M^+. From the law of conservation of energy, the photoejected electrons possess kinetic energy E_k, defined by

$$E_k = h\nu - I_i - \Delta E_{vib} - \Delta E_{rot} - \Delta E_{trans} \qquad (2)$$

where

I_i — the i'th ionization energy or energy required to remove the i'th electron from the molecular (or atomic) species M into the continuum to give a specific state of M^+,

ΔE_{vib}, ΔE_{rot} — the changes in vibrational and rotational energies upon ionization,

ΔE_{trans} — the change in translational energy between the electron and the ion.

The resultant photoelectron spectrum should possess discrete structure corresponding to the rotational and vibrational excitation energies, but as the experimental resolution is of the order of 20-25 meV (160-200 cm^{-1}) this is usually not sufficient to resolve rotational fine structure. However, discrete vibrational fine structure is often resolved. Thus, equation (2) can be rewritten as

$$E_k = h\nu - I_i - \Delta E_{vib} \qquad (3)$$

This is the fundamental equation of PES — measurement of E_k leads directly to the ionization energy and ΔE_{vib}.

This equation shows that the ion M^+ can generally be formed in several electronic states depending on the energy of the ionizing radiation used. The vacuum ultraviolet He Iα resonance emission (584.3 Å) is the most commonly used ionizing source, with an energy (hv=21.218 eV) sufficient to liberate valence electrons from most species.

Hence UVPES gives information pertaining to:

— The accurate ionization energy of a molecular species to a particular ionic state, giving the ordering of ionic states..

— Some molecular spectroscopic parameters of the ionic state, such as vibrational frequencies and ionic equilibrium bond lenghts for cases where vibrational structure is resolved.

UVPES provides accurate ionization energies that can be used in other branches of spectroscopy developed to study solely ionic species. The experimental ionization energies can also be used to calculate ionic heats of formation and bond dissociation energies [1].

Also the ordering and relative intensities of photoelectron bands can be used to test the theoretical model which is used to predict these quantities, e.g. UVPES data provide a good test of molecular orbital theory.

It is thus seen that UVPES is an important technique, both in itself and in assistance to the other branches of the rapidly expanding field of ion spectroscopy.

The basic requirements of a photoelectron spectrometer are pumping equipment capable of evacuating the apparatus to about 10^{-5} torr, a source of ionizing radiation, an ionization chamber, a gas sample inlet system, an electron energy analyser which only transmits electrons of a selected energy, an electron detector, amplification and recording equipment. These components are shown schematically in Figure 1. Photons generated in the source are directed onto sample molecules in the ionization chamber. Electrons can be ejected from all the accessible orbitals, provided that their binding energies are less than that of the incident photon energy. These ejected electrons, possessing kinetic energies E_k given by equation (3) enter the energy analyser. Once inside the analyser, the photoelectrons describe different trajectories depending upon their energies and the voltage applied to the analyser plates.

Electrons are detected usually using a single channel electron multiplier positioned at the image focal point of the analyser. The resultant signal coming from the detector is preamplified before passing into a conventional amplifier, discriminator and ratemeter. The resultant signal coming from the detector is preamplified before passing into a conventional amplifier, discriminator and ratemeter. Signals are recorded with equal and opposite sweep voltages being supplied to the analyser plates by a motor driven potentiometer. The spectrum obtained consists essentially of the count-rate registered by the transmitted electrons plotted against the kinetic energies, E_1, E_2, E_3,..., of the photoelectrons ejected.

The rapid advances of UVPES have stimulated developments and applications of quantum chemical methods of computing vertical ionization energies.

Koopmans' theorem [2] states that for removal of an electron from an orbital i in a closed-shell molecule, the negative of the orbital energy, $-\varepsilon_i$, computed in an ab-initio SCF calculation on the neutral molecule at the Hartree-Fock limit gives the best zeroth order approximation to the ith vertical ionization energy:

$$I_i^\circ = -\varepsilon_i \qquad (4)$$

However, this theorem ignores the effects of electron reorganization and correlation. In

practice, the experimental vertical ionization energy, I_i^{expt} can be related to Koopmans' theorem by the following expression:

$$I_i^{expt} = I_i^o - R + C \qquad (5)$$

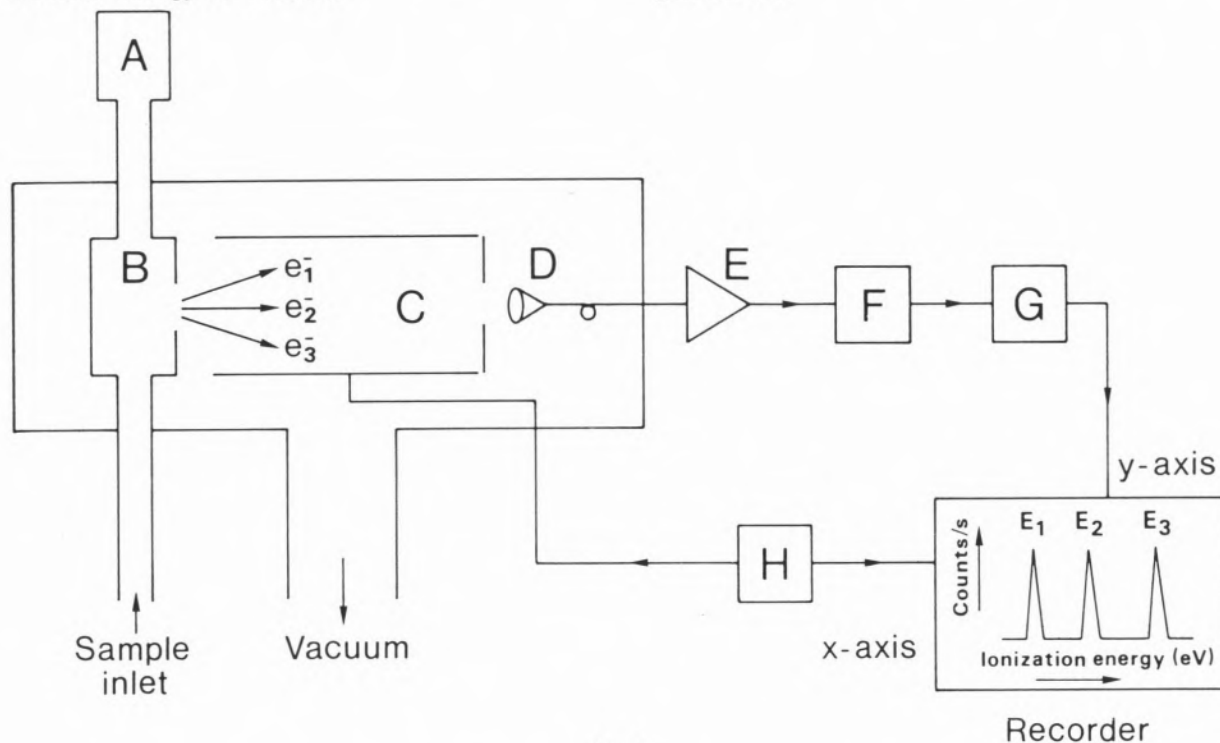where R is the reorganization energy resulting from ionization and C is the electron correlation energy correction.

The ethyl azide molecule will be mentioned here. Figure 2 shows the photoelectron spectrum of this azide. Observed and calculated ionization energies and assignments for the first two bands of this compound is also shown in this figure. The relevant molecular orbitals were shown in a style suggested by the computer produced diagrams of Jorgensen [5].

Fig. 1

Basic Components of a Photoelectron Spectrometer:
A — Light Source; B — Target Chamber; C — Analyser; D — Detector; E — Amplifier; F — Counter;
G — Ratemeter; H — Voltage Sweep.

Interpretation of the photoelectron spectra of some aliphatic azides has already been done with the aid of ab-initio calculations [3], using the GAUSSIAN 82 [4] computer program, as part of a general research project into open-chain aliphatic azides.

Prediction of the equilibrium geometries of the ground electronic states of the neutral azides under study has been achieved at the ab-initio SCF level gradient methods and the 4-31G basis set. From each equilibrium geometry, the vertical ionization energies were then computed.

At 9.914 eV the calculations give a non-bonding character to this molecular orbital, as the $2p_z$ atomic orbitals of N_1 and N_3 have the highest coefficients with opposite signs.

The first band at 10.02 eV of the photoelectron spectrum (figure 1) is intense and sharp indicating ionization from a non-bonding orbital. Consistent with the molecular orbital predictions we assign this band to the non-bonding orbital consequence of the combination of the $2p_z$ atomic orbital of N_1 and N_3.

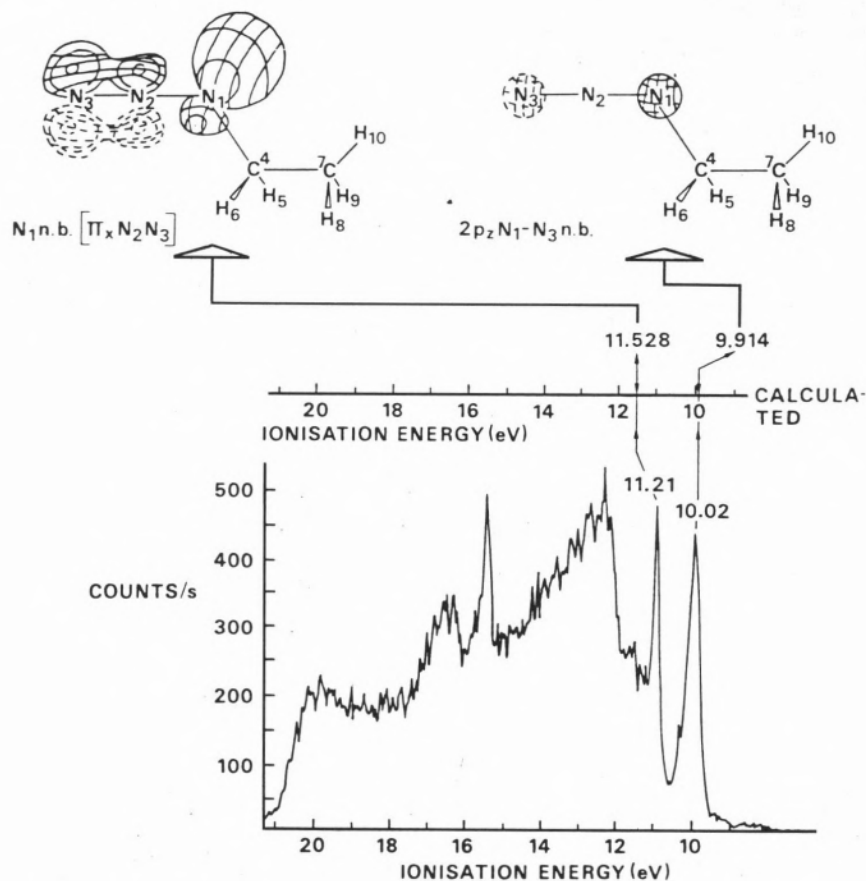According to the calculations, at 11.528 eV most of the electron density is concentrated on

Fig. 2

*Photoelectron spectrum, observed and calculated ionization energies and assignements
for the first two bands of ethyl azide.*

N_1. There is also a weakly bonding orbital between N_2 and N_3, since both contribute with their $2p_x$ atomic orbitals, the density being greater on N_3. Therefore, this orbital is non-bonding between N_1 and N_3 (largest contributions) and antibonding between N_1 and the weak π_x orbital existing between N_2 and N_3.

The large electron density concentrated on N_1 would produce a sharp band in the photoelectron spectrum. Since the band at 11.21 eV is sharp, assignment of this band to this orbital seems obvious.

The agreement between the calculated and experimental photoelectron spectrum is quite satisfactory. However, the preliminary results so far obtained will be improved in the near future by using the Møller-Pleset theory [6] in order to examine the influence of electron correlation on the ionization energies.

As well, the 6-31 G* [7] basis set will be used.

ACKNOWLEDGEMENT

REFERENCES

[1] J. M. DYKE, A. MORRIS, N. JONATHAN and M. J. WINTER, *Mol. Phys.*, **39**. 629 (1980).

[2] T. KOOPMANS, *Physica*, **1**, 104 (1933).

[3] M. L. S. L. COSTA and M. A. ALMOSTER FERREIRA, *J. Molec. Struct.*, in press.

[4] J. S. BINKLEY, M. J. FRISCH, D. J. DeFREES, K. RAHGAVA-CHARI, R. A. WHITESIDE, H. B. SCHLEGEL, E. M. FLUDER and J. A. POPLE, GAUSSIAN 82, Department of Chemistry, Carnegie-Mellon University, Pittsburgh, 1982.

[5] W. L. JORGENSEN and L. SALEM, The Organic Chemist's Book of Orbitals, Academic Press, London, 1973.

[6] C. MØLLER and M. S. PLESSET, *Phys. Rev.*, **46**, 618 (1934).

[7] T. CLARK, A. Handbook of Computational Chemistry, John Wiley and Sons, N. York, 1985.

RESUMO

Espectros de fotoelectrões e cálculos AB-INITIO

Espectroscopia de Fotoelectrões (UV) é a técnica mais eficaz para estudar a estrutura de valência de moléculas e iões. A característica saliente desta técnica é a sua capacidade de expulsar electrões de quaisquer dos níveis de energia ocupados numa molécula e, uma vez que cada um destes níveis tem uma energia de ionização diferente, só são seleccionados os electrões que se querem estudar em particular. De acordo com o Teorema de Koopmans, cada energia de ionização é igual, em valor absoluto, à energia do orbital. Fazendo uso desta aproximação, esta técnica dá a determinação experimental dum diagrama de orbitais moleculares. O rápido progresso da Espectroscopia de Fotoelectrões levou a um grande desenvolvimento dos métodos quânticos para calcular energias de ionização verticais. Neste trabalho, menciona-se a interpretação do espectro de fotoelectrões da azida etílica através de cálculos ab-initio.

M. NATÁLIA D. S. CORDEIRO
J. A. N. F. GOMES
Departamento de Química, Faculdade de Ciências,
Universidade do Porto
4000 Porto,
PORTUGAL

A. GONZÀLEZ-LAFONT
J. M. LLUCH
A. OLIVA
J. BERTRÁN
Departamento de Química, Facultat de Ciències,
Universitat Autònoma de Barcelona, Bellaterra (Barcelona),
SPAIN

AN INTERACTION POTENTIAL FOR THE Cu°-H₂O SYSTEM. APPLICATION TO A MONTE CARLO SIMULATION (*)

A two-body analytic potential for the interaction of the Cu° atom with the H₂O molecule has been determined by fitting to quantum energies of the monohydrate Cu°–H₂O. These, in turn, were computed by an ab initio method with effective core potentials for a set of 146 points in the Cu°–H₂O potential energy surface. In addition, the quality of the fit and the results obtained by applying this new interaction potential in a Monte Carlo simulation are examined.

1. INTRODUCTION

There is a continued interest in the studies of ionic aqueous solutions of transition metals. This interest derives from the fact that transition metals participate in many redox reactions in solution and the rates of such reactions are much influenced by the characteristics of their solvation shells.

Our final goal is the theoretical study of the solvent effects in the $2Cu^+$ (aq.) $\rightarrow$ Cu° (aq.) + Cu^{2+} (aq.) exchange reaction, using the Monte Carlo's method [1]. To begin with, we intend to simulate the aqueous solutions of the reagents and products of that reaction.

The application of Monte Carlo's method to these cases requires, however, the knowledge of the interaction potentials for the pairs water-water and water-metallic species. As to the potential of the $H_2O–H_2O$ pair, the analytical potential of Clementi et al [2] will be used, a potential which has been demonstrated to gove a good description of water in condensed state [3].

In what concerns the interaction potentials of the copper species, reasonable results have already been attained for the $Cu^+–H_2O$ system [4], with an heuristic procedure that uses, for the representation of this system's potential, an analytical function with adjustable parameters. These parameters were determined by fitting the chosen function to energy interaction values of the Cu^+ monohydrate, evaluated according to pseudo-potentials method of Barthelat et al [5]. The analytical function used was an expansion in the inverse powers of the internuclear distances.

The focus of the present work is the construction of an interaction potential for the $Cu^\circ–H_2O$ system, using the same kind of procedure and a similar analytical function. In fact, to perform the statistical study of the above referred exchange reaction, suitable interaction potentials for all the intervenient copper species are necessary.

In the next section, we will present the form of this analytical function applied herein to

the Cu°–H$_2$O system and, describe the main details of the interaction energy calculations, which were performed within the quantum model of Barthelat et al. Moreover, the results of these energy calculations are compared with the ones previously obtained for the Cu$^+$–H$_2$O system. The quality of the two fits is also compared. In section 3, the new Cu°–H$_2$O interaction potential is used in a Monte Carlo simulation of a Cu° aqueous dilute solution, in order to investigate the changes in the liquid structure of water produced by the Cu° atom. The results obtained in the simulation at 298K of the [Cu°(H$_2$O)$_{100}$] system are collected and analysed.

2. CONSTRUCTION OF THE Cu°–H$_2$O INTERACTION POTENTIAL

The form of the analytical function to use, was selected by our previous studies of Cu$^+$ hydrates [4] and also from other studies of transition metal systems, namely the Fe^{2+}–H$_2$O, the Fe$^+$–H$_2$O and the Fe°–H$_2$O systems [6]. As we have mentioned above, it is written as a combination of inverse powers of the several internuclear distances with the following structure:

$$V[Cu°-H_2O] = c_1 \left[1/r_a^2 - 1/2(1/r_b^2 + 1/r_c^2) \right] +$$
$$c_2 \left[1/r_a^3 - 1/2(1/r_b^3 + 1/r_c^3) \right] + c_3/r_a^4 +$$
$$c_4 \left(1/r_b^4 + 1/r_c^4 \right) + c_5/r_a^5 + c_6 \left(1/r_b^5 + 1/r_c^5 \right)$$
$$c_7/r_a^6 + c_8 \left(1/r_b^6 + 1/r_c^6 \right) + c_9/r_a^{12} +$$
$$c_{10} \left(1/r_b^{12} + 1/r_c^{12} \right) \qquad [1]$$

where r_a, r_b and r_c are the Cu°-oxygen and Cu°-hydrogens internuclear distances and c_i (i=1,2,..., 10) the adjustable parameters. It should be noted that the energy V[Cu°–H$_2$O], in eq. 1, is obtained in hartrees when the distances r_a, r_b and r_c are in bohrs. It is also important to stress that V[Cu°–H$_2$O] does not contain Coulombic terms as there are no electrostatic Coulomb interactions on the Cu°–H$_2$O system. No exponential terms have been included in that potential just to simplify

its later utilization on Monte Carlo's simulations.

The parameters c_i in the above equation were obtained by fitting the V[Cu°–H$_2$O] to the interaction energies of the Cu°–H$_2$O system, related to eleven orientations of the H$_2$O molecule around the Cu° atom. In this way, five planar and six non-planar configurations have been considered. The five planar ones differ in the values of angle α, as presented in Figure 1. The six non-planar configurations are constructed, from a configuration in which the H$_2$O molecule is in a plane perpendicular to the plane containing the Cu° atom, by successive rotations by angles β and γ, defined as shown in Figure 2. In all these orientations, the interaction energies, E[Cu°–H$_2$O], where computed for several Cu°–O distances, with the water molecule fixed at its equilibrium geometry, i.e., with r_{OH} = 0.9572 Å and $\angle$HOH = 104.5° [7].

As we have already mentioned, the energies E[Cu°–H$_2$O] were attained by means of the pseudo-potentials method of Barthelat and coworkers [5]. The appeal to this method can be justified by the obvious difficulties that an all-electron calculation of the E[Cu°–H$_2$O] energy points, on the above-considered orientations, would bring about. Program PSHONDO [8] was used on such calculations and we employed the pseudo-potentials parameters of Cu° and O atoms, together with the double-zeta valency basis set of the atoms Cu° (3d and 4s functions), O (2s and 2p functions) and H (1s function), which were suggested by the authors of this method [5].

In Figs. 1 and 2, the calculated Cu°–H$_2$O interaction energies, in a total of 146 points, are plotted, respectively, for the planar and non-planar configurations as functions of the internuclear distance Cu°–O. From these figures it can be seen that all the Cu°–H$_2$O studied configurations have a pronounced repulsive character, with the exception of the α=0° planar configuration. For this configuration, an energy minimum of –1.22 kJ mol^{-1} was found at a Cu°–O distance of 2.80 Å. This

binding energy was interpreted by those authors as the result of important water dipole-metal dipole induced attractions. However, the binding between H_2O and the Cu^o seems to be rather weak and, therefore, we don't expect to find a stable $[Cu^o(H_2O)_n]$ complex in solution at room temperature. It is worth noting that for the Cu^+ ion, a stable $[Cu^+(H_2O)_6]$ complex appears appears to exist in solution at 298 K [4] but, in this case, a much larger binding energy (-166.35 kJ mol^{-1}) at a much shorter copper-oxygen distance (2.05 Å) was obtained for the $\alpha = 0^o$ configuration.

The fitting of the $V[Cu^o-H_2O]$ function of equation (1) to these Cu^o-H_2O calculated energies was made by a least-squares procedure giving the following statistical parameters:

$$\mathbf{d} = 4.31 \text{ kJ mol}^{-1} \quad \text{and} \quad \mathbf{s} = 7.90 \text{ kJ mol}^{-1}$$

in which **d** stands for the average of absolute deviations and **s** for the average of square deviations. In fact, these parameters were improved in relation to the ones achieved on the Cu^+-H_2O fitting [4].

A list of the resulting c_i parameters for the $V[Cu^o-H_2O]$ potential is specified in Table I.

Table 1

Parameters of $V[Cu^o-H_2O]$ determined in the adjustment of the $E[Cu^o-H_2O]$ quantum energy points

Parameter	Adjusted value
c_1	-0.33372
c_2	$+7.81396$
c_3	-50.73922
c_4	-6.20687
c_5	$+44.73850$
c_6	$+70.92578$
c_7	-207.98939
c_8	$+123.98845$
c_9	-13571.56457
c_{10}	$+1522.24804$

The goodness of the present fitting can be judged with the above mentioned statistical parameters and, also, through examination of Figs. 1, 2 and 3.

On the first two figures, the Cu^o-H_2O quantum energies points are compared with the potential energy curves given by the $V[Cu^o-H_2O]$ function, for the two kinds of configurations analysed. In Fig. 3, the quantum energy points $E[Cu^o-H_2O]$ are plotted against those predicted by the $V[Cu^o-H_2O]$ function. The correlation between the two types of interaction energy values is rather good and, hence, we believe that this new Cu^o-H_2O potential will be appropriate to use in the subsequent Monte Carlo simulations.
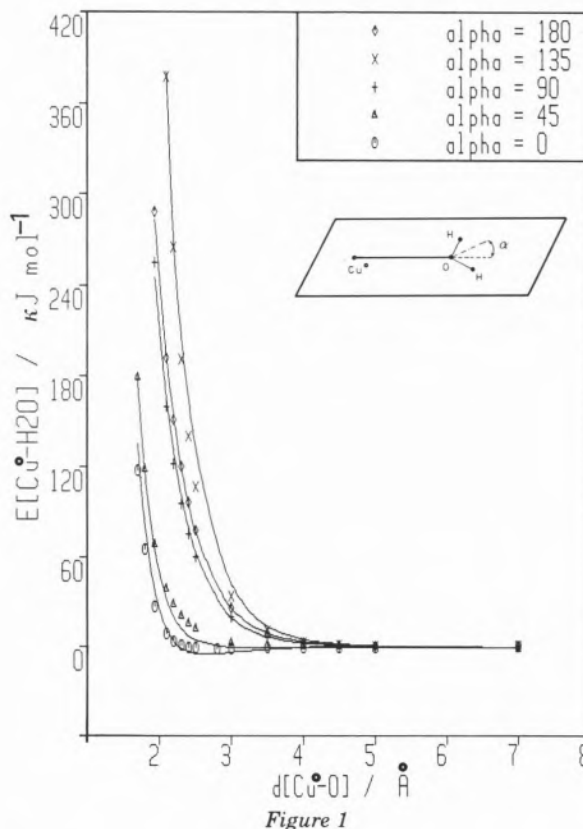
Figure 1

Potential energy curves for the Cu^o-H_2O in the planar configurations depicted. The points were calculated by the pseudo-potential method described in the text. The solid lines correspond to the fitted potential $V[Cu^o-H_2O]$
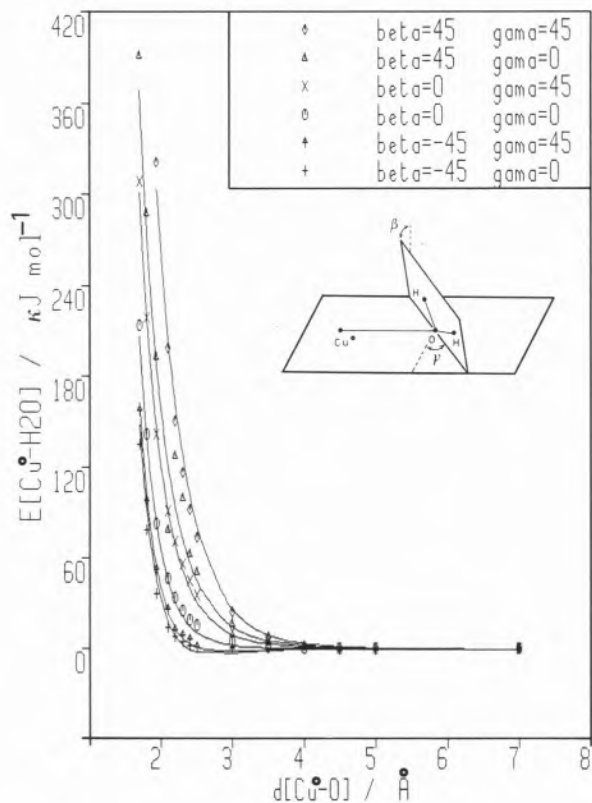
Figure 2

Potencial energy curves for the Cuº—H₂O in the non-planar configurations depicted. The points were calculated by the pseudo-potential method described in the text. The solid lines correspond to the fitted potential V[Cuº—H₂O]
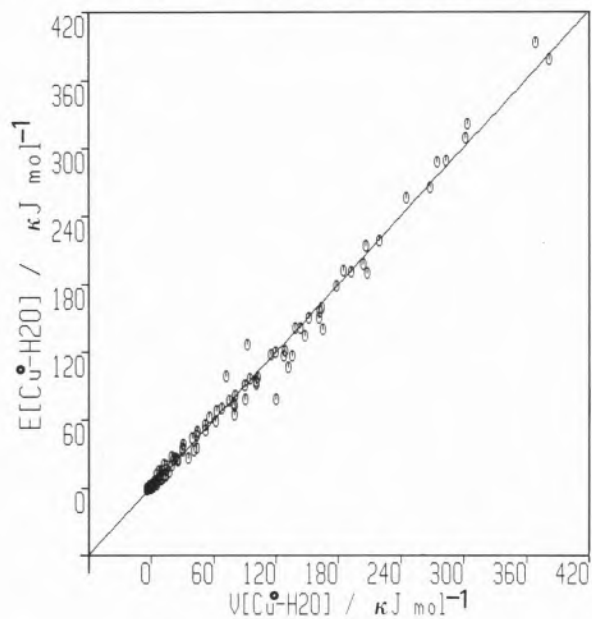

Figura 3

Comparison between calculated interaction energies of the Cuº—H₂O system and those resulting from the fit to potential V[Cuº—H₂O]

3. MONTE CARLO SIMULATION OF THE [Cuº(H₂O)₁₀₀] SYSTEM

In this work, the simulation of the [Cuº(H₂O)₁₀₀] system is the canonical (N,V,T) ensemble at T = 298 K has been done by Monte Carlo method [1], according to the Metropolis algorithm [10]. In this simulation, we used a cubic box with side lenghts of 15 Å in order to have a density of $\approx$ 1 g cm⁻³ for the 100 water molecules. Periodic boundary conditions have been introduced following the minimal image method. An initial configuration of the [Cuº(H₂O)₁₀₀] system has been achieved from a cubic distribution of water molecules, by placing the Cuº atom at the centre of the octahedron formed by the six nearest H₂O molecules. Statistical equilibration was attained after the simulation of 4000n configurations and, the simulation of another 4000n additional configurations was done afterwards.

In order to compute the energies of the configurations involved in the pair-potential approach, we used the following two-body potentials: the MCY potential [2] and the V[Cuº–H₂O] potential just described.

With the purpose of discussing the energy features of the [Cuº(H₂O)₁₀₀]system, we have determined the averages of the water-water and of the copper-water interaction energies per mol of water. An average water-water interaction energy of –37.17 kJ mol⁻¹ was obtained and, this value is quite close to the corresponding value for pure water, which has been computed using a box of similar side lenghts [11]. This clearly indicates that the Cuº atom is unable to modify the tetrahedral structure of water, at least in a significant way. The small value of –0.15 kJ mol⁻¹ found for the averaged copper-water interaction energy also confirms the above assumption.

There is another interesting value that can be determined on this simulation, i.e. the orientation parameter of the H₂O molecules in the [Cuº(H₂O)₁₀₀]. This parameter is defined as the average value of the cosine of the angle formed by the water molecule's dipolar moment

vector and the position vector of the respective oxygen atom, the origin of this position vector being fixed on the Cu^o atom. The magnitude of this orientation parameter can also be compared with the corresponding pure water value. We have found for the studied system an orientation parameter of -0.0010 which is almost null and analogous to that obtained ($+0.0028$) for pure water [11]. Again, this reflects that the water molecules are so hazardously oriented in the $[Cu^o(H_2O)_{100}]$ system as they are in pure water. The same conclusion can be reached by analysis of Figs. 4 and 5. where the copper-oxygen radial distribution function (RDF) and the running coordination number of Cu^o atom, $N(R)$, have been reported.

It shoud be mentioned that this number $N(R)$ has been taken as the average number of oxygen atoms within a sphere of radius R around the central Cu^o atom.

From Fig. 4, we can observe that in the copper oxygen RDF funcion no significant distinct peaks are found. On the contrary, this distribuition is very uniform along all the
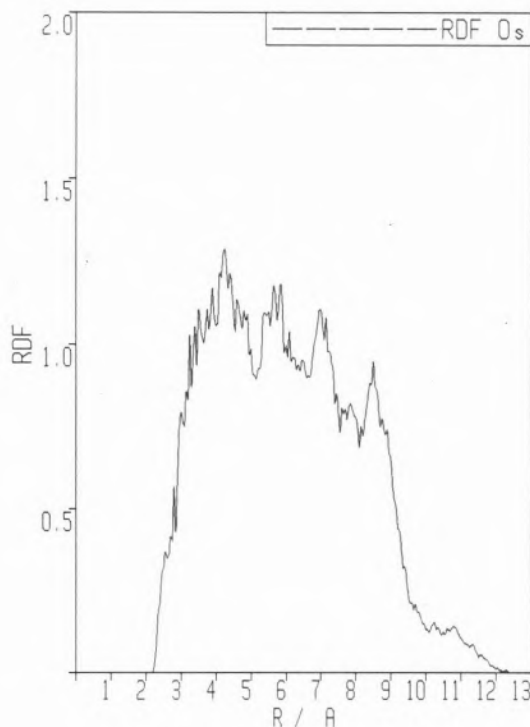

Figure 5

Running coordination number for the $[Cu^o(H_2O)_{100}]$ system at T=298K

Cu^o–O distances. In the same say, no plateau can be viewed on the $N(R)$ curve of Fig. 5.

All these trends can be explained by the feeble copper-water interaction energy, especially if this interaction energy value is compared with the one of -24.55 kJ mol^{-1} that has been achieved for the water-water interaction, employing the MCY potential [12].

Figure 4

Radial ion-oxygen distribution function for the $[Cu^o(H_2O)_{100}]$ system at T=298K

REFERENCES

[1] J. P. VALLEAU and S. G. WITTINGTON, in «Statistical Mechanics», Vol. A, Chap. 4, ed. by B. J. Berne, Plenum Press, New York (1977); J. P. VALLEAU and G. M. TORRIE, ibid., Chap. 5; W. W. WOOD, in «Physics of Simple Liquids», ed. by H. N. V. TEMPERLEY, J. S. ROWLINSON, and G. S. RUSHBROOKE, North-Holland, Amsterdam (1968), Chap. 5.

[2] O. MATSUOKA, E. CLEMENTI and M. YOSHIMINE, *J. Chem. Phys.*, **64**, 1351 (1976).

[3] E. CLEMENTI, in «Analytical Potentials from Ab-Initio Computations», «Chaire Francqui» Lecture Series; Part 4, IBM Corportation, New York (1986).

[4] M. N. D. S. CORDEIRO, J. A. N. F. GOMES, A. GONZÀLEZ-LAFONT, J. M. LLUCH, A. OLIVA and J. BERTRÁN, *J. Chem. Soc., Faraday Trans. 2*, **84**, 693 (1988).

[5] J. C. BARTHELAT, PH. DURAND and A. SERAFINI, *Mol. Phys.*, **33**, 181 (1971); CH. TEICHTEIL, J. P. MALRIEU and J. C. BARTHELAT, *ibid.*, **33**, 159 (1977); A. SERAFINI, J. C. BARTHELAT and PH. DURAND, *ibid.*, **36**, 1341 (1981).

[6] A. GONZÀLEZ-LAFONT, J. M. LLUCH, A. OLIVA and J. BERTRÁN, *Int. J. Quantum Chem.*, **30**, 663 (1986); A. GONZÀLEZ-LAFONT, J. M. LLUCH, A. OLIVA and J. BERTRÁN, *Int. J. Quantum Chem.*, in press.

[7] W. S. BENEDICT, N. GAILAR and F. K. PLYLER, *J. Chem. Phys.*, **24**, 1139 (1956),

[8] Adapted version of HONDO (QCPE program n.° 338).

[9] M. BLOMBERG, U. BRANDERMARK and P. SIEGBAHN, *Chem. Phys. Letters*, **126**, 317 (1986).

[10] N. METROPOLIS, A. W. ROSENBLUTH, M. N. ROSENBLUTH, A. H. TELLER and E. TELLER, *J. Chem. Phys.*, **21**, 1087 (1953).

[11] A. GONZÀLEZ-LAFONT, J. M. LLUCH, A. OLIVA and J. BERTRÁN, *J. Chem. Phys.*, **111**, 241 (1987).

[12] Z. SLANINA, *Chem. Phys. Letters*, **127**, 67 (1986).

RESUMO

Um potencial de interacção para o sistema Cu°—H$_2$O. Sua aplicação numa simulação de Monte Carlo.

Um potencial analítico para a interacção, a dois corpos, entre o átomo de Cu° e a molécula de H$_2$O foi determinado por ajuste das energias quânticas do monohidrato Cu°—H$_2$O. Estas energias foram por sua vez calculadas, recorrendo a um método ab initio com potenciais efectivos de cerne, para um conjunto de 146 pontos da superfície de energia potencial do sistema Cu°—H$_2$O. Além disso, são ainda examinados a qualidade do ajuste feito e os resultados obtidos na aplicação deste novo potencial de interacção a uma simulação de Monte Carlo.

JOÃO MORAIS CABRAL*
ANA MARGARIDA DAMAS*
PEDRO MORADAS FERREIRA**
* Sector de Biofísica, ** Sector de Bioquímica
Instituto de Ciências Biomédicas Abel Salazar
Universidade do Porto
4000 Porto
PORTUGAL

THE EFFECT OF SPECTRIN ON ERYTHROCYTE MEMBRANE ORDER. A STUDY USING ESR SPECTROSCOPY (❖)

The effect of spectrin on erythrocyte membrane order was studied analysing the ESR spectra of three different spin-label probes: 5-doxyl-stearic acid (5 DSA) which reports from a lipid site near the membrane surface, 16-doxyl-stearic acid (16 DSA) which reports from a deeper lipid site and 1-oxyl-2,2,6,6-tetramethyl-4-di-methyl-amino-piperidine-cethyl bromide (CAT 16) which is sensi-tive to events on the membrane surface into the lipid phase. These spin labels were incorporated into normal erythrocyte ghosts, spec-trin depleted vesicles and spherocyte ghosts and their ESR spectra were analysed in the temperature range of 7-57ºC. It was found that erythrocyte membranes, depleted of spectrin, displayed decrea-sed fluidity and a higher ordered environment. Similar, although smaller, diferences were found between membranes of normal ery-throcytes and spherocytes. The use of the spin probe CAT 16 has shown that substantial alterations occur, at the surface of normal membranes, when the temperature goes throurgh 40ºC.

INTRODUCTION

The major protein component of the mem-brane skeleton is spectrin which has a high molecular weight and is composed of two non-identical subunits (molecular weights 240 kDa and 220 kDa) that can associate in dimers or tetramers [11-18]. Spectrin interacts with the cytoplasmic surface of the red cell by non-co-valent associations with actin band 4.1 and ankyrin [10-16].

Hereditary deficiency in spectrin leads to a change in erythrocyte morphology which assumes a spheric shape. Two main factors may contribute to hereditary spherocytosis (HS): i) a quantitative deficiency of spectrin (1) and ii) a defective binding of spectrin to band 4.1 [5-6-19].

A number of evidences show that spectrin affects the properties of the membrane lipid bilayer [13-14-15]. One example was obtained from the microviscosity of the membrane of human erythrocytes which rapidly increases upon heating above 46-49ºC [17], the tempe-rature of spectrin denaturation. The use of electron spin ressonance has proved that this is a powerful technique for evaluating the motional properties of membrane lipids [2]. Maleimide spin labeling studies of purified spectrin have shown a transition of the pro-tein structure at 40ºC [12], which can be res-ponsible for the modification of membrane physicochemical properties.

The aim of this work is to evaluate the influence of the spectrin on membrane order, either by spectrin depletion of erythrocyte ghosts or using HS membranes.

We report on the spectral properties of erythrocyte membranes (normal and HS ghosts and spectrin depleted vesicles) labeled with 5-doxyl-stearic acid (5 DSA), 16-doxyl--stearic acid (16 DSA) and 1-oxyl-2,2,6,6-tetra-methyl-4-dimethyl-amino-piperidine-cethyl bromide (CAT 16). The use of such probes allows an insight into the motional properties of membrane lipids at various depths in the bilayer.

MATERIAL AND METHODS

If not stated otherwise, the following media were used:

— PMSF solution: phenyl-methylsulfonul fluoride 3 mM in ethanol

— lysis buffer: 7.5 mM NaH_2PO_4, sodium EDTA, 0.03 mM PMSF, pH 7.5

— extraction buffer: 0.2 mM sodium EDTA, 0.1 mM 2-mercaptoethanol, 0.03 mM PMSF, pH 7.5

— suspension buffer: 70 mM NaH_2PO_4, 100 mM KCl, 1 mM sodium EDTA, pH 7.5

Erythrocyte preparation: Erythrocytes were obtained from human blood provided by Serviço de Hematologia do Hospital Geral de Santo António (Porto). All experiments were performed no more than 48h after blood sampling. Removal of plasma and buffy coat (2000 rpm on a bench centrifuge, 10 min) was followed by five washings with physiological serum at 2000 rpm on a bench centrifuge (10 min). Hipotonic lysis was done by adding to the cell suspension the lysis buffer [3] and centrifugating at 2-4°C (at $3900 \times g$, 10 min). This process was repeted till ghosts appeared milky white.

Spectrin-depleted erythrocyte vesicles: Spectrin depletion was obtained adding to one volume of ghosts 10 volumes of the extraction buffer [3] for 30 min, at 37°C. Then a 20 min centrifugation (at $3900 \times g$, 2-4°C) followed. The whole procedure was repeted twice. The removal of spectrin was monitored by SDS polyacrylamide gel electrophoresis (7.5-15%) [8].

Spin labelling: the spin labels, 5-doxyl-stearic acid (5 DSA), 16-doxyl-stearic acid (16 DSA), were obtained from Sigma Chemical Co.. The cationic spin probe 1-oxyl-2,2,6,6-tetramethyl-t-dimethyl-amino-piperidine-cethyl bromide, USA). All the spin labels were dissolved in ethanol. Prior to labelling, an appropriate amount of ethanolic solution was placed in a teste tube and the solvent was evaporated in a nitrogen stream. The final concentration of the label in the sample was aproximately 9×10^{-5}M for 5 DSA and 16 DSA and 6×10^{-4}M for CAT16. Membranes were labelled by incubation for 30 minutes at room temperature. This incubation was followed by four washings ($3900 \times g$) in the suspension buffer. Membranes were sealed in 50 µl capillary micropippettes, for ESR measurements.

ESR measurements: ESR spectra were recorded on a Varian E-109 spectrometer equipped with a insert dewar and a nitrogen flow temperature control system Varian E-257. The temperature inside the sample cavity was monitored with a copper-constantan thermocouple (accuracy $\pm$ 0.5°C). The microwave power was kept at 10 mw and the microwave frequency was 8.99 GHz. The field sweep was 100 G with a scan time of 4 min. Modulation amplitudes of 4 G, 1.6 G and 2 G and time constants of 0.128 s, 0.250 s and 0.128 s were used for 5 DSA, 16 DSA and CAT16, respectively.

Analysis of ESR spectra: For the 5 DSA spectra, the order parameter (S) was calculated according to Gaffney [4] and Ingraham et al [7] ($S=0.568$ $(A_{||} - A_{\perp})a'$; $a' = (A_{||} + 2A_{\perp})/3$. This parameter is a measure of spin label order and motion, the theoretical limits being S=O for a completely fluid, isotropic system and S=1 for a completely rigid or ordered environment.

The spectra of the spin probe CAT16 were analysed in terms of the inner hyperfine splitting parameter $A_{\perp}$, which gives information on the hydrophilic part of the membrabe [9].

Finally the spectra of the spin probe 16 DSA were analised in terms of the rotational correlation time τ_o ($\tau_o = 6.5 \times 10^{-10}W_o$ ($\sqrt{h_o/h_{-1}}-1$). This is a motion parameter which is reasonably accurate for isotropic motion in the fast tumbling region. Large values for τ_o correspond to states of low fluidity.

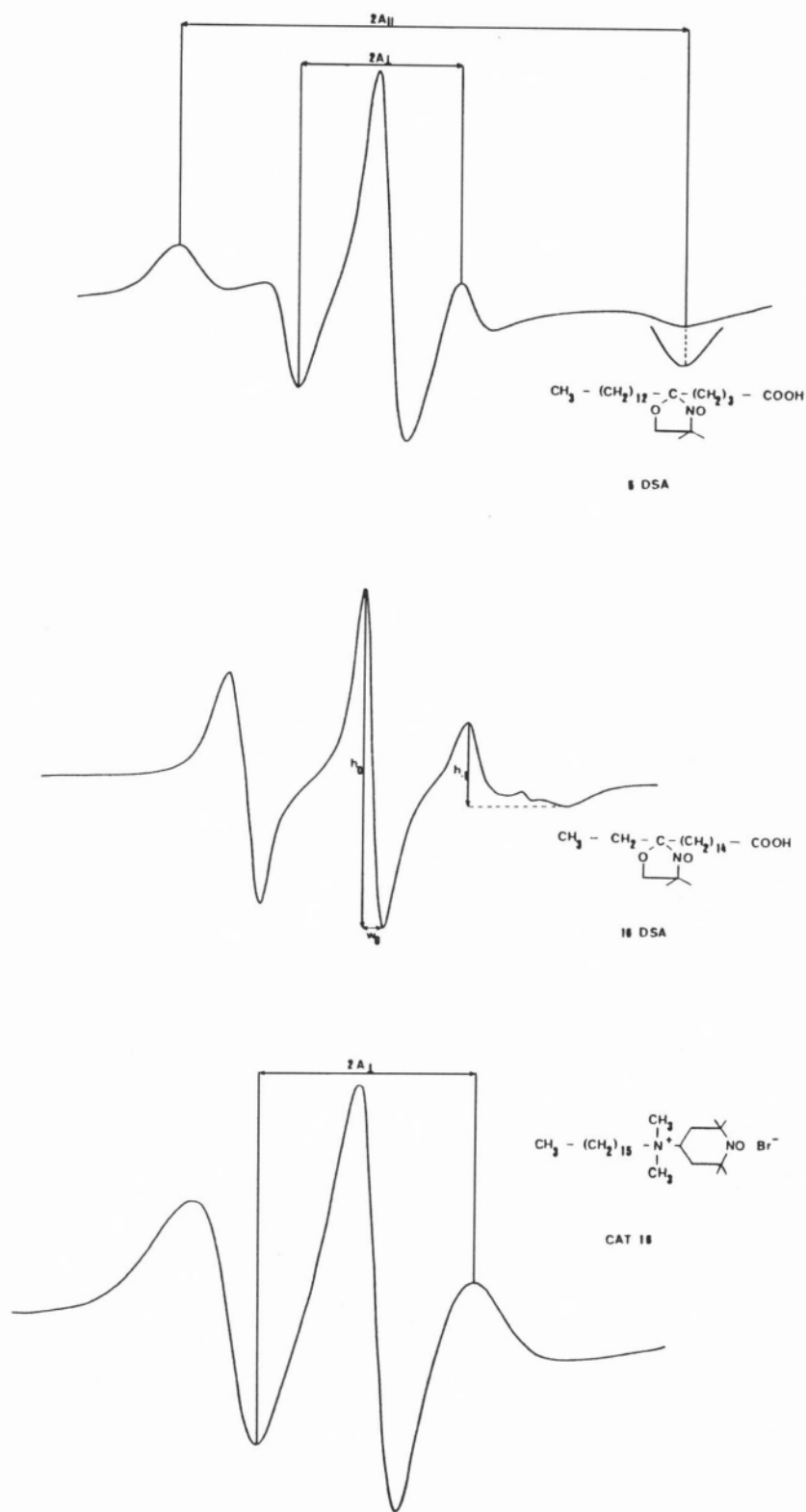The typica spectra of the spin probes together with the parameters used in further calculations are shown on figure 1.

Figure 1

The spectra of DSA, 16 DSA and CAT 16 spin probes together with the parameters used in the calculations

RESULTS

Spectrin depleted membranes: Proteins from ghosts incubated as described before were analysed by SDS-PAGE in order to assess the efficiency of spectrin removal. Using treated membranes, we verified that spectrin was not stained by Commasie Blue, which indicates that the depletion of spectrin was efficient.

ESR experiments: The effect of spectrin on membrane order was assayed at three depths

abrupt increase of $A_\perp$ above 40°C, which has already been reported as the temperature at which spectrin goes through a massive transition.

Experiments using 5 DSA: Fig. 3 shows the temperature dependence of the order parameter S for normal and HS membranes, as well as spectrin depleted vesicles. Spectrin extraction causes a significant increase of the order parameter at temperatures lower than 30°C. At higher temperatures, normal erythrocyte
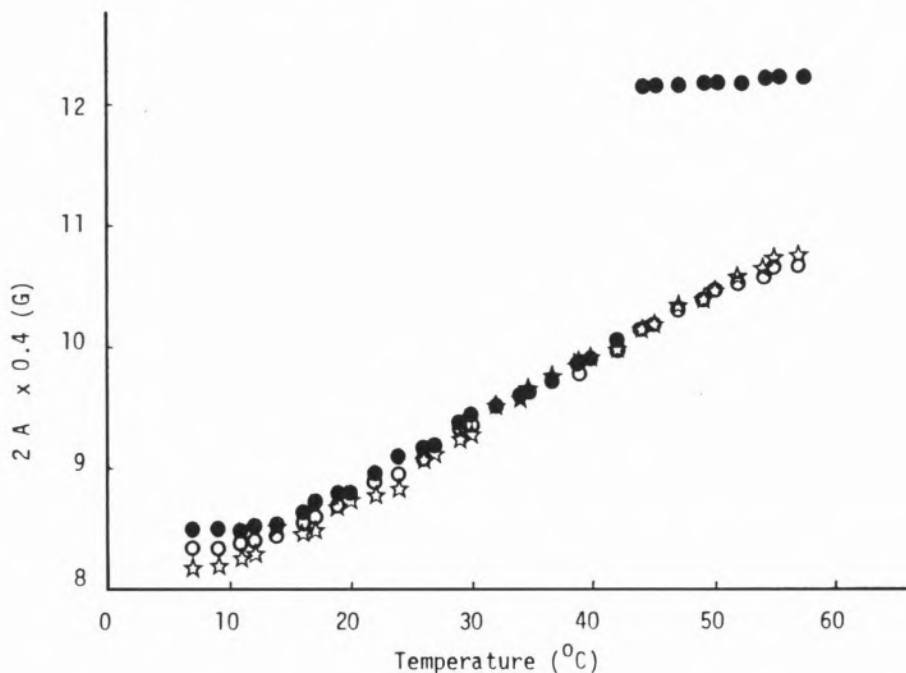

Figure 2

The dependence, on temperature, of the parameter $A_\perp$ of the spin probe CAT 16 incorporated in normal (●) and (☆) erythrocyte ghosts and in spectrin depleted vesicles (O)

of the membrane by the use of different spin probes. ESR spectra of all three probes, incorporated in normal and HS erythrocyte ghosts and in spectrin depleted vesicles, were recorded in the temperature range 7-57°C.

Experiments using CAT16: Figure 2 shows the dependence, on the temperature, of the inner hyperfine splitting parameter ($A_\perp$) of the spin probe CAT16 incorporated in ghosts and spectrin depleted vesicles. The temperature dependence of $A_\perp$ for HS membranes and spectrin depleted vesicles is very similar. In the case of erythrocyte ghosts, there is an

ghosts and spectrin depleted vesicles show approximately the same order parameter. HS membranes show, up to 20°C, order parameters between those of normal ghosts and spectrin depleted vesicles, but for temperatures above 30°C the order parameters are always higher than those associated with normal and spectrin depleted vesicles.

Experiments using 16 DSA; 16 DSA is a lipid spin probe used to explore the hydrophobic membrane core. Fig. 4 shows plots of the empirical parameter τ_0 as a function of temperature. From these plots, differences in

behaviour for all three cases are evident. The influence of the transition os spectrin at 40°C is observed just for ghosts. In what concerns HS membranes, τ_o changes, with temperature, much more rapidly then ghosts or even spectrin depleted vesicles.

temperature at which spectrin undergoes a massive transition. This change is due to changes of anisotropy of the probe movement or changes of the orientation of the N-O in the oxyl group in relation to the perpendicular axis to the membrane surface.
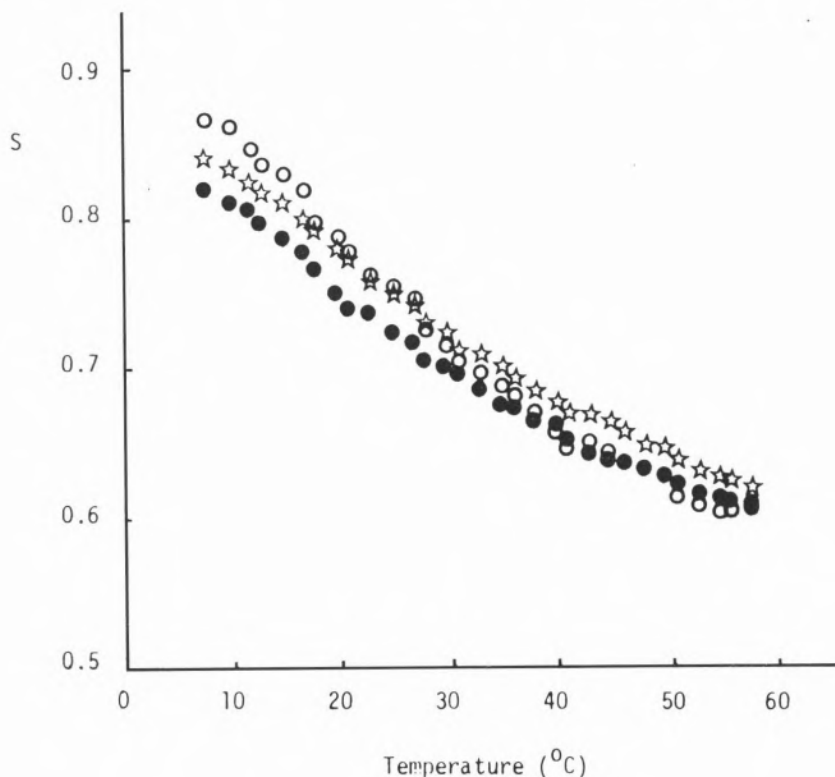

Figure 3

The temperature, dependence of the order parameter S of 5 DSA spin probe for normal (●) and HS (☆) erythrocyte ghosts and spectrin depleted vesicles (O)

DISCUSSION

As we pointed out before, a change in S or τ_o indicates a change in the range of motion (S) or in the rate of motion (τ_o). Upon spectrin extraction a significante increase of the order parameter, indicating a more ordered environment, was observed (Fig. 3). Similar effects were found by Sikorski and Kezierski when they compared the behaviour of erythrocyte ghosts and spectrin depleted vesicles [17]. The changes of the parameter $A_\perp$, as detected by the spin probe CAT 16 (Fig. 2), show that, in the case of normal ghosts, substantial alterations occur in the membrane at 40oC, the

Minetti et al [12], using the 16 DSA spin probe, indentified several structural transitions (40°C, 20°C, 8°C) in erythrocyte membranes. They have also shown that extraction of spectrin from those membranes abolishes the 40°C transition. However, our results showed a 40°C transition just for ghosts while the transition at 20°C, which is related to transitions in the lipid phase, is noticed in the three cases, being more evident in the HS membranes.

Our experiments, with erythrocyte membranes, show a «disordering» effect of the spectrin on the membrane lipid phase, mainly near the surface.
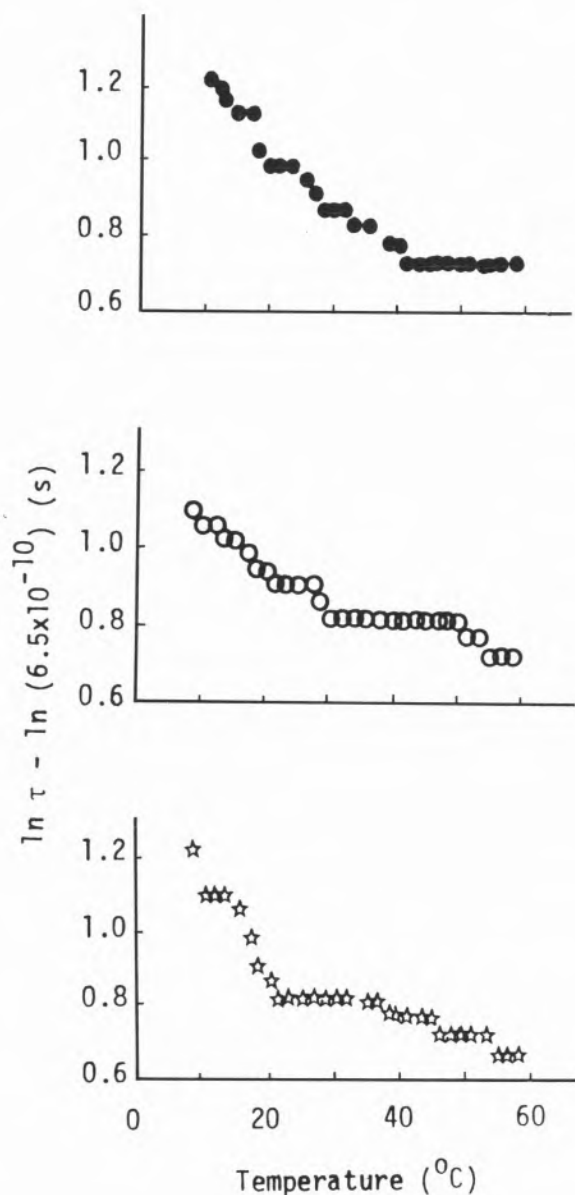
Figure 4

The rotational correlation time of 16 DSA spin probe incorporated in normal (●) and HS (☆) erythrocyte ghosts and spectrin depleted vesicles (O)

Comparison of the behaviour of the hidrophilic part of the membranes indicates that HS and spectrin depleted vesicles are very similar over the whole range of temperatures, In normal ghosts we could detect an important change of behaviour of the spin probe sited at the surface of the membrane, which is likely to be related with the transition that occurs in spectrin. The absence of such a transition in spectrin depleted vesicles and HS ghosts strongly supports the role of spectrin in the ordering of membrane lipids of normal red blood cells.

REFERENCES

[1] P. AGRE, J. F. CASELLA, W. H. ZINKHAM, C. MCMILLAN, V. BEMMET, *Nature*, **314**, 380 (1985).

[2] G. BENGA, in «Biochemical Research Techniques» (J. Wrigglesworth. ed.), pp 79-117, Joh. Wiley, London (1983).

[3] V. BENNETT, *Meth. Enzymol.*, **96**, 313 (1983).

[4] B. J. GAFFNEY, in «Spin Labeling. Theory and Applications» (I. J. Berlinier ed.) pp 567-571, Academic Press, New York (1975).

[5] S. R. GOODMAN, K. SHIFFER, L. CASORIA, M. E. EYSTER, *Blood*, **60**, 772 (1982).

[6] J. S. HILL, W. H. SAWYER, G. J. HOWLETT, J. WILEY, *Biochem. J.*, **201**, 259 (1981).

[7] L. M. INGRAHAM. P. C. BURNS, L. A. BOXER, R. L. BACHNER, R. A. HOAK, *J. Cel. Biol.*, **89**, 510 (1981).

[8] U. K. LAEMMLI, *Nature*, **227**, 680 (1970).

[9] G. LASSMANN and A. HERRMANN, *Stud. Biophys.*, **103**, 113 (1984).

[10] D. LITMAN, C. J. HSU, V. T. MARCHESI, *J. Cell Science*, **42**, 1 (1980).

[11] S. C. LIU, P. WINDISCH, S. KIM, J. PALEK, *Cell*, **37**, 587 (1984).

[12] M. MINETTI, M. CECCARINI, A. M. M. DI STASI, T. C. PETRUCCI, M. T. MARCHESI, *J. Cell Biochem*, **30**, 361 (1986).

[13] C. MOMBERS, P. W. M. VAN DIJCK, L. L. M. VAN DEENEN, J. DE GIER, A. J. VERKLEIJ, *Biochim. Biophys. Acta*, **470**, 152 (1977).

[14] C. MOMBERS, A. J. VERKJEIJ, J. DE GIER, L. L. M. VAN DEENEN, *Biochim. Biophys. Acta*, **551**, 271 (1979).

[15] C. MOMBERS, J. DE GIER, R. A. DEMEL, L. L. M. VAN DEENEN, *Biochim. Biophys. Acta*, **630**, 52 (1980).

[16] J. S. MORROW, D. W. SPEICHER, W. J. KNOWLES, V. T. MARCHESI, *Proc. Ntl. Acd. Sci.*, **77**, 6592 (1980).

[17] A. F. SIKORSKI, A. JEZIERSKI, *Studia Biophysica*, **113**, n.° 3, 193 (1986).

[18] D. W. SPEICHER, J. S. MORROW, W. J. KNOWLES, V. T. MARCHESI, *Proc. Ntl. Acd. Sci.*, **77**, 5673 (1980).

[19] P. D. YURCHENCO, D. W. SPEICHER, J. S. MORROW, W. J. KNOWLES, V. T. MARCHESI, *J. Biol. Chem.*, 9102 (1982).

RESUMO

O efeito do espectro sobre a ordem na membrana do eritrócito. Um estudo usando espectroscopia ESR

O efeito de espectrina, sobre a membrana de eritrócito, foi estudado por análise dos espectros de RPE das seguintes sondas paramagnéticas: 5 DSA, que dá informação sobre os lípidos perto da superfície da membrana, 16 DSA que dá informação sobre os lípidos no interior da membrana e CAT 16, que é sensível a modificações lípidicas à superfície da mesma. Estas sondas paramagnéticas foram incorporadas em membranas de eritrócitos normais, vesículas desprovidas de espectrina e membranas de esferócitos. Os seus espectros de RPE foram analisados numa gama de temperaturas entre 7-57°C. Concluiu-se que as membranas eritrocitárias, quando desprovidas de espectrina, têm menor fluidez e maior parâmetro de ordem. Diferenças semelhantes, embora menos evidentes, foram encontradas entre as membranas de eritrócitos normais e esferócitos. A utilização da sonda paramagnética CAT 16 mostrou a existência de grandes modificações, à superfície das membranas normais, quando a temperatura sobe acima de 40°C.

MARIA J. RAMOS
Departamento de Química, Faculdade de Ciências,
Universidade do Porto
4000 Porto
PORTUGAL

EMIL RODUNER
Physikalisch-Chemisches Institut der Universität Zürich,
Winterthurerstrasse 190,
CH-8057 Zürich,
SWITZERLAND

CALCULATION OF STRUCTURE AND HYPERFINE COUPLING CONSTANTS OF THE CYCLOHEXADIENYL RADICAL AND ITS MUONATED DERIVATIVE (*)

INDO calculations using a geometry based on advanced semiempirical calculations give improved values for hyperfine coupling constants and for corresponding shifts upon isotopic substitution by Mu in the methylene position of the cyclohexadienyl radical.

Previous calculations of hyperfine coupling constants in the cyclohexadienyl radical do not give satisfactory agreement with experimental numbers, in particular for the protons in the methylene group, but also for those in the ortho and para positions [1-2]. Assuming that this was mostly due to the crude approximation of the radical geometry we performed INDO calculations using the RHF version of MINDO/3. MNDO and AM1 optimised geometries for cyclohexadienyl [3]. Such an approach was successful previously for non-cyclic delocalised radicals [4]. The results are compared with those of earlier work and with experimental values in Table 1. Measured proton couplings are clearly better reproduced by the MNDO geometry whereas for ^{13}C the agreement between calculated and experimental values is slightly better for the AM1 geometry. The improvement is particularly pronounced for the methylene protons, although the MNDO predictions are still 50% high. Whereas the ortho and para proton couplings agree with experiment to within 10%, the meta proton couplings are a factor of two too large and do not depend much on the geometry. The meta proton couplings are a factor of two too large and do not depend much on the geometry. The latter seems to be a general result of INDO for protons adjacent to carbon atoms carrying negative spin population [4].

The MNDO geometry of the radical is given in Figure 1. The structure is predicted to be planar. The HCH bond angle at the methylene carbon which could affect the methylene coupling is 106° for the MNDO and AM1 resulting geometries and only slightly less with MINDO/3. Further comparison with other geometries shows that that the improvements found with MNDO are clearly related to an increased alternation effect in bond lengths as one goes from the methylene to the para carbon. Bond length alternation is important in and that this leads to satisfactory hyperfine coupling constants. *Ab-initio* methods which were previously applied to cyclohexadienyl give hyperfine couplings which scatter far

Table 1

INDO hyperfine coupling constants in mT

geometry	^{13}C nuclei				protons			
optimisation	ortho	meta	para	methylene	ortho	meta	para	methylene
standard [a]	1.79	−1.37	1.78	−1.76	−1.11	0.51	−0.98	9.76
INDO [b]					−1.09	0.54	−1.11	10.09
MINDO/3-RHF	1.75	−1.36	2.15	−1.72	−1.05	0.58	−1.20	7.72
MNDO-RHF	1.75	−1.35	2.18	−1.63	−1.02	0.54	−1.19	6.90
AM1-RHF	1.71	−1.31	2.07	−1.76	−1.03	0.53	−1.16	7.97
experiment [c]	1.41	−1.26	1.93	−1.22	(−)0.90	0.28	(−)1.33	4.78

[a] regular hexagon assumed, from *Pople, Beveridge and Dobosh* [1]
[b] *Yim and Wood* [1]
[c] values for protons from *Yim and Wood* [1], ^{13}C for C_6H_6Mu from ref. 10.

more about the experimental values than the ones derived from INDO [2].

Recently, the muonated cyclohexadienyl radical C_6H_6Mu, was detected and all nuclear hyperfine coupling constants reported [5]. Mu is a hydrogen-like one-electron atom with a positive muon as a nucleus. Chemically, it is

Figure 1

RHF-MNDO optimised structure of cyclohexadienyl with bond lengths in Å and angles in degrees.

regarded as a light isotope of hydrogen with a mass of only $^1/_9$ the mass of H [6]. The radical is formally derived by Mu addition to benzene, consequently Mu is bound in the methylene group. Comparison of the hyperfine coupling constants with those of C_6H_7 reveals considerable isotope shifts (see Table 2). Within the Born-Oppenheimer approximation the electronic energy hypersurface is the same for isotopic molecules. The shift must thus be a dynamic effect, and this is discussed in the following.

Optimised bond lenghts from *ab-initio* calculations yield equilibrium internuclear distances which correspond to a minimum on the potential energy surface. In contrast, semiempirical programmes such as MNDO are parametrised to reproduce experimental bond lengths which represent a dynamic average over vibrational modes. Bond length expectation values in an anharmonic potential are greater than the equilibrium internuclear distances, and they are isotope dependent. However, for conventional isotopes the effects are usually small, and therefore there is no separate parametrisation for isotopic molecules in semiempirical calculations. More dramatic effects are expected when isotopes as light as Mu are involved. More dramatic effects are expected when isotopes as light as
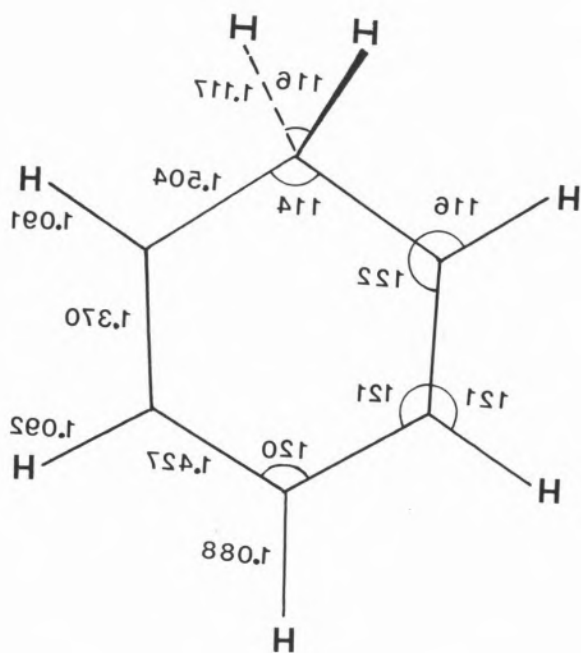
54

Table 2

Isotopic shift in % for absolute value of the hyperfine coupling constants of C_6H_6Mu relative to C_6H_7

methol	^{13}C nuclei				hydrogens				
	ortho	meta	para	methylene	ortho	meta	para	methylens muon	proton
MNDO [a]	−0.3	−0.2	−1.3	+9.4	−0.1	−0.5	−1.2	+25.1	−4.9
experiment [b]	–	–	–	–	−0.8	(−)3.8	−2.4	+20.5	−5.9

[a] see text
[b] from ref. 5.

Mu are involved. We have therefore calculated bond length expectation values for C-X diatomic species (X=D, H, Mu) in a Morse potential, using the exact wave functions and the Morse parameters given by Johnston and Parr [7]. For an equilibrium length of 0.1113 nm we have obtained values of 0.1134 nm (C-D), 0.1141 nm (C-H), and 0.1197 nm (C-Mu), i.e. the C-Mu bond is 4.9% longer than the C-H bond. Because of the low mass of Mu, one of the normal modes in C_6H_6Mu is to a good approximation a pure C-Mu stretching mode, just as in the diatomic case. However, the electrons adapt to the nuclear positions, and therefore the perturbation exerted by the longer C-Mu bond propagates through the molecule, in particular in delocalised systems. This effect was approximated in a MNDO calculation where the C-Mu bond was increased by 4.9% over the corresponding value in C_6H_7 and kept fixed while the remaining geometry parameters were relaxed. This results mainly in a shorter second methylene C-H bond by 0.3% and also in shorter C-C bonds to the methylene carbon by 0.25%. Except in the methylene group the symmetry plane is nearly retained. INDO coupling constants were calculated with this new geometry. The isotope shifts relative to C_6H_7 are given and compared with the experimental values in Table 2. We note quite excellent agreement, in particular for the large values of the methylene nuclei. Furthermore, conforming with the experiment, the effect is predicted to be nega-tive and larger for the para than for the ortho hydrogen. For the small meta couplings relative experimental errors are large, and comparison with calculated shifts is not meaningful. A large shift is also predicted for the methylene ^{13}C coupling, but experimental data are unfortunately not available for unsubstituted C_6H_7.

The analysis shows that the increased bond length of C-Mu provides the key to an understanding of isotope shifts in hyperfine couplings of rigid muonated radicals. It is expected to be relevant also in more flexible species such as ethyl [8], where the dominant effect on isotope shifts has been shown to be due to isotope dependent barriers of internal rotation [9]. Nevertheless, the static approach used to simulate a dynamic phenomenon can only be a first step. A more advanced treatment should calculate the expectation value of the hyperfine coupling constant for the vibrations in an anharmonic potential directly. This should then also describe the temperature dependence of the couplings.

REFERENCES

[1] J. A. Pople, D. L. Beveridge and P. Debosh, *J. Amer. Chem. Soc.*, **90**, 4201 (1968); M. B. Yim and D. E. Wood, *J. Amer. Chem. Soc.*, **97**, 1004 (1975); P. Bischof, *J. Amer. Chem. Soc.*, **98**, 6844 (1976).

[2] D. M. Chipman, *J. Chem. Phys.*, **78**, 4785 (1983).

[3] M. J. S. Dewar and D. M. Storch, *J. Amer. Chem. Soc.*, **107**, 3898 (1985).

[4] J. C. Walton, *Rev. Chem. Intermed.*, **5**, 249 (1984).

[5] P. W. Percival, R. F. Kiefl, S. Kreitzman, D. M. Garner, S. F. J. Cox, G. M. Luke, J. H. Brewer, K. Nishiyama and K. Venkateswaran, *Chem. Phys. Letters*, **133**, 465 (1987).

[6] D. C. Walker, *J. Phys. Chem.*, **85**, 3960 (1981).

[7] P. M. Morse, *Phys. Rev.*, **34**, 57 (1929); H. S. Johnston and Ch. Parr, *J. Amer. Chem. Soc.*, **85**, 2544 (1963).

[8] S. F. J. Cox, T. A. Claxton and M. C. R. Symons, *Radiat. Phys. Chem.*, **28**, 107 (1986).

[9] M. J. Ramos, D. McKenna, B. C. Webster and E. Roduner, *J. Chem. Soc., Faraday Trans. 1*, **80**, 255 (1984); M. J. Ramos, D. McKenna, B. C. Webster and E. Roduner, *J. Chem. Soc., Faraday Trans.1*, **80**, 267 (1984); T. A. Claxton and A. M. Graham. *J. Chem. Soc., Chem. Commun.*, 1167 (1987).

[10] R. F. Kiefl, P. W. Percival, J. C. Brodovitch, S. K. Leung, D. Yu, K. Venkateswaran and S. F. J. Cox, *Chem. Phys. Letters*, **143**, 613 (1988).

RESUMO

Cálculos de estrutura e de constantes de acoplamento hiperfino do radical hexadienilo e do seu derivado por substituição muónica

Cálculos INDO, usando uma geometria baseada em cálculos semiempíricos, dão origem a valores melhorados de constantes de acoplamento hiperfinas e correspondentes deslocamentos do radical ciclohexadienilo.

BALTAZAR DE CASTRO
JOSÉ PEREIRA
Departamento de Química
Faculdade de Ciências do Porto
4000 Porto
PORTUGAL

ESTUDO DA ESTABILIDADE DO SISTEMA TERNÁRIO ZINCO/CITIDINA/ /GLICILGLICINA POR ESPECTROSCOPIA DE R.M.N. DE 13C (*)

Fez-se o estudo em solução aquosa do sistema ternário zinco (II)/ citidina/glicilglicina por RMN de 13C, tendo-se determinado as constantes de associação Zn(II)/citidina na presença e ausência de glicilglicina, obtendo-se valores de 0,3 ± 0,2 M e 1,7 ± 0,9 M, respectivamente. Este resultado parece permitir excluir efeitos cooperativos significativos entre os ligandos que favoreçam a coordenação da citidina ao catião zinco. Reinterpretam-se resultados anteriormente apresentados na literatura que apontavam para a formação preferencial do complexo ternário zinco(II)/citidina/glicilglicinato, em solução de cloreto de zinco, em termos da interacção dos iões cloreto com a região NH₂/C(5)–H da citidina que induzem um desvio químico significativo em H–5.
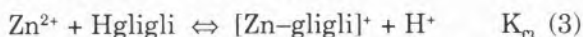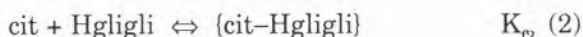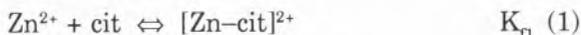
INTRODUÇÃO

A ocorrência de interacções não covalentes entre os ligandos em complexos ternários de metais de transição tem sido alvo do maior interesse nos últimos anos, nomeadamente devido ao papel preponderante que pode ter na especificidade das ligações de catiões metálicos a proteínas, enzimas, ADN e ARN. A sua importância tem sido avaliada em sistemas do tipo MLL' sobretudo por titulação potenciométrica (pH) e por espectrometria de ressonância magnética nuclear (RMN) [1]. Sistemas ternários com um nucleótido, um catião metálico divalente (Zn, Cu, Ni, Mg, Ca, Cd, etc.) e um outro ligando orgânico, quelante e com átomos dadores de azoto, têm sido estudados como modelos para a interacção dos catiões metálicos com o ADN e o ARN em processos de replicação, de transcrição e de tradução celulares [1]. Igual atenção tem sido dada à complexação por aminoácidos e pequenos péptidos de catiões divalentes na presença de outros ligandos de interesse biológico, como é o caso dos nucleótidos e nucleósidos [2,3].

Em todos estes estudos, particular importância tem sido dada aos factores que estabilizam a formação de complexos ternários mistos, com incidência nas interacções hidrofóbicas, de empilhamento e de formação de pontes de hidrogénio entre os dois ligandos coordenados [1,4].

Foi sugerido por Li *et al.* [5] a ocorrência de fenómenos cooperativos na formação de complexos entre a citidina (cit), catião zinco (II) e a glicilglicina (Hgligli), a patir da observação de que os desvios químicos do protão H-5 da citidina na presença de zinco aumentavam com adição de glicilglicina. Na sequência desses resultados, foi estudado o equilíbrio químico em solução aquosa nos sistemas binários Zn-citidina, citidina-glicilglicina e no sistema ternário citidina-Zn-glicilglicina, como primeira fase da avaliação da importância de interacções não covalentes

entre aminoácidos e nucleósidos no equilíbrio de complexação com catiões divalentes diamagnéticos. Neste sistema são possíveis os seguintes equilíbrios:

$$Zn^{2+} + cit \Leftrightarrow [Zn-cit]^{2+} \qquad K_{f1} \quad (1)$$

$$cit + Hgligli \Leftrightarrow \{cit-Hgligli\} \qquad K_{f2} \quad (2)$$

$$Zn^{2+} + Hgligli \Leftrightarrow [Zn-gligli]^+ + H^+ \qquad K_{f3} \quad (3)$$

$$[Zn-gligli]^+ + cit \Leftrightarrow \{cit-[Zn-gligli]\}^+ \quad K_{f4} \quad (4)$$

MÉTODO EXPERIMENTAL

A glicilglicina (Merck) e a citidina (Aldrich) foram utilizadas tal como adquiridas, sem purificação adicional. As soluções de nitrato de zinco e nitrato de cálcio foram preparadas a partir do respectivo sólido hidratado e tituladas com soluções padrão de EDTA. As soluções de KNO_3 foram preparadas a partir do sólido condicionado. Na preparação de todas as soluções foi usada água desionizada e bidestilada em quartzo.
Na determinação de K_{f1} utilizaram-se soluções 0,10 M em citidina e com concentrações de zinco de 0,05; 0,10; 0,20 e 0,30 M (concentrações para além da qual se observou precipitação de hidróxido de zinco). Esta experiência foi repetida com cálcio e potássio, este último em concentrações de 0,15; 0,30; 0,60; 0,90 M. Na determinação de K_{f4} utilizaram-se soluções 0,10 M em citidina e 0,05; 0,10; 0,20; 0,30 M em glicilglicina e com as concentrações de zinco referidas acima. No estudo da interacção citidina-glicilglicina usaram-se quer soluções de 0,10 M em citidina e concentrações variáveis de glicilglicina (0,05; 0,10, 0,20 e 0,30 M), quer soluções 0,10 M em glicilglicina com concentrações variáveis de citidina. O pH de todas as mostras foi ajustado a 6.15 ± 0.05 por adição de solução concentrada de HNO_3 e/ou NaOH.
Os espectros RMN de ^{13}C foram obtidos num espectrómetro Brucker AC200 à frequência fundamental de 47.3 MHz usando um «lock» externo de D_2O. Os desvios químicos foram medidos em Hertz relativamente a t-butanol, utilizado como referência interna.
Para o cálculo das constantes de formação dos complexos $[Zn(cit)]^{2+}$ e $[Zn(cit)(gligli)]^+$ foram utilizados os desvios químicos dos átomos de carbono da citidina. Atendendo a que os equilíbrios (1) e (4) são rápidos, e designando por M a concentração de catião zinco livre e complexado ao anião glicilglicinato, por L a concentração de citidina livre, por ML a concentração do complexo de citidina com zinco e por L_0 a concentração total de citidina, o desvio químico observado para cada átomo de carbono da citidina em solução é dado por:

$$\delta_{obs}^{Zn} = (L/L_0)\delta_L + (ML/L_0) \, \delta_{ML} \qquad (3)$$

onde δ_L e δ_{ML} são os desvios químicos do ligando livre e do ligando complexado, respectivamente. Conjuntamente com a definição da constante de formação

$$K_f = ML / (M \, L) \qquad (4)$$

é possível deduzir uma relação entre K_f e os desvios químicos observados:

$$(5)$$

$$\Delta_{obs} = \frac{M_0 + L_0 + \dfrac{1}{K_f} - \sqrt{\left(M_0 + L_0 + \dfrac{1}{K_f}\right)^2 - 4\,L_0 M_0}}{2\,L_0} \Delta_{max}$$

(onde M_0 representa a concentração total de nitrato de zinco), sendo $\Delta_{obs} = \delta_{obs}^{Zn} - \delta_L$ e $\Delta_{max} = \delta_{ML} - \delta_L$
A equação (5) contém dois parâmetos a calcular: K_f e Δ_{max}. A resolução iterativa do sistema de equações obtido utilizando vários valores de concentração de catião zinco, permite obter os valores de K_f e Δ_{max} a partir dos desvios químicos observados, Δ_{obs} [6].
A utilização dos desvios químicos da citidina livre, δ_L, como referência, embora forneça valores plausíveis para as constantes de formação dos complexos, não atende à variação da força iónica pelo que foram utilizados os desvios químicos observados para os átomos de carbono da citidina em soluções com nitrato de cálcio ou nitrato de potássio. Neste caso, o

tratamento matemático dos resultados processa-se de forma análoga à descrita atrás, mas com $\Delta_{obs} = \delta_{obs}{}^{Zn} - \delta_{obs}{}^{Ca \ ou \ K}$ e $\Delta_{max} = \delta_{ML} - \delta_{obs}{}^{Ca \ ou \ K}$, em que $\delta_{obs}{}^{Ca \ ou \ K}$ representa o desvio químico de um átomo de carbono da citidina em soluções de nitrato de cálcio ou de nitrato de potássio com a mesma força iónica.

Na determinação de K_f para o complexo ternário, não foi considerado o equilíbrio (1), uma vez que a formação do complexo [Zn–gligli]+ ocorre em extensão apreciável (o pK, determinado potenciometricamente, é aproximadamente igual 3,13 e não é afectado pela presença da citidina [5]) o que permite desprezar a reduzida concentração de Zn2+ coordenado unicamente à citidina.

RESULTADOS E DISCUSSÃO

A análise prévia do sistema glicilglicina-citadina em solução permitiu excluir qualquer interacção significativa entre os dois ligandos, pelo menos que se traduzisse em alteração nos desvios químicos de 13C dos espectros de RMN de soluções com os dois ligandos, relativamente aos de glicilglicina e da citidina livres.

O cálculo das constantes K_{f1} e K_{f4} utilizando como referência os desvios químicos da citidina livre, forneceu valores próximos da unidade, embora com uma dispersão significativa em torno do valor médio ($K_f \approx 1,2 \pm 1$) que se pode atribuir à variação da força iónica.

A utilização dos valores de $\delta_{obs}{}^{Ca}$ como referência, permite eliminar nos desvios químicos de soluções de citidina com catião zinco o efeito da força iónica do meio, sem introduzir interacções específicas com a citidina, pois embora o catião cálcio mostre ligeira tendência para se ligar à citidina em dimetilsulfóxido (DMSO) [7], não é de esperar que isso aconteça em água [8]. Esta observação é suportada pela concordância dos valores calculados para as constantes de equilíbrio (ver figura 1 e tabela 1) utilizando $\delta_{obs}{}^{Ca}$ como referência e pela semelhança entre estes valores e os obtidos utilizando $\delta_{obs}{}^{K}$ de soluções de citidina com
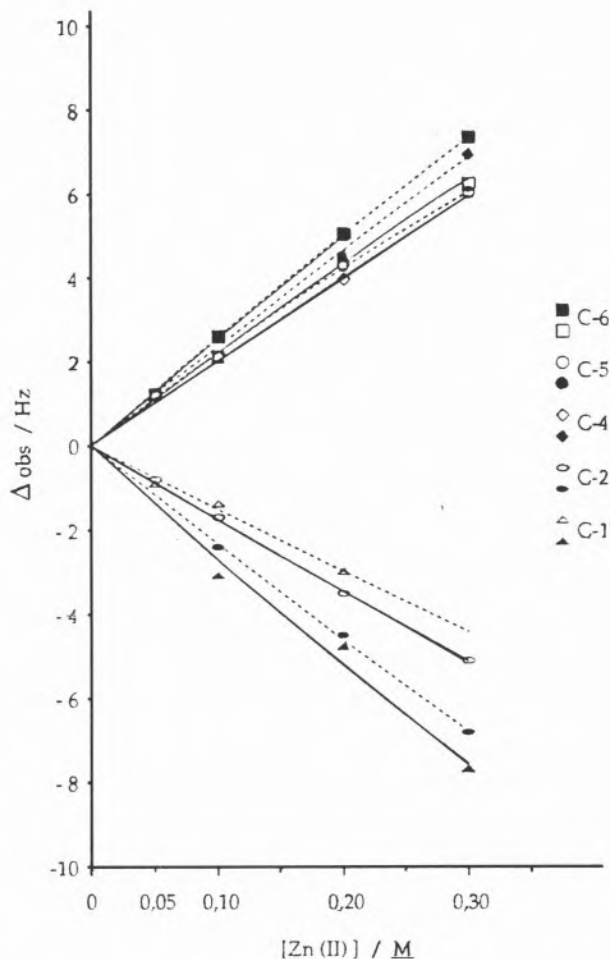

Figura 1

Representação gráfica de Δ_{obs} em função de [Zn(II)]. A preto estão indicados os pontos correspondentes ao sistema ternário citidina-Zn-glicilglicina e a branco os pontos correspondentes ao sistema binário Zn-cit

Tabela 1

Constantes de formação de Zn²⁺ e [Zn(gligli)]⁺ com citidina, calculados para cada átomo de carbono (ver texto)

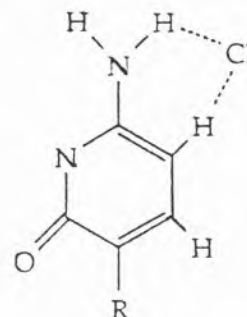| Zn2 + Citidina					
C2	C4	C5	C6	C1´	Média
0.177	0.148	0.607	0.289	0.126	0.26±0.20

[Zn(gligli)]⁺ + Citidina					
C2	C4	C5	C6	C1´	Média
1.25	1.14	3.45	1.76	0.76	1.7±0.9

nitrato de potássio como referência. Aliás, esta última observação, conjuntamente com a semelhança dos valores dos desvios químicos para soluções de cálcio e potássio com a mesma força iónica, sugere que não deve ocorrer formação de ligações entre o catião metálico do grupo IIA e a citidina em solução aquosa, sendo os desvios químicos originados unicamente por variação de força iónica. Para o cálculo de constantes de formação, a utilização de um catião divalente em solução é preferível (atendendo ao número e carga das espécies em solução) para compensar o efeito da força iónica, pelo que os valores referidos de K_f utilizam δ_{obs}^{Ca} como referência.

Na figura 1 estão representados os desvios Δ_{obs} em função da concentração de $Zn(NO_3)_2$ para os carbonos da citidina que apresentam maiores desvios químicos, para os sistemas Zn-citidina e citidina-Zn-glicilglicina. As curvas para os dois sistemas são praticamente idênticas, não diferindo entre si, para cada átomo de carbono, de mais de 1,5 Hertz (0,03 ppm). A constante de formação calculada em ambos os sistemas é a média das constantes obtidas para os carbonos que apresentam maior desvio químico; C-2, C-4, C-6, C-5 e C-1′. A análise do sistema Zn-citidina forneceu o valor $0,3 \pm 0,2$ M para a constante de formação do complexo [Zn-citidina]²⁺, valor menor do que se obteve para o complexo {cit-[Zn-gligli]}⁺ no sistema citidina-Zn-glicilglicina: $1.7 \pm 0,9$ M.

Estes resultados mostram que a formação do complexo [Zn-citidina]²⁺ em solução aquosa ocorre em pequena extensão, que é menor que a observada em DMSO, para a qual é referido um valor de $\approx$ 4,1 M [7]. Por outro lado, a pequena diferença entre os valores da constante de formação na presença e ausência de glicilglicina sugere que não deve ocorrer nenhum efeito cooperativo significativo entre a glicilglicina e a citidina que favoreça a coordenação da citidina no zinco, contrariamente ao que foi sugerido anteriormente. Esta última observação foi baseada em desvios químicos de ¹H para o protão H-5 da citidina na presença e ausência de glicilglicina numa solução aquosa de cloreto de zinco e citidina, e

em que se observaram desvios químicos maiores para o protão H-5 da citidina na presença de glicilglicina [5]. No entanto, os resultados de Li *et al* podem ser explicados com base na existência de uma interacção do anião cloreto com o grupo N3/C4-NH₂ da citidina (esquema 1) [7,8].

Esquema 1

Representação da interacção possível entre o anião cloreto e o grupo $NH_2/C(5)-H$ da citidina

Para as concentrações elevadas de $ZnCl_2$ utilizadas, deve ocorrer em solução a formação de pares iónicos Zn^{2+}/Cl^- que provoca uma diminuição da concentração de anião cloreto livre. Por adição de glicilglicina, a quase totalidade do zinco em solução passa a estar coordenado ao anião glicilglicinato (para o pH utilizado, a coordenação ocorre pelo átomo de azoto do grupo amino terminal [10], e a formação de pares iónicos irá ocorrer em menor extensão, o que aumenta a concentração de cloreto livre e logo favorecerá a interacção com a base. Por outro lado, o anião nitrato utilizado neste estudo, não demonstrou perturbar os desvios químicos da citidina [8] e o efeito da coordenação aniónica fica assim obviado.

AGRADECIMENTOS

BIBLIOGRAFIA

[1] H. J. SIGEL, *Angew. Chem.*, **92**, 421 (1982); H. SIGEL, *J. Inorg. Nucl. Chem.*, **39**, 1903 (1977); P. R. REDDY, B. M. REDDY, *Polyhedron*, **5**, 1947 (1986); R. TRIBOLET, R. B. MARTIN, H. SIGEL, *Inorg. Chem.*, **26**, 638 (1987).

[2] S. M. WANG, R. K. GILPIN, *Talanta*, **32**, 329 (1985).

[3] J. J. LED, *J. Amer. Chem. Soc.*, **107**, 6755 (1985); K. PRASAD, A. K. RAO, M. S. MOHAN, *J. Coord. Chem.*, **16**, 251 (1987).

[4] H. SIGEL, R. MALINI-BALAKRISHNAN, U. K. HARING, *J. Amer. Chem. Soc.*, **107**, 5137 (1985); R. MALINI-BALA-KRISHNAN, K. H. SCHELLER, U. K. HARING, R. TRIBOLET, H. SIGEL, *Inorg. Chem.*, **24**, 2067 (1985).

[5] K. C. TEWARI, J. LEE, N. C. LI, *Trans. Farad. Soc.*, **66**, 2069 (1970).

[6] L. G. MARZILLI, B. CASTRO, J. P. CARADONNA, R. C. STEWART, C. P. VAN VUUREN, *J. Amer. Chem. Soc.*, **102**, 916 (1980).

[7] T. YOKONO, S. SHIMOKAWA, SHOMA, *J. Amer. Chem. Soc.*, **97**, 3827 (1975).

[8] C.-H. CHANG, L. G. MARZILLI, *J. Amer. Chem. Soc.*, **96**, 3656 (1974).

[9] R. B. MARTIN, *Acc. Chem. Res.*, **18**, 32 (1985).

[10] D. L. RABENSTEIN, S. LIBICH, *J. Inorg. Chem.*, **11**, 2960 (1972).

[11] S. M. WANG, N. C. LI, *J. Amer. Chem. Soc.*, **90**, 5069 (1968).

ABSTRACT

Stability of the termary system zina/cytidine/glycyl-glycin as studied by ^{13}C-NMR spectroscopy

The study of the ternary sistem zinc(II)/cytidine/glycylgly-cine in aqueous solution by ^{13}C NMR spectroscopy allowed the determination of Zn(II)/cytidine formation constants in the presence and absence of glycylglycine, the constants being 0.3 ± 0.2 M and 1.7 ± 0.9 M respectibly. Significant cooperative efects between the ligands in the coordination of cytidine to zinc cation are therefore excluded. Previous results presented in the literature for this system, implying a preferencial formation of the ternary complex in aqueous solution of zinc chloride, are reinterpreted in terms of an induced shift due to a reverse charge chelate between the chloride ion and cytidine through the $NH_2/C(5)$-H moiety.

M. BROTAS DE CARVALHO
J. PIRES
Centro de Química Física e Radioquímica — INIC
Faculdade de Ciências da Universidade de Lisboa
R. Escola Politécnica, 58
1200 Lisboa
PORTUGAL

F. RAMÔA RIBEIRO
Grupo de Estudos de Catálise Heterogénea
Instituto Superior Técnico
Av. Rovisco Pais
1096 Lisboa Codex
PORTUGAL

INFLUÊNCIA DOS CATIÕES SÓDIO E NÍQUEL NA CAPACIDADE DE ADSORÇÃO DE AZOTO E DE n-HEPTANO EM MORDENITES

Determinaram-se as isotérmicas de adsorção de azoto a 77K e de n-heptano a 298K, sobre várias formas de mordenite: sódica, protónica e formas contendo diferentes teores em níquel. As capacidades adsortivas foram estimadas por aplicação do modelo de Dubinin-Radushkevich, tendo-se concluído que, em relação ao azoto, essa capacidade é máxima para a mordenite protónica, diminuindo com o aumento do teor em níquel e sendo mínima para a mordenite sódica independentemente da permuta parcial de sódio por níquel.

As capacidades de adsorção em n-heptano das diferentes amostras seguem a mesma sequência obtida para o azoto, embora os valores registados sejam muito mais baixos, pois, devido às dimensões das suas moléculas, o n-heptano não tem acesso aos canais de menores dimensões da mordenite.

INTRODUÇÃO

As mordenites são zeólitos muito utilizados na indústria petroquímica [1]. Frequentemente introduz-se na sua estrutura, por permuta iónica, um metal de transição (por exemplo o níquel) para melhorar a estabilidade catalítica. As mordenites são silico-aluminatos cristalinos, cuja fórmula empírica é $M_{8/n}(AlO_2)_8(SiO_2)_{40} \cdot 24 H_2O$, onde n, é a valência do catião de compensação M [2].

A estrutura cristalina da mordenite apresenta grandes canais paralelos, de secção elíptica $(0,75 \times 0,59nm)$, interseptados numa direcção perpendicular por canais mais estreitos $(0,29 \times 0,57nm)$ também paralelos entre si.

O catião de compensação é normalmente o sódio, podendo ser facilmente permutado por outros catiões que podem influenciar as propriedades do zeólito e, nomeadamente, a sua capacidade de adsorção.

Diversos estudos têm sido efectuados para determinar o efeito dos catiões nas propriedades texturais das mordenites, não estando porém bem esclarecidas a extensão e as causas da alteração da porosidade.

O objectivo deste trabalho é estudar a influência dos catiões sódio e níquel nas propriedades de adsorção da mordenite. Realizaram-se para o efeito estudos de adsorção de azoto a 77K e de n-heptano a 298K nas várias amostras preparadas.

PARTE EXPERIMENTAL

1 — *Preparação das amostras*

A preparação das várias amostras estudadas foi feita a partir de uma forma sintética da mordenite sódica (Zeolon 900Na da Norton Company) identificada por NaM. Submeteu-se este zeólito a uma sequência de três permutas com uma solução de NH_4NO_3 (2 mol dm^{-3}), eliminando-se aproximadamente 98% (em massa) do sódio inicial, e obteve-se a forma intermédia, NH_4M, que foi posteriormente calcinada num forno tubular horizontal, sob um

fluxo de ar de 4 l/h com o seguinte regime de aquecimento: o aumento da temperatura de 298 a 623K foi feito a uma velocidade de 150K/h, mantendo-se esta temperatura durante 30 minutos. Em seguida, elevou-se a temperatura à velocidade de 300K/h, até 773K, conservando-se o sistema a esta temperatura por mais 4 horas. Este protocolo de calcinação, a que se recorreu para obter a forma protónica, HM, foi também posteriormente seguido na preparação das outras formas de mordenite.

Para introduzir o catião níquel na estrutura da mordenite, usaram-se os seguintes procedimentos, que conduziram respectivamente aos produtos designados por NiNaM(38), NiHM(25), NiHM(32) e NiHM*(32).

A amostra NiNaM(38) foi obtida por permuta iónica de NaM com uma solução aquosa de Ni $(NO_3)_2$ (2 mol dm^{-3}) e posterior secagem a 373K. As formas NiHM(25) e NiHM(32) foram obtidas a partir da forma intermédia, NH_4M, por permuta iónica com uma solução aquosa de $Ni(NO_3)_2$ de molaridade respectivamente 0,5M e 2M, seguida de calcinação à temperatura final de 773K, segundo o método acima descrito para obtenção da forma HM.

A forma NiHM*(32) foi obtida a partir da forma HM por permuta iónica com uma solução aquosa de $Ni(NO_3)_2$(2 mol dm^{-3}), seguida de secagem a 373K.

Entre parêntesis indica-se a taxa de permuta (percentagem mássica) em relação à quantidade de sódio inicial.

2 — Medidas de adsorção

As medidas de adsorção de azoto a 77K e de n-heptano a 298K realizaram-se pelo método volumétrico, num sistema de alto vácuo construído em Pyrex.

As leituras de pressão foram efectuadas através de um sensor da MKS Baratron, tipo BAS-1000, e de um sensor Shaevitz, ambos para pressões até 1000 torr, previamente calibrados com manómetro de mercúrio e catetómetro. As experiências com n-heptano foram realizadas numa zona restrita da instalação com torneiras do tipo J-Young com êmbolos de teflon e sem qualquer lubrificação.

Antes da determinação das isotérmicas de adsorção as amostras foram submetidas a um tratamento de desgaseificação durante 6 horas a 673K, sob um vazio inferior a 8 mPa.

Em todos os sistemas considerados, detectaram-se processos de adsorção muito lentos, pelo que foi necessário prolongar os tempos de medida para cerca de 15 a 20 horas, conforme a zona da isotérmica.

RESULTADOS E DISCUSSÃO

As isotérmicas de adsorção de azoto a 77K e de n-heptano a 298K nas várias amostras estão representadas, respectivamente, nas Figuras 1 e 2, e a sua análise permite tirar várias conclusões. As isotérmicas de adsorção do azoto e do n-heptano são do tipo I, de acordo com a classificação da IUPAC [3], e, em ambos os casos, as quantidades adsorvidas são máximas
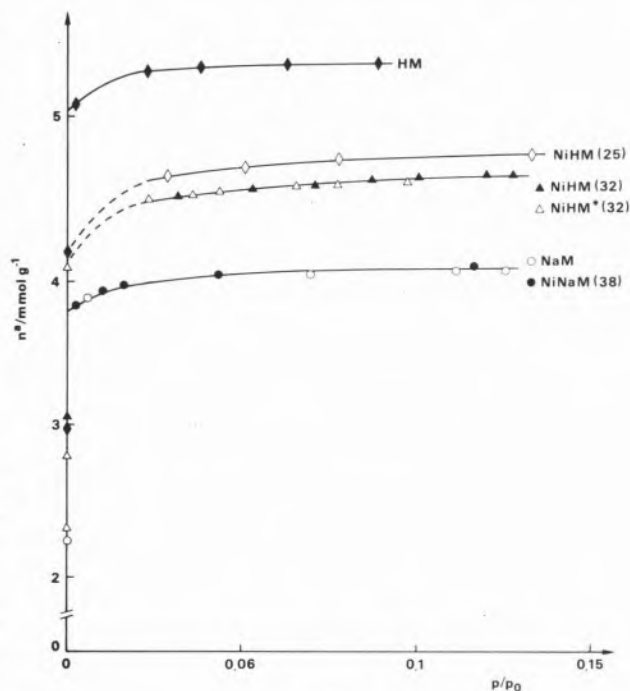

Figura 1

Isotérmicas de adsorção de azoto a 77K nas diferentes formas da mordenite.
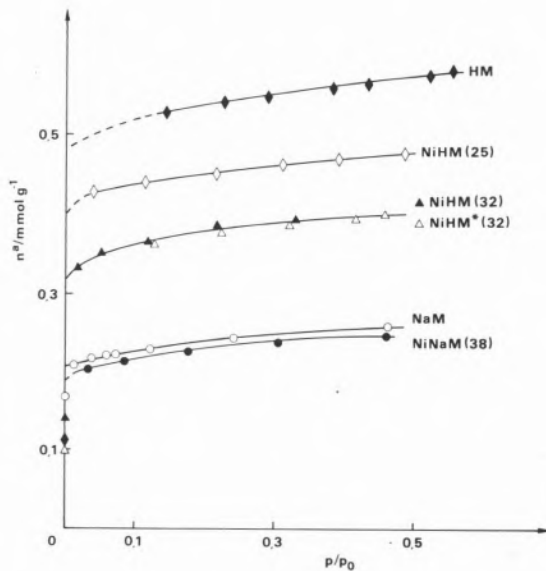
Figura 2

*Isotérmicas de adsorção de n-heptano a 298K
nas diferentes formas da mordenite.*

para a forma protónica da mordenite. As mordenites NiHM(25) e NiHM(32) obtidas por permuta com níquel e posteriormente calcinadas, têm uma capacidade de adsorção superior, quer à da forma NaM, quer à da forma NiNaM(38), obtida por permuta directa do sódio com o níquel. Por outro lado, para as diferentes amostras de mordenite preparadas, as quantidades adsorvidas são sempre maiores no caso da adsorção de azoto a 77K do que no da adsorção de n-heptano a 298K em condições de pressão relativa idênticas.

Em sólidos microporosos, as capacidades de adsorção podem ser estimadas por aplicação do modelo de Dubinin-Radushkevich (D:R.) de acordo com a equação [3,4]:

$$\log W = \log W_0 - (B/2,303) (T/\beta)^2 \log^2(p/p_0)$$

onde W representa a quantidade adsorvida à pressão relativa p/p_0, W_0 é a quantidade máxima adsorvida (capacidade microporosa) e T a temperatura. Os parâmetros B e β são respectivamente a denominada constante estrutural do adsorvente e o coeficiente de similaridade que depende do adsortivo.

As Figuras 3 e 4 ilustram a aplicação deste modelo respectivamente aos dados obtidos na adsorção do azoto a 77K e do n-heptano a 298K. Na zona linear dos gráficos, determinaram-se os valores correspondentes à capacidade microporosa $W_0(cm^3 g^{-1})$ das várias mordenites (Tabela 1).

É de notar que os valores de W_0 assim determinados, são muito próximos dos obtidos através de uma representação de Langmuir. Este aspecto foi já verificado noutros sistemas estudados neste laboratório [5] e resulta do facto de que as isotérmicas de adsorção de gases ou
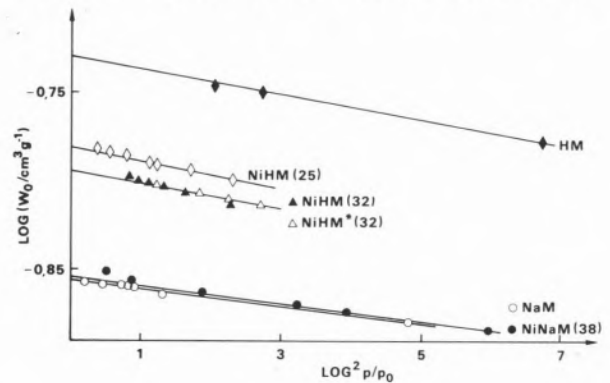

Figura 3

*Representações de Dubinin-Radushkevisch das isotérmicas
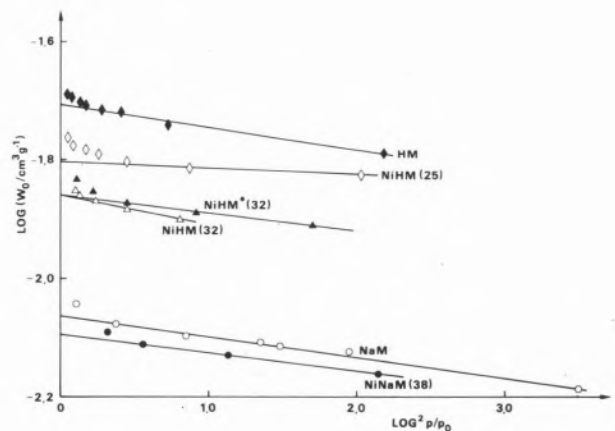de adsorção de azoto a 77K nas diferentes formas
da mordenite.*

Figura 4

*Representação de Dubinin-Radushkevisch das isotérmicas
de adsorção de n-heptano a 298K
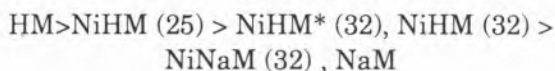nas diferentes formas da mordenite.*

Tabela 1

Capacidades microporosas, estimadas pelo modelo (D.R.),
aplicado à adsorção de azoto a 77K e de n-heptano a 298K

MORDENITE	$W_0/cm^3 g^{-1}$	
	azoto	n-heptano
NaM	0,14	0,034
NiNaM	0,14	0,033
NiHM(32)	0,16	0,057
NiHM*(32)	0,16	0,057
NiHM(25)	0,17	0,066
HM	0,19	0,081

vapores em zeólitos são quase exclusivamente do tipo I.

Como se pode verificar pela análise da Tabela 1, a capacidade microporosa (W_0) obtida no caso da adsorção de azoto em HM foi de 0,19 cm^3g^{-1}. Este valor é muito próximo do volume poroso da mordenite (0,199 cm^3g^{-1}) encontrado na bibliografia [6, 7] e traduz a acessibilidade do azoto a praticamente toda a rede porosa da forma protónica. Esta conclusão é compreensível, pois as dimensões estimadas das moléculas de azoto (0,3 ×0,4nm) permitem a sua entrada nos dois tipos de canais, da estrutura zeolítica embora nos de menores dimensões (0,29 ×0,57nm) o acesso possa implicar alguma deformabilidade da molécula.

Ainda relativamente ao azoto, conclui-se que o volume de saturação depende da natureza e teor do catião presente na estrutura zeolítica diminuindo segundo a sequência:

HM>NiHM (25) > NiHM* (32), NiHM (32) > NiNaM (32) , NaM

É de salientar que, nas duas formas da mordenite, NiHM* (32) e NiHM (32), em que o ião níquel foi introduzido por processos diferentes, respectivamente permuta iónica com HM para obtenção do NiHM* (32) e permuta iónica com a forma intermédia NH_4M para obtenção de NiHM (32), se obtiveram resultados de adsorção idênticos.

Nas experiências com n-heptano as quantidades adsorvidas pelas diferentes amostras variaram na mesma sequência verificada para o caso do azoto (Tabela 1). No entanto, os volumes adsorvidos são, mesmo no caso da forma protónica, sempre inferiores ao volume total dos canais mais largos. Isto pode em parte ser explicado pelo facto das moléculas do n-heptano, cuja secção transversal tem um diâmetro estimado em 0,49nm, não poderem penetrar nos canais de menores dimensões.

Para os sólidos NaM e NiNaM (38) não se registaram diferenças nos resultados de adsorção do azoto e do n-heptano, sugerindo este facto que o sódio residual, existindo em quantidade ainda apreciável na forma NiNaM tem um efeito predominante na limitação da capacidade adsortiva.

Analisando o efeito dos catiões sódio e níquel na redução da capacidade adsortiva da mordenite protónica, podem tirar-se as seguintes conclusões: entre as formas HM e NaM tanto em relação ao azoto como ao n-heptano existe uma diferença no valor do volume de saturação de 0,05cm^3g^{-1}. Analogamente entre os zeólitos HM e NiHM (32) essa diferença é de 0,03 e 0,02 para o azoto e n-heptano respectivamente, e entre HM e NiHM (25) de 0,02 para os dois adsortivos.

Estes resultados, atendendo a que as moléculas do n-heptano não têm acesso aos canais mais estreitos, levam a supôr que a influência dos catiões na capacidade adsortiva se faz sentir essencialmente nos canais de maior abertura.

REFERÊNCIAS

[1] F. RAMÔA RIBEIRO, et al., «Zeolites: Science and Technology», Martinus Nijhoff Publishers, The Hague, 1984.
[2] R. M. BARRER, «Zeolites and Clay Minerals as Sorbents and Molecular Sieves», Academic Press, London, 1973.
[3] Reporting Physisorption Data for Gas/Solid Systems, *Pure Appl. Chem.*, **57**, 604 (1985).
[4] S. J. GREGG, K. S. W. Sing, «Adsorption, Surface Area and Porosity», Academic Press, 1982.
[5] J. PIRES, M. BROTAS DE CARVALHO, F. LEMOS, F. RAMÔA RIBEIRO, M. GUISNET, *Reaction Kinetics and Catalysis Letters*, **37**, 49 (1988).
[6] D. W. BRECK, «Zeolite Molecular Sieves», J. Wiley, London, 1974.
[7] R. M. BARRER, F. R. S., D. L. PETERSON, Proc. Roy Soc., **A 280**, 466 (1984).

ABSTRACT

Influence of sodium and nickel cations on the adsorption capacity of nitrogen and of n-heptane for mordenites.

The adsorption isotherms of nitrogen at 77K and of n-heptane at 298K were obtained for different forms of mordenite: sodium mordenite, protonic mordenite and mordenite with different contents of nickel. The capacity of adsorption was estimated by the equation of Dubinin-Radushkevich, with the following conclusions: for nitrogen the capacity is higher for the protonic mordenite, decreases with the increase of the nickel content, and is minimum for the sodium mordenite before or after exchange with nickel. The adsorption capacity of n-heptane of different samples follows the same order obtained for nitrogen. However the values determined with n-heptane are lower than with nitrogen, as the molecule of n-heptane, due to its diameter, is unable to access to the narrower channels of mordenite.

M. BROTAS DE CARVALHO
M. ALICE CONCEIÇÃO
Departamento de Química da Faculdade de Ciências de Lisboa
PORTUGAL

M. R. SALES GRADE
Centro de Química Física e Radioquímica INIC
Lisboa
PORTUGAL

CARACTERIZAÇÃO DE CARVÕES MICROPOROSOS POR ADSORÇÃO DE N_2 E CO_2

Por adsorção de gases (N_2 e CO_2) provou-se que o carvão activado Norit PK 1-3 e produtos obtidos a partir deste por impregnação com metais se caracterizam por uma distribuição muito estreita de microporos, de dimensões moleculares, para além de uma certa mesoporosidade.

Neste tipo particular de textura, discute-se a aplicação dos vários modelos de análise das isotérmicas (ponto B, Langmuir, Dubinin-Radushkevitch, BET, método t e de Pierce).

1 — INTRODUÇÃO

A caracterização de sólidos microporosos feita através da análise das isotérmicas de adsorção de gases constitui um problema complexo que não está inteiramente resolvido nem do ponto de vista teórico nem do da aplicação prática [1,2].

Quando os adsorventes apresentam simultaneamente microporos (com abertura, d, inferior a 2nm) e mesoporos (2<d<20nm) como acontece, por exemplo, na maioria dos carvões activados, nenhum dos métodos correntes para determinação do «volume de microporos» é, em geral, considerado satisfatório. Também neste caso, a aplicação da equação BET aos dados da adsorção de N_2 a 77K, de uso tão generalizado, conduz a valores de «área BET» com significado pouco preciso. Com efeito, por vezes, estes resultados divergem muito dos valores das «áreas específicas aparentes» estimadas por outros métodos de análise da isotérmica de azoto ou da análise de isotérmicas de outros gases, ou ainda dos valores obtidos por medidas de calorimetria.

Na análise da textura deste tipo de sólidos recorre-se frequentemente, para além do azoto, ao dióxido de carbono [3]. Admitindo que os poros dos adsorventes são, em princípio, igualmente acessíveis ao N_2 e ao CO_2, cujas dimensões moleculares críticas são equivalentes, o facto das experiências com CO_2 serem conduzidas a temperaturas muito mais elevadas poderá ser uma razão de preferência por este gás. E, considerando que a temperatura favorece a difusão nos poros mais estreitos, seria de prever que os «volumes de microporos», ou «áreas específicas aparentes», determinados com CO_2 à temperatura de 195K fossem superiores aos determinados com N_2 a 77K. Verifica-se na literatura que este é, de facto, o caso mais corrente, embora sejam citadas algumas excepções em que a «área» obtida com CO_2 é um pouco inferior à determinada com N_2.

O trabalho que se apresenta, sobre estudos de adsorção de N_2 e CO_2 em carvão activado e de adsorção de N_2 em produtos obtidos a partir

daquele material por impregnação com metais, permitiu obter uma correcta caracterização das superfícies e simultaneamente fazer algumas considerações sobre a validade dos métodos vulgarmente usados para determinação de texturas.

2 — PARTE EXPERIMENTAL

2.1 — *Instalação e Técnica Experimental*

As isotérmicas de adsorção foram determinadas numa instalação volumétrica convencional, equipada com dois manómetros de Hg, respectivamente em U e do tipo McLeod, e um Pirani. Os volumes foram calibrados com mercúrio e por expansão de hélio, da forma habitual, tal como vem descrito em [4]. O espaço morto, que se fez variar de 116 a 218 cm^3, com inclusão dos sucessivos volumes de uma bureta de gases, manteve-se termostatizado, com oscilações de temperatura inferiores a 0,5K. As temperaturas na célula de adsorção foram de 77,4 ± 0,1K e 195,0 ± 0,2K, respectivamente, nas experiências com N_2 e com CO_2.

Empregou-se hélio, azoto e dióxido de carbono com um grau de pureza superior a 99,95%, fornecidos em recipientes apropriados para que a sua transferência fosse feita sem contaminação.

O método foi testado com uma experiência de adsorção de N_2 a 77,4K, numa substância padrão, TK 800 da firma Degussa, de Área (BET) = 166 ± 2 m^2g^{-1} [5], tendo-se obtido uma dispersão experimental que não excedeu os 3%.

Em todas as experiências de adsorção, os carvões activados foram previamente desgaseificados durante quatro horas à temperatura de 500K e com um vazio da ordem de 10^{-2} Pa, constatando-se uma perda de cerca de 17% em peso, correspondendo esta diferença à humidade, que é recuperada quando a amostra é exposta ao ar.

Nas experiências com N_2 provou-se que o equilíbrio de adsorção era atingido em tempos inferiores a 10 minutos. Para obter a curva de desadsorção e evitar os erros devidos ao não equilíbrio entre a temperatura ambiente e a do interior do espaço morto, quando o gás é deslocado da célula que mergulha no azoto líquido, prolongaram-se os tempos de contacto para 30 minutos.

Os resultados que se apresentam referem-se à massa de carvão no final das experiências de adsorção.

2.2 — *Adsorventes*

O carvão activado Norit PK 1-3, de densidade aparente 0,25 g cm^{-3} e uma granulometria superior a 1,0mm em 88% da massa, foi utilizado sem qualquer tratamento prévio e é referenciado neste trabalho por «carvão AC».

Os produtos impregnados a partir deste carvão foram preparados no Centro de Engenharia do Porto e têm as seguintes designações e características: AC/Fe (com 4,6% de Ferro); AC/Co (com 8,05% de Cobalto) e AC/Ni (com 4,20% de Níquel) [6].

A isotérmica de N_2 em carvão AC foi traçada com dados obtidos em três experiências realizadas com amostras diferentes do carvão, que variaram entre 0,1 e 0,6g. Nos restantes ensaios usaram-se quantidades de carvão de cerca de 0,1g.

3 — RESULTADOS

3.1 — *Adsorção de N_2 em carvão AC*

Os resultados apresentados nas figuras 1 e 2 traduzem uma isotérmica de adsorção do tipo II/IV na classificação da IUPAC [7], e mostram que a curva de desadsorção não é única, mas depende das condições em que é obtida.

A pressões moderadas, de P/P° inferior a 0,6, a isotérmica inicial parece reversível (Fig. 1), porém, sempre que é excedido aquele valor, observa-se, na desadsorção, uma histerese residual que virtualmente se mantém até à origem da isotérmica (Fig. 2). Verificou-se que esta histerese desaparece com a desgaseificação a temperaturas mais elevadas.
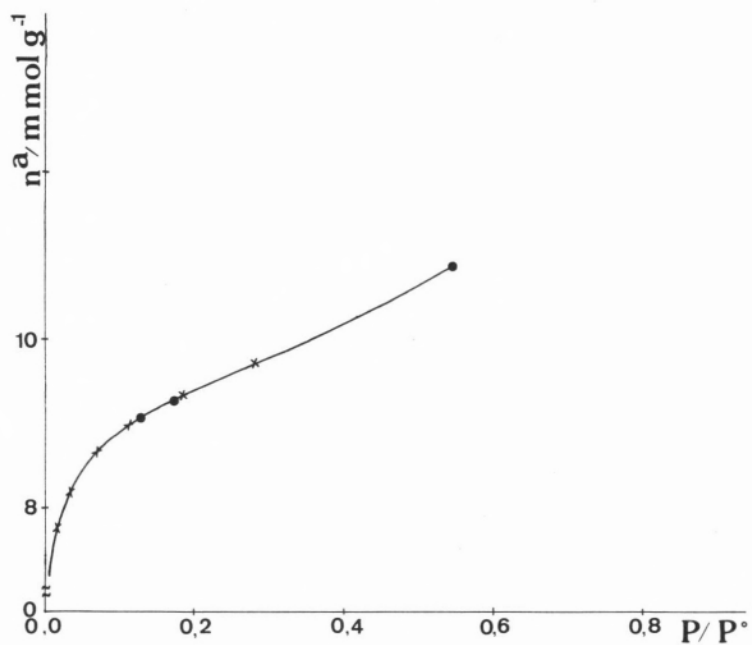
Figura 1

Isotérmica de adsorção de azoto em carvão Norit PK 1-3 a 77,4K (● adsorção; × desadsorção)
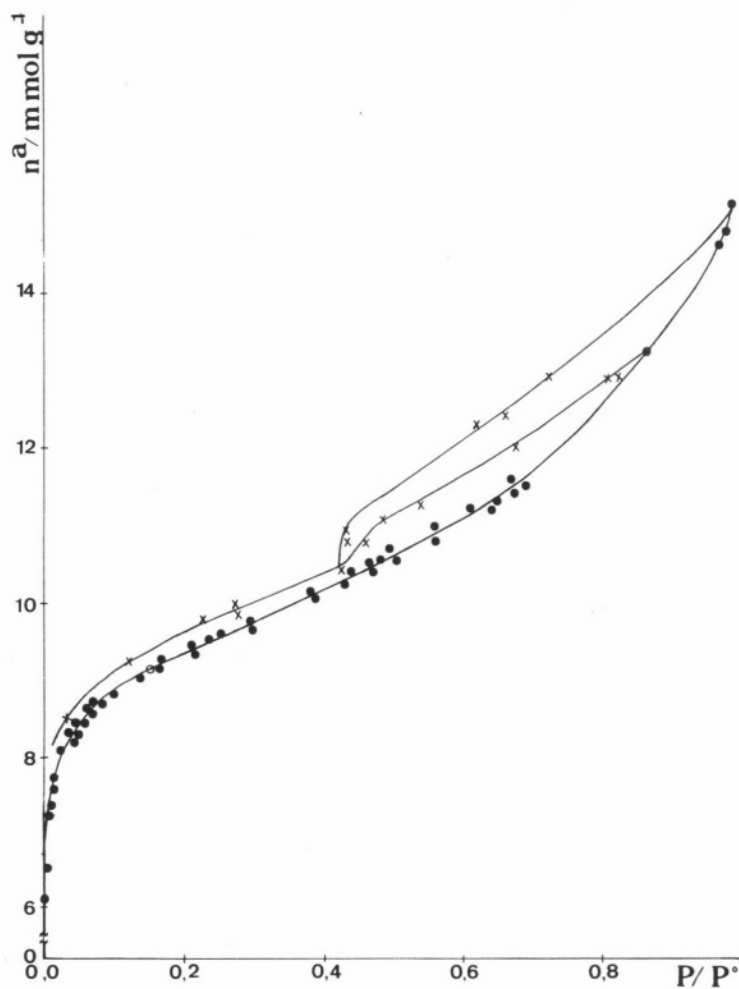

Figura 2

Isotérmica de adsorção de azoto em carvão Norit PK 1-3 (● adsorção; × desadsorção)

A adsorção não reversível, que se detecta a pressões relativas entre 0,42 e 0,96 e que é devida à estrutura mesoporosa do adsorvente, caracteriza-se por ciclos de histerese do tipo H3, que indicam uma provável existência de poros em forma de fenda, ou poros com orifícios de acesso muito estreito formados em agregados de partículas [7].

Procedeu-se, em primeira lugar, à análise da parte inicial da isotérmica de adsorção recorrendo-se aos modelos de Langmuir, Dubinin-Radushkevitch (DR) e ao método do ponto B, que permitem fazer uma estimativa da capacidade equivalente da monocamada, n^a_m, e consequente valor da área específica, A, ou área específica aparente, A_{ap}, no caso de os adsorventes serem também microporosos [8]. Os métodos «t» e de Pierce foram aplicados numa zona mais extensa das isotérmicas, até aos valores máximos da pressão relativa [8].

Apresentam-se, na Tabela I, os resultados das várias equações e respectivos intervalos em que foram aplicadas, sendo de assinalar que, em toda a gama de valores de pressões relativas, os dados de adsorção foram tratados por dois ou mais métodos.

Pela equação de Langmuir obteve-se um valor de n^a_m = 9,09 mmol g^{-1}, que é praticamente igual ao que corresponde ao do ponto B, determinado sobre a isotérmica, e que é cerca de 15% superior ao valor estimado com o modelo BET.

Mostra-se na figura 3 a representação de Dubinin-Radushkevitch que, igualmente, lineariza a isotérmica de adsorção até uma pressão relativa de 0,08. O valor da ordenada na origem, que, segundo alguns autores [9], pode, em certos casos, traduzir a capacidade da monocamada, n^a_m, é também muito seme-
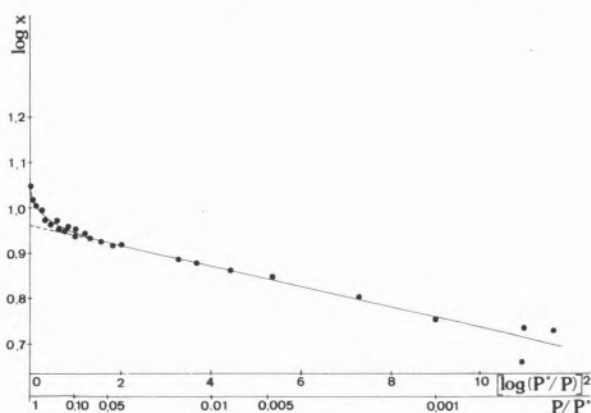

Figura 3

Representação de Dubinin-Radushkevitch (DR)
(x = quantidade adsorvida de azoto a 77,4 K
em carvão AC (mmol g^{-1}).

Tabela I

Resultados da análise da isotérmica de N_2 a 77,4 K em carvão AC

Método Int. aplicação (P/P°)	Ponto B 0,015	Langmuir 0-0,15	DR 0,001-0,08	BET (c >1000) 0,005-0,15	t 0,08-0,90	Pierce 0,42-0,96	R. Gurvitch 0,96
n^a_m/mmol g^{-1}	9,11	9,09	9,24	7,82	—	—	—
A_{ap}/m^2 g^{-1}	887 ± 6	886 ± 10	900 ± 5	763 ± 4	—	—	—
n^a_{par}/mmol g^{-1}	—	—	—	—	2,03	2,03	—
A_{par}/m^2 g^{-1}	—	—	—	—	198 ± 5	198	—
n^a_{mic}/mmol g^{-1}	—	—	—	—	6,79	—	—
V_{mic}/cm^3 g^{-1}	—	—	—	—	0,237 ± 0,005	—	—
V/cm^3 g^{-1}	—	—	—	—	—	—	0,499 ± 0,003

n^a_m, A_{ap} — capacidade equivalente da monocamada e área específica aparente
n^a_{par}, A_{par} — capacidade da monocamada e área específica de mesoporos
n^a_{mic}, V_{mic} — capacidade e volume de microporos com abertura inferior a 0,4 nm
V — volume total de poros

lhante ao valor calculado pela equação de Langmuir.

Para analisar a parte da isotérmica de adsorção correspondente a $P/P^o > 0,08$ aplicou-se «o método t» que se baseia numa comparação com curvas de referência obtidas em sólidos não porosos de materiais apropriados. Utilizou-se a curva padrão de Lippens e de Boer que, na bibliografia, é correntemente usada no estudo da textura de carvões [10].

Como pode observar-se na fig. 4, a representação n^a versus t é linear numa grande extensão da pressão relativa, correspondendo este intervalo a valores de espessura da camada adsorvida, t, compreendidos aproximadamente entre 0,4 e 0,8nm, dando a indicação da inexistência de microporos com aberturas de pelo menos 0,8nm até 1,6nm.
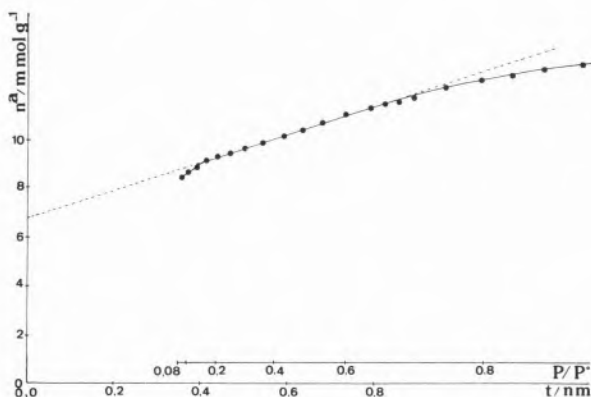

Figura 4

Representação t. (t- espessura estimada da camada adsorvida de azoto em carvão AC)

Através do declive desta recta estimou-se a capacidade da monocamada parcial, n^a_{par}=2,03 mmol g⁻¹, atribuível à área externa ou área de poros com abertura superior a cerca de 1,6nm.

Da extrapolação da mesma recta até ao eixo das ordenadas, obteve-se o valor da capacidade de microporos muito estreitos, com largura igual ou inferior a 0,8nm, n^a_{mic}=6,79 mmol g⁻¹.

É interessante verificar que a soma das duas quantidades calculadas pelo método t, n^a_{par} e n^a_{mic}, perfaz um valor muito semelhante ao valor da capacidade equivalente da monocamada, n^a_m, estimado por três dos métodos anteriormente citados, de Langmuir, de Dubinin e do método do ponto B.

Aplicou-se ainda o método de Pierce à curva de desadsorção, definida entre as pressões relativas de 0,42 e 0,96. Admitindo poros cilíndricos, com raio superior a 1,7 nm, obteve-se um valor de área cumulativa de 198 m²g⁻¹.

Com os valores de n^a_m e n^a_{par} calcularam-se, respectivamente, os valores estimados da área específica aparente A_{ap} e da área específica parcial A_{par}, admitindo para o N_2 uma área de influência, na monocamada, de 0,162 nm². O volume de microporos foi calculado a partir do valor de n_{mic} e o volume total de poros, pela regra de Gurvitch, considerando que o N_2 adsorvido está no estado líquido com um volume molar de 35 cm³ mol⁻¹.

3.2 — *Adsorção de CO₂ sobre carvão AC*

A adsorção de dióxido de carbono em carvão AC, à temperatura de 195K, processa-se em duas fases distintas, sendo a primeira muito rápida, à semelhança do que acontece com a adsorção de N_2 a 77,4K, e a segunda muito lenta como pode verificar-se na figura 5, onde se regista a evolução da pressão ao longo do tempo no sistema CO_2 — carvão AC.
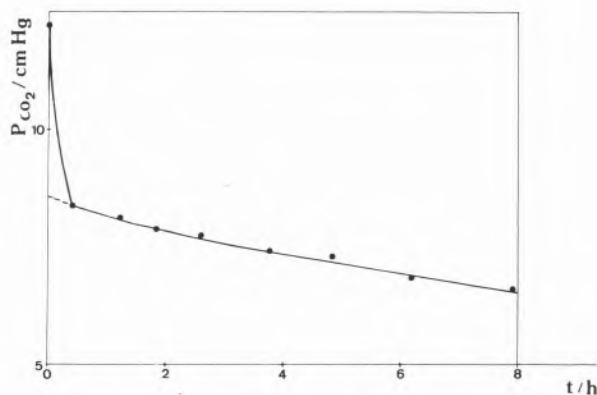

Figura 5

Evolução da pressão ao longo do tempo. Condições iniciais: 0,234 g de carvão AC e 1,33 mmol de CO₂.

A quantidade adsorvida correspondente a tempo zero permitiu calcular, pelo método BET, o valor da área específica que corresponde a uma adsorção quase instantânea do CO_2.

Usando os valores limites mais vulgarmente encontrados na bibliografia para a área de ocupação do CO_2 na monocamada, respectivamente, de 0,163 e 0,195 nm², chega-se á conclusão que a área parcial do carvão que é facilmente acessível a este gás, compreendida entre 164 e 196 m²g⁻¹, representa apenas cerca de um quinto da área específica total aparente.

3.3 — Adsorção de N_2 em carvões impregnados

Os dados da adsorção do N_2 a 77,4K, determinados até pressões relativas de 0,1 nos carvões impregnados, foram analisados pela equação de Langmuir, tal como aconteceu no caso do carvão AC.

As áreas específicas aparentes, que aparecem na Tabela II, apresentam variações que são da mesma ordem de grandeza da dispersão experimental o que mostra que o processo da impregnação não afectou significativamente a textura do carvão original.

Tabela II
Áreas específicas aparentes (m²g⁻¹)
estimadas pelo método de Langmuir

carvão AC	—	89×10
carvão AC/Fe	—	91×10
carvão AC/Co	—	90×10
carvão AC/Ni	—	87×10

4 — CONCLUSÕES

A análise conjunta dos resultados experimentais da adsorção de N_2 e de CO_2, em carvão Norit PK 1-3, permitiu chegar a interessantes conclusões acerca da textura deste adsorvente, o que não teria sido possível se se dispusesse apenas dos dados de adsorção de um destes gases.

Observaram-se efeitos de peneiração molecular em relação aqueles dois adsorvatos, raramente citados na bibliografia, que mostraram que, neste carvão activado, existe uma quantidade apreciável de poros penetráveis pelo azoto e onde não entram com facilidade as moléculas de dióxido de carbono.

Considerando a semelhança entre as dimensões moleculares de N_2 e do CO_2 (respectivamente com diâmetros de Pauling 0,30 e 0,37 nm [11] e diâmetros cinéticos críticos de 0,38 e 0,39 nm [12]), concluiu-se que, neste caso, se deve tratar de um tipo muito uniforme de microporos, com aberturas muito estreitas, da ordem de grandeza do tamanho daquelas moléculas, seguramente inferiores a 0,4 nm.

Verificou-se, por outro lado, que a área específica do carvão, onde se processa uma adsorção rápida de CO_2, é da mesma ordem de grandeza da área específica parcial de mesoporos, concluindo-se, deste modo, que praticamente não existem microporos para além dos de largura inferior a 0,4 nm.

Esta conclusão, completa a análise feita pelo método t à isotérmica de adsorção de N_2, segundo a qual apenas foi possível estabelecer um limite superior de 0,8 nm para o diâmetro equivalente de microporos, e um volume total destes de cerca de 0,24 cm³ g⁻¹.

Nas experiências com azoto, detectou-se uma histerese de adsorção, a pressões relativas reduzidas, que põe ainda de manifesto a existência de uma pequena percentagem de poros mais estreitos, onde a acessibilidade deste gás está condicionada a um valor mínimo da pressão, provavelmente devido à falta de rigidez da estrutura do carvão.

A irreversibilidade nos processos de adsorção-desadsorção do azoto, evidenciada na Figura 2, entre pressões relativas de 0,42 e 0,96, mostra claramente que o adsorvente apresenta também mesoporosidade, a que corresponde uma área parcial de 198 m² g⁻¹, de acordo com as estimativas feitas tanto pelo método de Pierce como pelo método t (Tabela I).

Em relação aos resultados da área específica aparente, apresentados na Tabela I, somos levados a supôr que, por se tratar de um sólido com microporosidade de dimensões moleculares, se pode atribuir um significado físico (relacionado com a soma das capacidades de microporos e da monocamada de mesoporos), aos valores concordantes obtidos pelos métodos de Langmuir, de DR e do ponto B. As áreas BET, pelo contrário, parecem evidenciar mais uma vez que o modelo não se ajusta às condições reais da superfície, não devendo ser considerado na caracterização de sólidos microporosos.

AGRADECIMENTOS

REFERÊNCIAS

[1] J. M. M. MARTINEZ, F. F. REINOSO e M. M. SABIO, Carbon 24, 255 (1986).
[2] M. M. DUBININ, Carbon 21, 359 (1983).
[3] B. RAND, J. Coll. Interface Sci., 56, 337 (1976).
[4] A. RUIZ PANIEGO, M. BROTAS CARVALHO, Anales de la Real Sociedad Española de Quimica y Fisica, 67, 705 (1971).
[5] D. H. EVERETT, G. D. PARFITT, K. S. W. SING, R. WILSON, J. Appl. Chem. Biotechnol, 24, 199 (1974).
[6] J. L. FIGUEIREDO, M. C. A. FERRAZ, «Comunicação no 1.º Congresso Mediterrâneo de Engenharia Química», Barcelona, 1978.
[7] Reporting Physisorption Data for Gas/Solid Systems. Pure Appl. Chèm., 57, 603 (1985).
[8] S. L. GREGG e K. S. SING, Adsorption, Surface Area and Porosity, Academic Press, Londres (1967). 2.ª Ed. (1982).
[9] M. G. KAGANER, Zhur. Fiz. Khim, 32, 2202 (1959).
[10] B. C. LIPPENS e J. H. DE BOER, J. Catalysis, 4, 319 (1965).
[11] D. W. BRECK, Zeolite Molecular Sieves. Structure, Chemistry, and Use. Wiley Interscience (1974), p. 636.
[12] R. C. REID, J. M. PRAUSNITZ, T. K. SHERWOOD, The Properties of Gases and Liquids. McGraw-Hill Co. 3.ª Ed. (1977), p. 678.

ABSTRACT

Characterization of microporous carbons by adsorption of N_2 and CO_2

Through adsorption of gases (N_2 and CO_2), it has been shown that the activated carbon Norit PK 1-3 and the products obtained from it by impregnation with metals can be characterized by a very fine distribution of micropores with molecular sizes, and also some mesoporosity.
In this particular type of texture, it is discussed the application of several models for isotherms analysis (point B, Langmuir, Dubinin-Radushkevitch, BET, method t and Pierce).

A. M. P. S. GONÇALVES DA SILVA
C. A. NIETO DE CASTRO
V. A. M. SOARES
Centro de Química Estrutural, Complexo I
1096 Lisboa Codex
PORTUGAL

A. O. S. MACZEK
Departament of Chemistry
The University
Sheffield S3 7HF
UNITED KINGDOM

REFRACTIVES INDEXES AND EXCESS MOLAR VOLUMES OF THE SYSTEM BENZENE + TOLUENE AT 303 K

An accurate method for measuring the composition of liquid mixtures using differential refractometry is presented. The refractometer used can easily detect changes in refractive index of the order of 1 part in 10[7], and so can be applied to the determination of small changes in composition. The refractive indexes of binary mixtures of benzene + toluene have been measured at 303.15 K and compared with absolute measurements made with a Pulfrich refractometer. The results show that is is possible to detect changes in refractive index with an uncertainty amounting to no more than a few parts per million. For the system studied here, this corresponds to a change in mole fraction of the order of 0.001.

Excess molar volumes as a function of composition were evaluated for this system using the Lorenz-Lorentz equation. The molar excess volume for an equimolar mixture was found to be +0.080 cm³ mol⁻¹. Comparision with available literature data suggests that the present values are accurate to within ± 0.001 cm³ mol⁻¹.

INTRODUCTION

Differential refractrometry of the type used in high pressure liquid chromatography is often sufficiently sensitive to detect changes in refractive index of the order of one part in 10^7; the technique can provide a very accurate means of measuring very small changes in composition. In our laboratory in Lisboa we have developed a method, using a commercial differential refractrometer (Waters Model R401), which allows us to measure the relative adsorption on activated charcoal and silica of liquid compounds which are chemically very similar. The first such system to be studied was the adsorption by silica from benzene + toluene mixtures.

Benzene and toluene have very similar values of refractive index [1]; the difference in refractive index for the pure components is only 0.00352 at 303.15K. This suggests that a change in mole fraction of 0.001 will produce a change in refractive index of the order of only 3×10^{-6}. Such small change in refractive index can be measured reliably only with a differential device.

In this work we present the experimental values of refractive index obtained in mixtures of benzene + toluene at 303K and also the excess molar volumes calculated using the Lorenz-Lorentz equation. A comparison with literature results is shown in the last part of this note.

PROCEDURE

The differential device operates by comparing the refractive index of a test sample with that of a reference fluid; the output signal is related to the difference in refractive index, Δn, between sample and reference; this relation is linear providing Δn does not exceed 0.001. Consequently, in order to obtain a full curve of refractive index vs. mole fraction $(0 < x < 1)$ a series of intermediate reference fluids must be used. Toluene (Fluka, > 99.5% GLC) was taken as the first refe-

rence fluid and Δn was measured for several toluene-rich mixtures up to a composition x_1' is benzene such that the refractive index at this composition differed by no more than 0.001 from that of pure toluene. This mixture (x_1') was then taken as the second reference and Δn was measured for a further set of compositions from x_1' to x_1'', once again within 0.001 of the refractive index of x_1'. This procedure was followed up to a mole fraction of benzene x_1 of about 0.5, and then repeated in the reverse direction starting with pure benzene (Fluka, > 99.5% GLC) as the first reference, until a mole fraction of toluene $x_2 = 0.5$ had been reached. Measurements were carried out at the wavelength of the sodium D-line.

The experimental value for a particular composition x_j was obtained using the expression

$$n_j = n_{b,t} + \sum_{j=1}^{N} \Delta n_j \qquad (1)$$

where $n_{b,t}$ referes either to benzene or to toluene (depending on which was the first reference fluid chosen) and the summation is taken over all N intermediate references mixtures. Such a method is clearly very prone to the accumulation of intermediate reference errors which would show up as a mis-match at $x = 0.5$ between the two sides of the refractive index vs. mole fraction curve. The absence of any such mis-match gives us confidence in the reliability of our experimental procedures.

For binary mixtures, the molar refraction, R_m, in terms of the molar volume, V_m, is given by:

$$R_{m,12} = \left[\frac{n_{12}^2 - 1}{n_{12}^2 + 2}\right] V_{m,12} = x_1 R_{m,1} + x_2 R_{m,2} \qquad (2)$$

where

$$R_{m,i} = \left[\frac{n_i^2 - 1}{n_i^2 + 2}\right] V_{m,i} \qquad (3)$$

Using (2) and (3) one gets for the molar excess volume V^E :

$$V^E = V_{m,12} - x_1 V_{m,1} - x_2 V_{m,2}$$

$$= \left[\left(\frac{n_{12}^2 + 2}{n_{12}^2 - 1}\right)\left(\frac{n_1^2 + 2}{n_1^2 - 1}\right) - 1\right]V_{m,1}x_1 +$$

$$\qquad (4)$$

$$+ \left[\left(\frac{n_{12}^2 + 2}{n_{12}^2 - 1}\right)\left(\frac{n_2^2 + 2}{n_2^2 - 1}\right) - 1\right]V_{m,2}x_2$$

RESULTS

The experimentally measured refractive indexes and the derived molar volumes are shown as a funcion of composition in Table I. In Figure 1, the excess refractive index (defined for a binary solution as $n^E = n_{12} - (n_1 x_1 + n_2 x_2)$) is plotted against

Table I

Refractive index and molar volume at 303K for $C_6H_6 + C_6H_5CH_3$

x_1	n	V_m/cm^3 mol^{-1}
0.0	1.49126[α]	107.444
0.0186	1.491290	107.123
0.0371	1.491322	106.804
0.0737	1.491380	106.174
0.1457	1.491499	104.934
0.2847	1.491790	102.532
0.3738	1.492014	100.986
0.4432	1.492214	99.779
0.4942	1.492377	98.890
0.5442	1.492550	98.016
0.5934	1.492733	97.154
0.6417	1.492927	96.307
0.6892	1.493131	95.472
0.7359	1.493346	94.649
0.7818	1.493565	93.840
0.8269	1.493798	93.043
0.8712	1.494035	92.259
0.9149	1.494276	91.485
0.9578	1.494524	90.724
0.9737	1.494619	90.442
0.9869	1.494699	90.207
1.0	1.49478[α]	89.974

α — values obtined from reference [1]

the benzene mole fraction x_1, together with the results at 301K of Trew and Spencer [2] and some recent unpublished measurements at 303K by Maczek and Humphreys [3].

Although the excess funtion n^E has no particular theoretical significance, this method of

mended by Myers and Scott [4]. The optimum degree of the fit k was found using the criteria of minumum variance. The series in equation (5) converges rapidly and a value of k=2 is adequate to describe the experimental points. As the excess refractive index curve is only
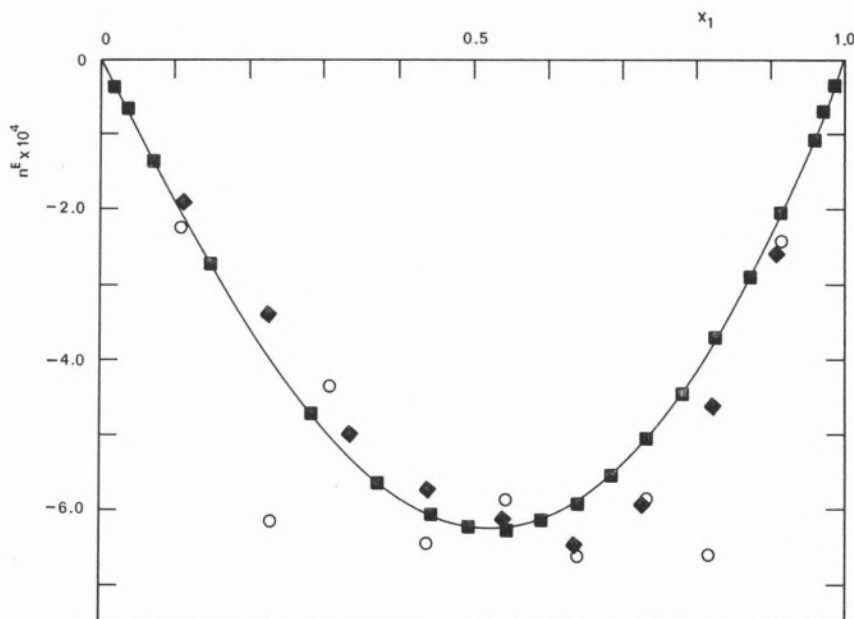
Figure 1

The excess refractive index n^E for the system benzene+toluene at 303K
as a function of mole fraction of benzene

◆ — Maczek and Humphreys [3]
O — Trew and Spender [2], at 301K
■ — present work

presentation reveals very clearly any experimental uncertainty in the raw data, and provides an immediate visual test of their internal consistency.

The fitted curve in Figure 1 has been obtained using an equation of the Redlich-Kister type

$$n^E = x_1 \ x_2 \ \sum_{j=0}^{k} \ a_j \ (1 - 2x_1)^j \qquad (5)$$

with the coefficients a_j found by a least-squares method using a fitting program recom-

slightly skewed, there is no need for an additional skweing parameter, as described by Myers and Scott [4], in order to fit the data. The optimised parameters for this fit are:

$$a_0 = (-24.96 \pm 0.03) \times 10^{-4}$$
$$a_1 = (3.186 \pm 0.063) \times 10^{-4}$$
$$a_2 = (2.073 \pm 0.130) \times 10^{-4}$$

with a root mean square deviation for the fit of 1.56×10^{-6} units of refraction index.

The absolute data of Maczek and Humphreys [3] lie close to our data but are slightly more skewed; the results of Trew and Spencer [2] show considerable scatter around the least-squares curve.

The results show that our method can detect changes in refractive index with an uncer-

$V_{m,2}$ for the pure components were taken from reference 1. In Figure 2 we show the calculated values and a curve fitted to equation with the same form than equation (5) by the method of Myers and Scott [4] as used earlier. Once again the series converges rapidly and an order of fit k=2 is adequate to describe the
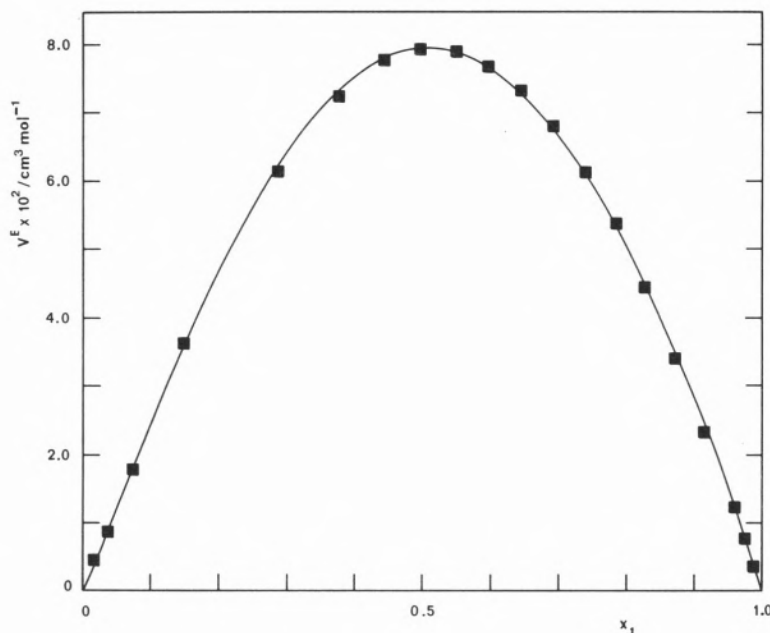
Figura 2

The excess volume V^E for the system benzene+toluene at 303K as a function of mole fraction of benzene

tanty that amounts to no more than a few parts per million. For the system benzen + toluene this corresponds to an uncertainty in mole fraction of about ± 0.001. This system, in which the difference in the refractive index of the pure components is so small, is a very stringent test of the method we propose for measuring small changes in composition, and illustrates how useful differential refractro-metry can be in the pursuit of this experimental objective.

The excess molar volumes were calculated from equation (4); the molar volumes $V_{m,1}$ and

derived data. The optimised parameters for this fit are:

$$a_0 = (+31.81 \pm 0.07) \times 10^{-2} \text{ cm}^3 \text{ mol}^{-1}$$

$$a_1 = (-1.782 \pm 0.147) \times 10^2 \text{ cm}^3 \text{ mol}^{-1}$$

$$a_2 = (-4.121 \pm 0.302) \times 10^2 \text{ cm}^3 \text{ mol}^{-1}$$

with a root mean square deviation of 0.0004 cm^3 mol^{-1}.

Figure 3 shows a deviation plot between the experimental points and the value evaluated with the fit. It can be seen that no experimen-

tal point deviates from the fit by more than 0.001 cm³ mol⁻¹. Table II contains some literature values [5,8] for the molar excess volume at equimolar composition together with the results obtained by us. A graphical comparison is made in Figure 4.
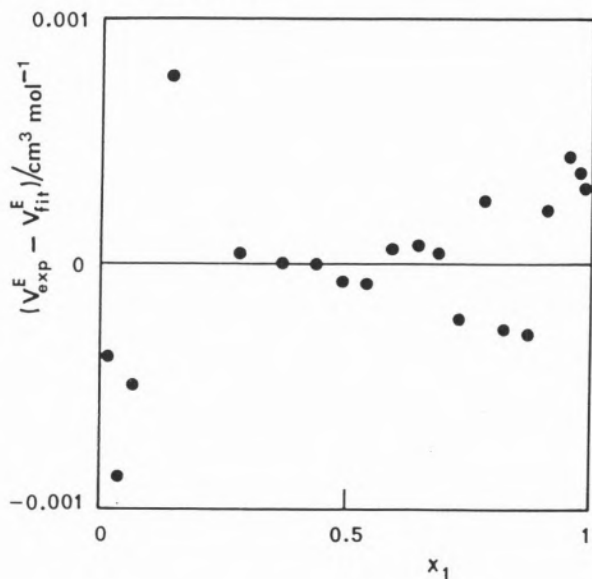

Figure 3

The deviations between the measured excess volumes and the values given by the numerical fit

Over so small a temperature range it is reasonable to assume a linear variation of V^E with temperature. on this basis, as Figure 4 shows, our result lend support to those of Ocon *et al.* [5] and Murakami *et al.* [7], but lies outside the mutual uncertainties of the results of Iguchi [8] and of Diaz-Pena and Delgado [6]. The excess molar volume is very small (of the order of 0.1 cm³ mol⁻¹) and we believe that

Table II

Equimolar excess volume data for $C_6H_6 + C_6H_5CH_3$

T/K	$10^6 \, V^E / m^3 mol^{-1}$	Reference
273	0.108 ±0.002	5
298	0.044 ±0.003	6
298	0.088 ±0.002	7
303	0.050 ±0.005	8
303	0.080 ±0.001	Present work

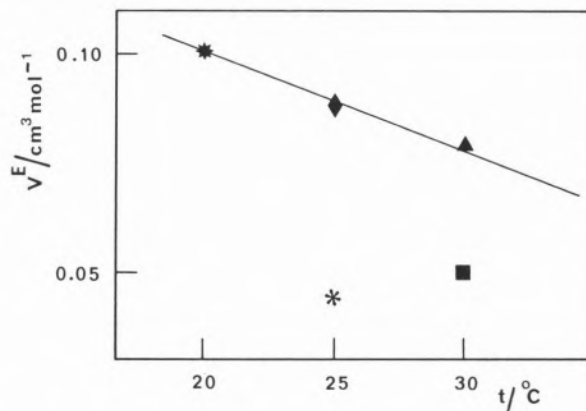our method provides a relatively straightforward means of measuring such small quantities.

Figure 4

The equimolar excess volume V^E for the system benzene+toluene as a function of temperature

* — Ocon *et al.* [5]
* — Diaz Peña *et al.* [6]
♦ — Murakami *et al.* [7]
■ — Iguchi *et al.* [8]
▲— present work

ACKNOWLEDGEMENTS

REFERENCES

[1] J. TIMMERMANS, in *«Physico-Chemical Constants of Pure Organic Compounds.*, Vol. 2, Elsevier Publishing Co., Amsterdam (1965).
[2] V. C. G. TREW and J. F. SPENCER, *Trans. Faraday Soc.,* **32**, 701 (1936).
[3] A. O. S. MACZEK and C. A. HUMPHREYS, unpublished results; Absolute measurements made with a Pulfrich refractometer.
[4] D. B. MEYERS and R. L. SCOTT, *Ind. Eng. Chem.,* **55**, 43 (1963).
[5] J. OCON, G. TAJO and L. ESPADA, *An. Quim.,* **65**, 727 (1969).

[6] M. Diaz-Pena and J. N. Delgado, *An. Quim.*, **73**, 24 (1967).

[7] S. Murakami, V. T. Law and G. C. Benson, *J. Chem. Therm.*, **1**, 397 (1969).

[8] A. Iguchi, *Kagaku Sochi*, **10**, 74 (1968).

RESUMO

Índice de refracção e volume molar de excesso do sistema benzeno + tolueno a 303 K

Apresenta-se um método de grande exactidão para determinação da composição de misturas líquidas binárias através da refracto-metria diferencial. O refractómetro usado detecta facilmente variações de índice de refracção da ordem de 1 em 10^7 pelo que pode ser utilizado na determinação de pequenas variações de composição. Mediram-se os índices de refracção de misturas binárias de benzeno + tolueno a 303.15 K e compararam-se com as medidas absolutas feitas com um refractómetro Pulfrich. os resultados mostram que é possível medir variações de índice de refracção com uma incerteza não superior a algumas partes por milhão. para o sistema estudado isto corresponde a uma variação de fracção molar da ordem de 0.001.

Os volumes molares de excesso em função da composição foram determinados através da equação de Lorenz-Lorentz. O volume molar de excesso encontrado para a mistura equimolar foi 0,080 cm^3 mol^{-1}. A comparação deste valor com os valores experimentais encontrados na literatura sugere que os resultados presentes têm uma exactidão de ± 0,001 cm^3 mol^{-1}.

LAURA M. ILHARCO
A. F. DO VALE
J. LOPES DA SILVA
Centro de Química Física Molecular, Complexo I do INIC
Instituto Superior Técnico
1096 Lisboa Codex
PORTUGAL

A CHAMBER FOR SPECTROSCOPIC STUDIES OF ORGANIC VAPOURS

A chamber designed to study photochemical and photophysical properties of organic vapours is described. Some results obtained in absorption and fluorescence experiments performed with it are presented.

1. INTRODUCTION

For spectroscopic studies of organic vapours, different apparatus have been designed in order to produce the vapour, control and measure its temperature and pressure. They usually consist of an irradiation cell and a side arm, where vaporization of the product is carried out. Both compartments being made of pyrex or quartz, their heating requires the use of external metal furnaces. Temperatures are measured by thermocouples or platinum resistance thermometers placed in the furnaces walls [1, 5].

In the present work a chamber of this kind is described, which presents some interesting characteristics: as it is made of stainless stell, the walls themselves are the furnaces and the temperatures are taken inside the chamber, in the bulk vapour, which means that they are more accurate measures of the real temperatures. Of known dimensions, this chamber is suitable for experiments performed when only the vapour phase is present and in conditions of phase equilibrium (solid or liquid//vapour).

2. DESCRIPTION

The diagram of the chamber is displayed in Fig. 1. It also consists of two compartments: the vaporization cell (V. C.), where the solid or liquid is introduced and vaporized, and the irradiation cell (I. C.), where the vapour is irradiated. They communicate through a tube, whose dimensions were optimized in order to satisfy two contradictory conditions: be narrow and long enough so that temperature gradients were significant along the tube but not in either cell and be large and short enough to guarantee a rapid establishment of thermal equilibrium; the best compromise was obtained for a length of 15mm and a diammeter of 2mm.

The vacuum sealing on the cover of the V. C. is assured by a pure gold O-ring. All the remaining O-rings indicated in Fig. 1 are in

fluoro-carbon rubber (Aerospace Material Specification 7278E), previously annealed to 150°C. They do not degase and are mechanically resistant to the temperatures and pressures of work.
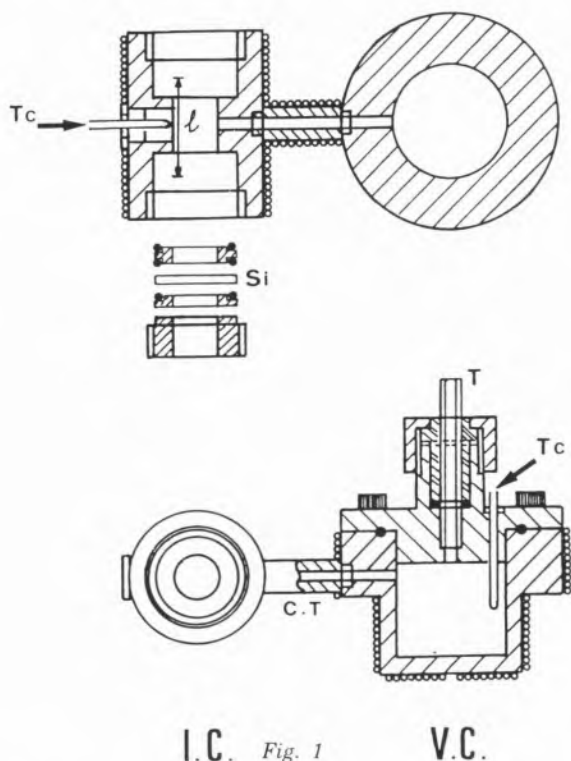
I.C. *Fig. 1* V.C.

Diagram of the vapour chamber: I. C. — irradiation cell; V. C. — vaporization cell; C. T. — communication tube; T — Pyrex tube which connects the chamber to a vacuum line; Tc — thermocouples; l — radiation path length; Si — fused silica windows; ● — pure gold O-ring; ● — fluoro-carbon O-rings; ○ — thermocoax heating elements.

The vapour chamber may be connected to a vacuum line through the glass tube (T) placed on top of the V. C.

The interior volume of the chamber, including the glass tube up to the level where it is sealed, was determined both by calculations and by filling with water at 20°C as 5.25 ± 0.01 cm³.

The two cells are thermostatized separately by means of Thermocoax heaters (reference ZAZ Ac 10 from S. A. Sodern), made of nickel chromium 80/20, with a resistivity of 108 μΩ/cm, and with low resistance cold ends of nickel chromium tube with CuZr filling. The insulating material is high purity MgO and

the sheath of austenitic stainless stell. The outer diammeter is 1.0 cm and the total length was conveniently dimmensioned according to the power needed to heat each cell (the communicating tube was included, for this purpose, in the irradiation cell). The heating elements were coiled around the chambers and, to improve thermal contact, metal wrappers were fixed around the heating elements.

Temperatures are measured by Thermocoax thermocouples of iron-constantan, with 18-8 stainless stell sheath and characterized by an output voltage of approximately 55 μV/°C. Their external diammeter is of 2mm. They are silver-brazed, respectively to the V. C. cover and to the wall of the I. C. (see Fig. 1), the hot junction being inserted in a suitable cavity not to interfere with the radiation path. The thermocouples are connected to Pastocomp temperature controllers (PD model) having a sensitivity higher than 0.5°C in the measured value.

Some care had to be taken in order to correct the thermocouples readings: as may be seen in Fig. 1, the hot junction was placed too close to the cell walls in the I. C., and so its information could be influenced by conduction through the thermocouple sheath. Tests were made placing a similar but insulated thermocouple in the bulk vapour, in the middle of radiation path. A curve of these last readings *versus* the values obtained with the brazed thermocouple was used as a calibration. The same kind of tests showed that this problem did not occur in the V. C..

Each system thermocouple-controller was calibrated separately by comparison with the readings of calibrated Hg thermometers immersed in water and in oil baths, for temperatures between 15 and 220°C, exactly in the same conditions as the thermocouples.

Fused silica windows were used in the I. C., but they can obviously be replaced by windows made of any other adequate material. The optical path length through the vapour, once the setting is complete, is 17.60 ± 0.05 mm.

3. EXPERIMENTS PERFORMED WITH THE CHAMBER. RESULTS

As mentioned before, visible or UV absorption of organic vapours may be studied with this chamber at different temperatures, either at constant concentration either in equilibrium of phases (the concentration depending, in this case, on the temperatures of both cells [6]).

The first kind of measurements requires an accurate knowledge of the vapour concentration. In order to minimize the errors in such determination, the compound, previously degased, must be weighed under vacuum atmosphere in a microanalytical balance. As the weight of the whole chamber largely exceeds the capacity of such balances, an appropriate Pyrex device was designed for this purpose (see Fig. 2). It consists of a bulb (A) where the substance is introduced, a con-
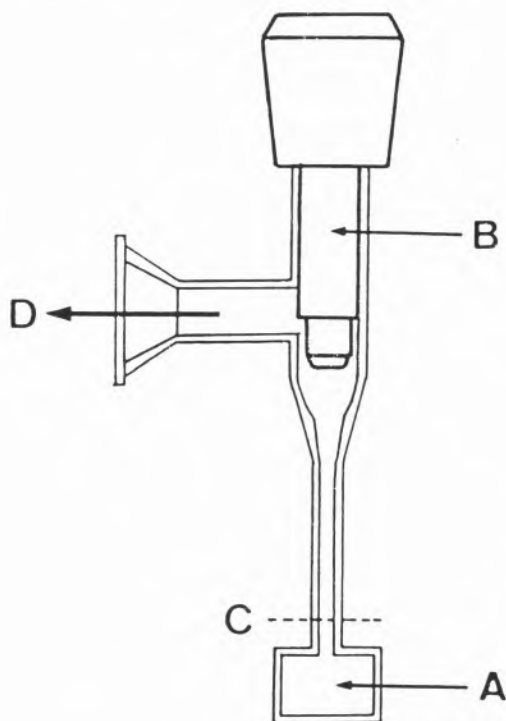

Fig. 2

*Pyrex glass device to prepare the vapour samples: **A** — bulb where the product is introduced; **B** — Teflon stopcock; **C** — level where it is sealed off; **D** — connection to vacuum line.*

nection to a vacuum line (D), where Viton O-rings are used, and a «Rotaflo» tap (B) with Teflon stopcock, to avoid any contaminations produced by the currently used vacuum grease.

To prepare the vapour samples, the following procedure is used: the device, previously cleaned, is evacuated to nearly 10^{-4} Pa. After closing tap B, it is weighed in a microanalytical balance Mettler M5/S5 (W_A). The piston is removed and an approximately known volume of the liquid (or weight, if a solid) is introduced in the bulb (A) through the top. It is then degased by the classic vacuum technique. After several freeze-pump-thaw cycles, (B) is closed and the weight of the whole apparatus is determined (W_B). The bulb, immersed in liquid nitrogen, is sealed off at level C and introduced in the V. C., which is evacuated and also sealed. A ring in stainless stell with a sharp point has been previously placed on the bottom of V. C., just bellow the bulb, which may then be broken from the outside, by a mechanical impulse. Afterwards, vaporization carries out.

The vapour concentration in the chamber, C, is calculated by the simple expression:

$$C = \frac{(W_B - W_A) \,/\, MW}{V}$$

where MW is the compound molecular weight and V the total useful volume of the chamber (V = 5.193 cm^3, after deducing the volumes of the glass sherds, the pointy piece and the thermocouples ends inside the cells).

Absorption spectra were recorded in Perkin Elmer Spectrophotometers, models 552 and Lambda 5. Fluorescence spectra were obtained in transmission, with a home-built spectrofluorometer [7], using a helium-cadmium ion laser from Spectra-Physics, model 185, as a source. Benzene Uvasol from Merck, purity > 99.7& and para-xylene puriss, from Fluka, purity > 99.5%, were used without further purification. Pyrene puriss, from Fluka was zone-refined before use.

A — Absorption spectra at constant vapour concentration were studied thermostatizing both cells at the same temperature: T(I. C.) = T(V. C.). About twenty minutes after each temperature change, the reproducibility of the spectra was excellent, providing a good evidence for the stabilization inside the chamber.

The symmetry forbidden transition $^1B_{2u} \leftarrow {^1A_{1g}}$ of benzene vapour, centered at ≈ 260nm, has been studied in these conditions, as a function of temperature. Concentrations covered the range: 1×10^{-4} to 5.5×10^{-2} M and temperatures were changed from the minimum value corresponding to total vaporization of the product to 418 K. A similar study was carried out for para-xylene, in the same region of wavelengths. The intensity variation with temperature, expressed as a function of absorbance and of the spectra integrated area, as well as the dependence on temperature of the vibronic components of these electronic transitions have been reported elsewhere [8] and are still being studied in our laboratory. Here, just to illustrate the chamber's possibilities, we present some of the spectra obtained for benzene and para-xylene (Figs 3 and 4), where the variations of absorbance with temperature for different vibronic transitions are clearly brought out.

B — When working with saturated vapours and to avoid condensation on the walls of the I. C., it must be maintained at a slightly higher temperature than the V. C.: T(I. C.) > T(V. C.). In this case, the amount of product introduced in the bulb need not to be known, providing it is in excess to guarantee an equilibrium of phases. In order to achieve stabilization after each change in the V. C. temperature (i. e., to obtain reproducible spectra), a period of about one hour must be respected. Twenty minutes proved to be enough when only the temperature of the I. C. was changed. These spectra were useful in the development of a method to determine saturated vapour concentrations, as a function of the temperatures of both cells. That work, which involves the fitting of interesting molecular parameters, is reported elsewhere [6].
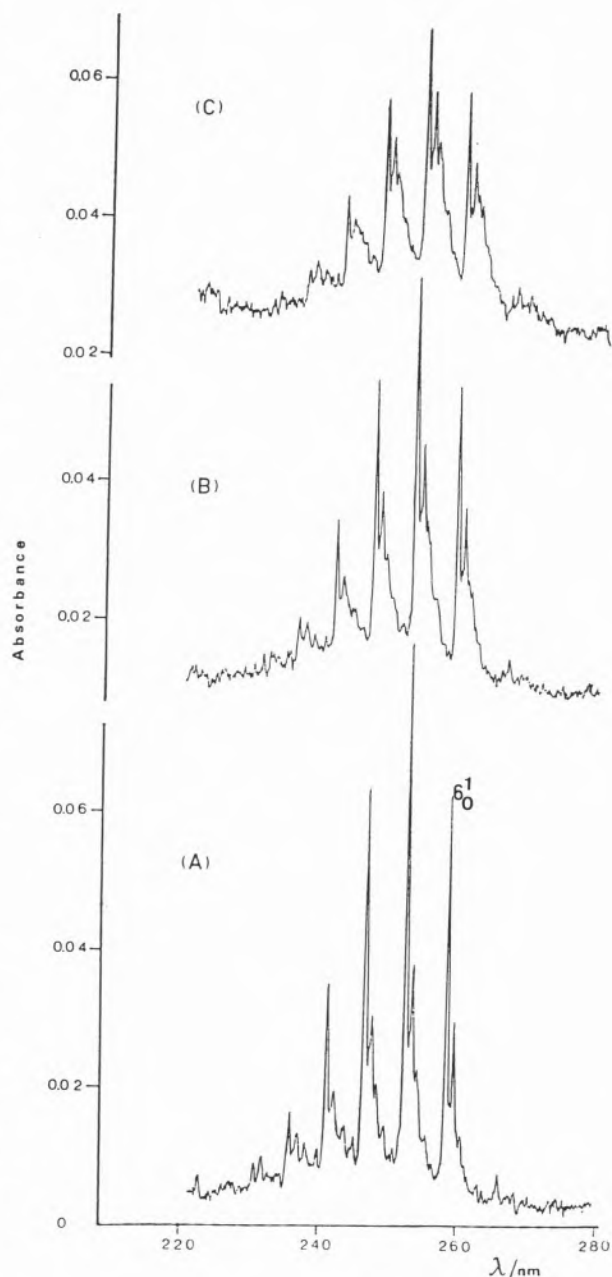

Fig. 3

Absorption spectra of benzene vapour (transition $^1B_{2u} \leftarrow {^1A_{1g}}$) obtained for a concentration of 1.5×10^{-4} mol dm^{-3} at different temperatures: (A) – T = 303 K; (B) – T = 353 K; (C) – T = 403 K.
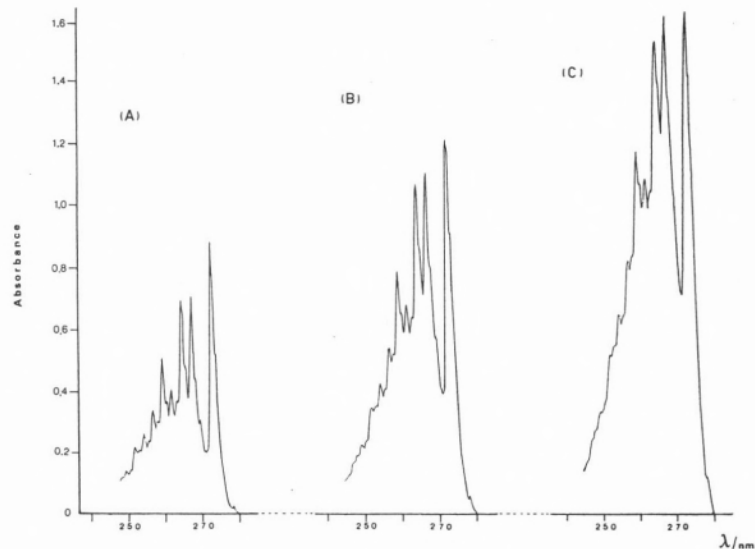
Fig. 4

Absorption spectra of para-xylene vapour for a concentration of 9.8 × 10⁻³ mol dm⁻³:
(A) – T = 335 K; (B) – T = 353 K; (C) – T = 413 K;

To test the convenience of the vapour chamber for working with low vapour pressure compounds (solids at normal temperature), absorption of saturated pyrene vapour to the second excited singlet state and fluorescence from the first singlet state were also studied as functions of both temperatures. As may be observed from Fig. 5, a very good reso-
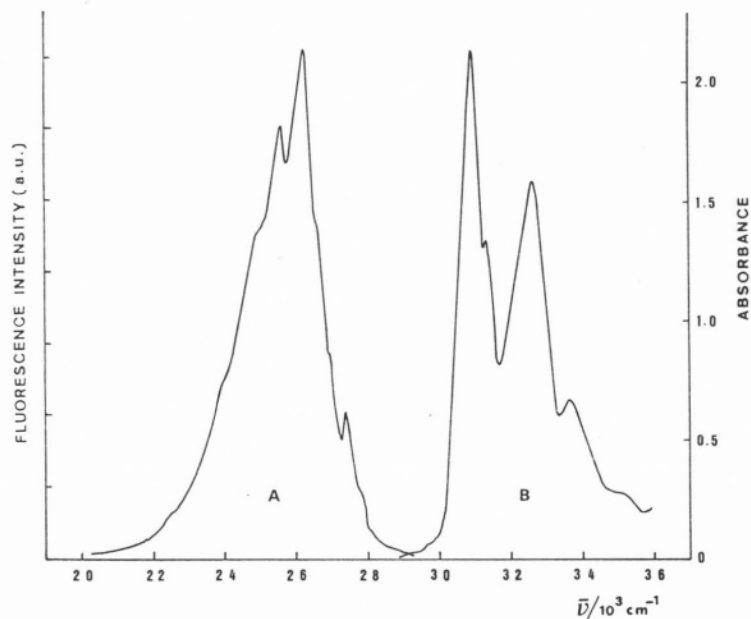

Fig. 5

A — *Non corrected fluorescence spectrum of pyrene vapour excited at 30769 cm⁻¹ (λ_exc = 3250 Å of an He-Cd ion laser), for T(V. C.) = 469 K and T(I. C.) = 498 K.*
B — *Absorption of pyrene vapour to the second excited singlet state, for T(V. C.) = 469 K and T(I. C.) = 498 K.*

lution was obtained for the fluorescence spectra when compared with others published [9, 10] (*).

4. CONCLUSION

The spectra obtained with the chamber described here, particularly in the case of benzene, have already been the subject of an extensive study [11]. Nevertheless, it is still of interest to improve the experimental conditions in which they are obtained, in order to clarify some questions related to the nature of the states involved and to the quenching mechanisms in the vapour phase. It seems clear that this chamber presents some advantages when compared to other similar apparatus: innherent to the fact that the walls themselves are the furnaces and that temperatures are taken in the bulk vapour, there is a more accurate control and knowledge of both temperatures. This allows the vapour concentration in the irradiation cell to be known more accurately, either for low concentration ranges (constant concentration experiments used concentrations as low as 10^{-4} M) or for high concentrations (particularly when working in equilibrium of phases). Moreover, the excellent reproducibility of the spectra supplied a good evidence for the establishment of thermodynamical equilibrium at each temperature (or pair of temperatures) of work.

(*) In both kinds of absorption experiments reported in this work, a base line was recorded and memorized in the spectrophotometer before breaking the Pyrex bulb containing the product.

REFERENCES

[1] J. FERGUSON, L. W. REEVES and W. G. SCHNEIDER, *Can. J. Chem.*, **35**, 1117 (1957).
[2] A. NAKAJIMA, *Bull. Chem. Soc. Japan*, **45**, 1687 (1972).
[3] E. PANTOS, J. PHILIS and A. BOLOVINOS, *J. Mol. Spectrosc.*, **72**, 36 (1978).
[4] S. HIRAYAMA and D. PHILLIPS, *J. Phys. Chem.*, **85**, 209 (1981).
[5] A. DAVIS, M. J. PILLING and M. J. WESTBY, *Chem. Phys.*, **63**, 209 (1981).
[6] LAURA M. ILHARCO, A. F. DO VALE and J. LOPES DA SILVA, *Chem. Phys.*, **111**, 137 (1987).
[7] J. M. G. MARTINHO and J. C. CONTE, *J. Lumin*, **22**, 271 (1981).
[8] LAURA M. ILHARCO, *Tese de Doutoramento*, I. S. T., Lisboa, 1987.
[9] A. NAKAJIMA, *Bull. Chem. Soc. Japan*, **44**, 3272 (1971).
[10] C. J. WERKHOVEN, T. DEINUM, J. LANGELLAR, R. P. H. RETTSCHNICK and J. D. W. VAN VOORST, *Chem. Phys. Lett.*, **30**, 504 (1975).
[11] Good reviews for benzene may be found in:
— R. B. CUNDALL, D. A. ROBINSON and L. C. PEREIRA, «Extitation and de-excitation of benzene», in *Advances in Photochemistry*, ed. J. N. PITTS, JR., G. S. HAMMOND and K. GOLLNICK, Vol. **10**, 147-219 (1977).
— G. HERZBERG, «*Molecular Spectra and Molecular Structure*», Vol. **2**, Van Nostrand, New York, 1966.
— M. B. ROBIN, «*Higher Excited States of Polyatomic Molecules*», Academic Press, London, 1975.
— J. M. HOLLAS, «*High Resolution Spectroscopy*», Butterworth's, London, 1982.

RESUMO

Uma câmara para estudo espectroscópico de vapores orgânicos

Descreve-se uma câmara em aço inóx, projectada para o estudo de propriedades fotoquímicas e fotofísicas de vapores orgânicos. Apresentam-se alguns resultados obtidos em experiências de espectroscopia de absorção e fluorescência.

M. MANUELA MOTTA
C. FERREIRA DE MIRANDA
Departamento de Química
Universidade de Évora
7000 Évora
CECUL — Centro de Electroquímica e Cinética das Universidades de Lisboa
1200 Lisboa
PORTUGAL

ADSORPTION OF MOLYBDATE BY CLAY MINERALS — II — MONTMORILLONITE AND ILLITE

The adsorption of molybdate by montmorilonite and illite was investigated at 25°C and 40°C in a 0.01 M sodium chloride background medium. A maximum of adsorption was observed at pH=3.8 for montmorrilonite and at pH=4.0 for illite. Both clay minerals adsorb less molybdate at 40°C than at 25°C. The adsorption isotherms can all be fitted to the Langmuir equation. The limiting values are 1.98 mg Mo and 1.80 mg Mo per gram of montmorrilonite at 25°C and 40°C, respectively; the correspondig values for illite are 0.424 mg Mo and 0.270 mg Mo per gram of adsorbent. The adsorption isotherms can be approached by straight lines and adsorption treated as a partition problem for molybdenum concentrations in solution lower than 0.2 μg cm⁻³ for montmorillonite and lower than 3 μg cm⁻³ for illite at 25°C, with Kd equal to (15.3 ± 1.6) × 10² cm³ g⁻¹ for montmorillonite and equal to (5.9 ± 0.2) cm³ g⁻¹ for illite. Estimations of free energy, enthalpy and entropy of adsorption are presented for both clay minerals and for kaolinite as well.

1 — INTRODUCTION

The importance of molybdenum in agriculture and the determining role of clay minerals in the fixation and mobility of this element in soils have been reviewed in a previous publication [1].

Adsorption of molybdate by clay minerals is also interesting from the point of view of testing and comparing the performance of models which are currently being applied to the adsorption of ions by oxides, hydrous oxides and clay minerals [2-7]. Whereas a number of studies are available concerning another important nutrient, phosphate (*Cf.* ref. 2 and literature cited therein), data are relatively scarce for other specifically adsorbed anions. Adsorption of molybdate by oxides [8, 9, 10] and by clay minerals [8, 11] has been investigated but litle information [12] seems to be available concerning its adsorption isotherms by clay minerals.

We have recently investigated the adsorption of molybdate by kaolinite [13]. In the present paper we report a similar study of the adsorption isotherms of molybdate by montmorillonite and illite at 25°C and at 40°C and also data on the 40°C isotherm for the system molybdate/kaolinite.

2 — EXPERIMENTAL

Montmorillonite was obtained from FLUKA. X-ray diffraction analysis of this material showed, besides the characteristic line of montmorillonite at 1.5 nm, a weak line at 1.0 nm indicating only a few per cent illite. Illite was obtained from CLAY MINERALS SOCIETY, SOURCE CLAY MINERALS REPOSITORY. The X-ray pattern showed the two characteristic lines of illite at 0.496 nm and 1.0 nm; no other lines were observed thus indicating no contamination with other minerals.

Sedimentation analysis in hexametaphosphate medium yielded the particle size distri-

Table I

Particle size distribution for montmorillonite and illite

Mineral	> 50 µm	50-20 µm	20-2 µm	2-0.5 µm	< 0.5 µm
	(%)	(%)	(%)	(%)	(%)
Montmor-illonite	12.6	10.3	44.7	21.0	9.9
Illite	17.0	24.1	28.9	17.0	11.4

bution shown in table I. Specific $BET_{(N2)}$ areas are 220 m² g⁻¹ and 21 m² g⁻¹ for montmorillonite and for illite, respectively.

Preliminary experiments allowed to choose clay solution ratios equal to 10 g dm⁻³ for montmorillonite and to 50 g dm⁻³ for illite in order to obtain a conveniently measurable distribution of molybdate between solid and liquid phases. The initial Mo concentration ranged from 3 to 100 µg cm⁻³ for montmorillonite and from 1 to 250 µg cm⁻³ for illite. The initial pH of the suspensions in adsorption experiments was 4.0 for montmorillonite and 8.9 for illite, which were the pH the suspensions of these clays spontaneously assumed in 0.01 M NaCl medium.

Each adsorption equilibrium was carried out in three replicates. Equilibrium was reached in less than 24 hours in every case. In experiments at varying imposed pH, the suspensions were ajusted to the desired pH allowed to equilibrate overnight. The appropriate amount of molybdate solution was then added and the final pH measured after the exchange equilibrium was reached. The pH drift was always less than 0.8.

Experimental details concerning the equilibration procedure and the determination of molybdenum by flameless atomic absorption were given in a previous paper [13].

3 — RESULTS AND DISCUSSION

a) pH

The dependence of molybdenum adsorption on pH is shown in figures 1 and 2. A maximum is

reached at pH=3.8 for montmorillonite and at pH=4.0 for illite, both values being close to the pKa of the $HMoO_4^-$ as it could be antecipated from the theory of Hingston *et al* [14] and as we also observed in the case of kaolinite [13].
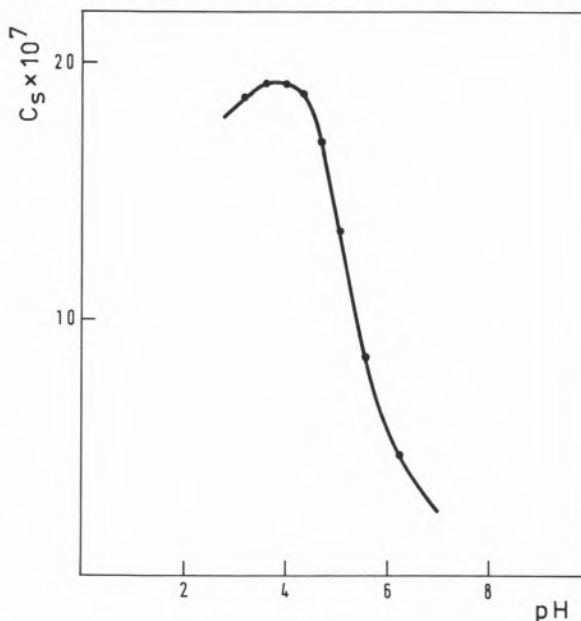

Figure 1

Adsorption of molybdate by montmorillonite: dependence on pH. 1 g montmorillonite; 100 cm³ 0.01 M NaCl; Co(Mo) = 2.0 g cm⁻³.
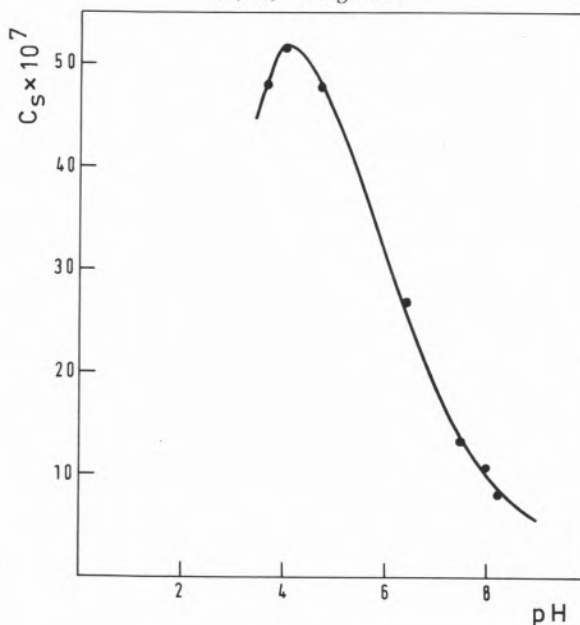
Figure 2

Adsorption of molybdate by illite: dependence on pH. 1 g illite; 100 cm³ 0.01 M NaCl; Co(Mo) = 10 g cm⁻³.

b) **Molybdenum concentration. Temperature**

Adsorption isotherms for montmorillonite and illite are shown in figures 3 and 4 for 25°C and 40°C respectively, pH remained unchan-

The four curves are all of L type (Giles classification [15]), molybdate showing less affinity for illite than for montmorillonite, and both minerals adsorbing less molybdate at 40°C than at 25°C.
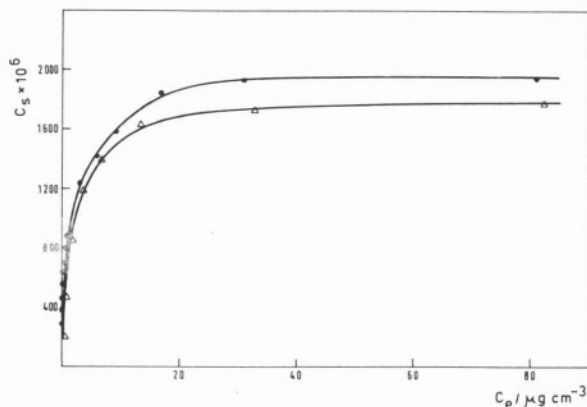

Figure 3

Adsorption isotherms for molybdate on montmorillonite in 0.01 M NaCl medium: ● 25°C (3.98 ≤ pH ≤ 4.05), △40°C (3.85 ≤ pH ≤ 4.45)
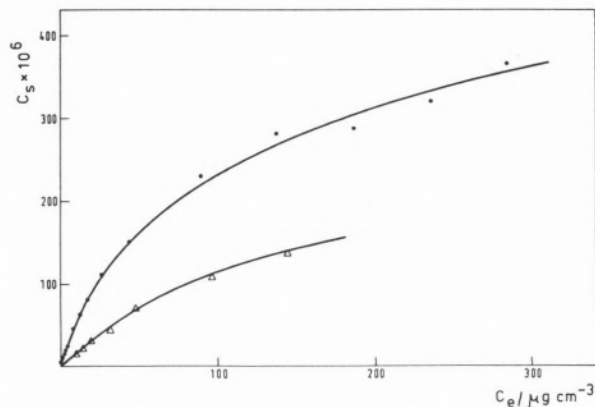

Figure 4

Adsorption isotherms for molybdate on illite in 0.01 M NaCl medium: ● 25°C (pH = 8.90), △ 40°C (pH = 8.20)

ged during equilibration in the case of illite, owing to the buffering effect due to the high clay/solution ratio which was convenient to employ. As to montmorillonite, pH changed from 4.0 to at most 4.8 in the course of equilibration.

The isotherms at 25°C can be fitted to the Langmuir equation (Figs. 5 and 6), yielding for the linearized form

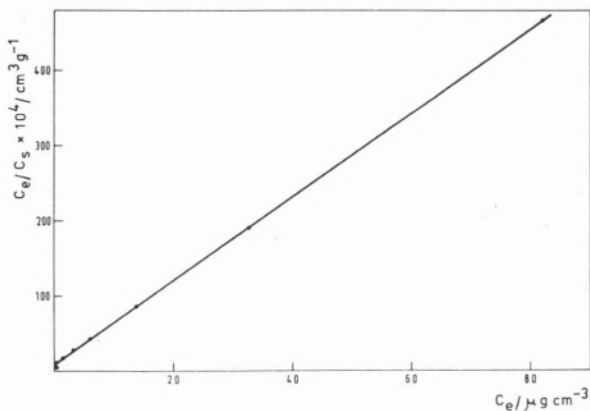$$\frac{C_e}{C_s} = 5.06 \times 10^{-4} \, C_e + 7.50 \times 10^{-4} \qquad (1)$$

Figure 5

Langmuir plot for the adsorption isotherm of molybdate by montmorillonite at 25°C
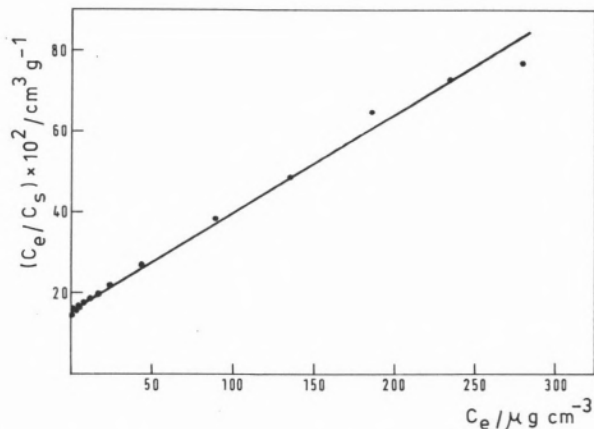

Figure 6

Langmuir plot for the adsorption isotherm of molybdate by illite at 25°C

for montmorillonite, and

$$\frac{C_e}{C_s} = 0.236 \times 10^{-2} C_e + 16.06 \times 10^{-2} \qquad (2)$$

for illite, where C_e and C_s are the equilibrium Mo concentration in the liquid and solid phases expressed in $\mu g\ cm^{-3}$ and $\mu g\ Mo\ g^{-1}$ clay respectively.

The differences between calculated and experimental values amount to $9.4 \pm 3.2\%$ and to $4.4 \pm 0.9\%$ for montmorillonite and for illite respectively; these are to be compared with the variation coefficient for the experimental C_s, $2.2 \pm 0,3\%$. The fit is therefore reasonably good for illite but less so for montmorillonite. This may be connected with increasing affinity between molybdate and the adsorbent on going from illite to kaolinite and then to montmorillonite under our experimental conditions, namely an ionic strength of 0.01 M. Actually, all the isotherms being of L type, illite may nevertheless be considered to show some tendency to C-type behaviour and montmorillonite to H-type behaviour.

For molybdenum concentrations in solution lower than $0.2\ \mu g\ cm^{-3}$ for montmorillonite and lower than $3\ \mu g\ cm^{-3}$ for illite, the isotherms can be described by straight lines:

$$C_s = 15.3 \times 10^2 C_e \qquad (C_e < 0.2\ \mu g\ cm^{-3}) \quad (3)$$

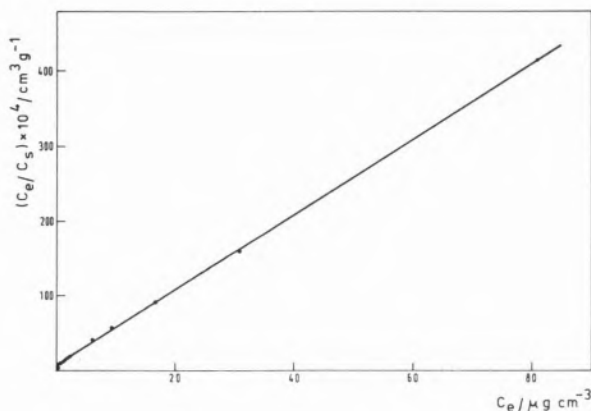for montmorillonite, and

$$C_s = 5.9\ C_e \qquad (C_e < 3\ \mu g\ cm^{-3}) \quad (4)$$

The differences between calculated and experimental values amount to $8 \pm 3\%$ for montmorillonite and $4 \pm 2\%$ for illite. The adsorption equilibrium can thus be characterized in these concentration ranges by a single parameter, the distribution coefficient, Kd, which is equal to $(15.3 \pm 1.6) \times 10^2\ cm^3\ g^{-1}$ for montmorillonite and equal to $(5.9 \pm 0.2)\ cm^3\ g^{-1}$ for illite.

Since molybdenum concentration in soil solution is tipically lower than 3 ppm, adsorption of molybdenum by illite as a soil constituent can be treated as a simple partition problem. The same is true for kaolinite as we have shown in a previous paper [13]. As to montmorillonite, a two parameters equation, like Langmuir's, will be required in order to describe the behaviour of molybdenum in montmorillonitic soils.

The isotherms at 40°C can also be fitted to the Langmuir equation (Figs. 7 and 8) yielding for the linearized form

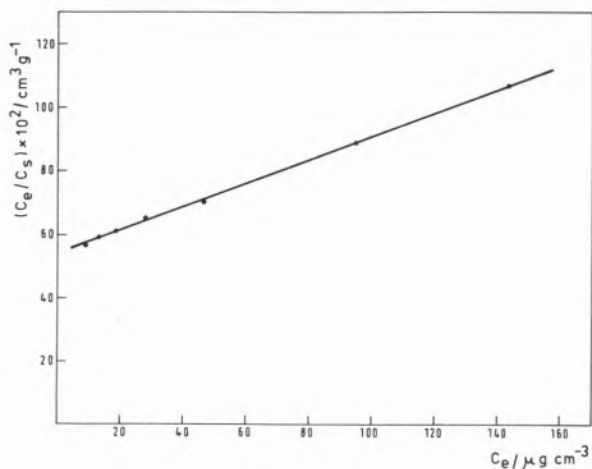$$\frac{C_e}{C_s} = 5.57 \times 10^{-4} C_e + 7.99 \times 10^{-4} \qquad (5)$$

Figure 7

Langmuir plot for the adsorption isotherm of molybdate by montmorillonite at 40ºC

Figure 8

Langmuir plot for the adsorption isotherm of molybdate by illite at 40ºC

for montmorillonite, and

$$\frac{C_e}{C_s} = 0.370 \times 10^{-2}\, C_e + 54.04 \times 10^{-2} \quad (6)$$

for illite. The differences between calculated and experimental values amount to $3.1 \pm 1.3\%$ and to $0.9 \pm 0.3\%$ for montmorillonite and illite respectively.

For low molybdenum concentrations the isotherms approach to straight lines as it was found at 25°C; partition coefficientes at 40°C are, however, unlikely to be useful in soil chemistry studies since this is not a common temperature in soils.

c) Equilibrium constants and thermodynamic functions

The fact that Langmuir equation adequately describes the adsorption equilibria we investigated makes it easy to advance preliminary estimation of the pertinent thermodynamic functions.

If speciation is ignored both in the liquid and the solid phases, the general stoicheometric equation can be put forward

$$\overline{S}OH(s) + H_2MoO_4(aq) + xH^+(aq) =$$
$$= \overline{S}MoO_4H_{1+x}^{x+}(s) + H_2O \quad (7)$$
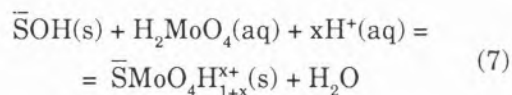
corresponding to the conditional constant

$$K = \frac{C_s}{(C - C_s)\, C_e\, [H^+]^x} \quad (8)$$

wherefrom the relationship

$$\frac{C_e\, [H^+]^x}{C_s} = \frac{1}{KC} + \frac{1}{C}\, C_e\, [H^+]^x \quad (9)$$

can be derived. ($\overline{S}$ stands for one equivalent of the clay mineral and C for its exchange capacity for molybdate in the same units as C_s).

Now, whereas a good fit to equation (9) can be obtained with x=0, poor fitting resulted whenever stoicheometrically meaningfull values of x ranging from +2 to −1 were tried. In any case, a sistematically better agreement bet-

ween experimental and calculated values of C_s was observed when $x \to 0$. This suggests that equations (7) and (9) may be re-writen as

$$\overline{S}OH(s) + H_2MoO_4(aq) =$$
$$= \overline{S}\,MoO_4H(s) + H_2O \quad (10)$$
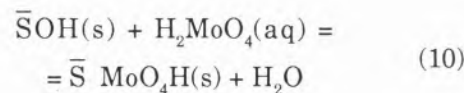
and

$$\frac{C_e}{C_s} = \frac{1}{K_L C} + \frac{1}{C}\, C_e \quad (11)$$

equation (11) being the linearized form of Langmuir equation. The moderate increasing of pH which accompanies molybdate adsorption in the case of montmorrilonite (and also kaolinite) should then be attributed to the readjustment of the acid-base equilibrium for the clay

$$\overline{S}O^-(s) + H_2O = SOH(s) + OH^-(aq) \quad (12)$$

upon the adsorption of molybdate, which consumes the SOH species. Potentiometric titrations of the clay suspensions corroborate this view.

Let it be pointed out that the Langmuir constant K_L is obtained from the extrapolation of the straight line (11) to the axis of ordinates: it therefore corresponds to an estimation of the equilibrium constant K for reaction (10) at zero Mo concentrations in both aqueous and solid phases. K_L may thus be taken as a fair approximation of the thermodynamic constant for the adsorption equilibrium. After conversion to molar concentration units for molybdenum in solution, it then referes to the following standard states under ideal conditions: unit molar concentration for molybdate in solution; and 0.5 mole fraction both for $\overline{S}OH(s)$ and for $\overline{S}MoO_4H(s)$.

The usual treatment of the equilibrium constants next yields the results that are summarized in table II, where data for kaolinite is also included for comparison.

Confidence intervals were estimated on the basis of the Langmuir fit, neglecting the cor-

Table II

Thermodynamic functions for the adsorption of molybdate by clary minerals

Function	Kaolinite	Montmorillonite	Illite
K(298K)	$(10.9 \pm 0.3) \times 10^3$	$(65 \pm 6) \times 10^3$	$(1.41 \pm 0.07) \times 10^3$
K(313K)	$(2.57 \pm 0.09) \times 10^3$	$(67 \pm 5) \times 10^3$	$(0.66 \pm 0.01) \times 10^3$
ΔG° / kJ.mol^{-1}	-23.0 ± 0.1	-27.4 ± 0.2	-18.0 ± 0.1
ΔH° / kJ.mol^{-1}	-75 ± 2	2 ± 2	-39 ± 1
ΔS° / kJ.mol^{-1}.K^{-1}	-174 ± 1	98 ± 2	-72 ± 1

relation of the errors in the ordinates and in the abscissae; a more rigorous calculation would be rather involved and probably unjustified. Precision confirms that estimates of ΔH° and ΔS° are possible and the results significant, even if only two temperatures were investigated. Accuracy, on the other hand, depend on how reliable the identification of K with K_L proves to be.

The driving force for the adsorption of molybdate by montmorillonite is of an entropic nature under our experimental conditions. The same has been found by Muljadi *at al.* [16] in the case of the adsorption of phosphate by kaolinite at pH = 5; the authors report zero enthalpy, -20 kJ.mol^{-1} free energy (at 20°C) and $+63$ J.mol^{-1}.K^{-1} standard entropy for the exchange reaction. The values shown in table II are of similar magnitude, with the exception of the entropy of adsorption of molybdate by kaolinite which may seem too high. However, if the adsorption of molybdate by kaolinite is to a certain extent assimilated to a bidimensional formation of aluminum molybdate (without significant simultaneous re-arrangement of exchangeable cations) the high entropy decrease is perhaps not surprising, if it is also born in mind that the standard entropy of formation or ferrous molybdate, for which data are available, is equal to -335 J.mol^{-1}.K^{-1} [17].

A more refined thermodynamic treatment, based on the use of the Gibbs-Duhem equation, in order to obtain, from the conditional constants the thermodynamic equilibrium constants as well as the activity coefficients in the solid phases [18], depends on the confirmation of the stoicheometry of the adsorption reaction. This, on its turn, requires a detailed knowledge of the acid-base equilibria for the clays. The same is true if the adsorption equilibrium constants (and the thermodynamic functions) are to be derived from model considerations using, for instance, the constant capacitance model [2]. The acid-base behaviour of the clay minerals we have studied is therefore under investigation at present.

ACKNOWLEDGEMENTS

REFERENCES

[1] M. M. Motta Batista and C. F. Miranda, *O Molibdénio nos Solos*, INIC, Lisboa (1981).

[2] S. Goldberg and G. Sposito, *Soil Sci. Soc. Am. J.*, **48**, 772 (1984).

[3] W. Stumm, R. Kummert and L. Sigg, *Croat. Chem. Acta*, **53**, 291 (1980).

[4] J. Westall and H. Hohl, *Adv. Colloid Interface Sci.*, **12**, 265 (1980).

[5] H. Hohl, L. Sigg and W. Stumm, *In: M. C. Kavanaugh and J. O. Leckie (ed.) Particulates in water.* Adv. Chem. Ser. n.° 189, p.l. Am. Chem. Soc., Washington DC (1980).

[6] J. W. Bowden, S. Nagarajah, N. J. Barrow, A. M. Posner and J. P. Quirk, *Aust. J. Soil Res.*, **18**, 49 (1980).

[7] P. W. Schindler, *In: M. A. Anderson and A. J. Rubin (ed.) Adsorption of inorganic at solid-liquid interfaces*, p.l. Ann Arbor Science, Ann Arbor, MI (1981).

[8] L. H. P. Jones, *J. Soil Sci.*, **8**, 313 (1957).

[9] E. D. Reyes and J. J. Jurinak, *Soil Sci. Soc. Am. Proc.*, **31**, 637 (1967).

[10] R. M. McKenzie, Aust. J. Soil. Res., **21**, 505 (1983).

[11] B. K. G. Theng, *N. Z. Sci.*, **14**, 1040 (1971).

[12] P. J. Phelan and S. W. Mattigod, *Clays Clay Miner.*, **32**, 45 (1984).

[13] M. M. G. Motta and C. F. Miranda, *Rev. Port. Quim.*, **27**, 505 (1985).

[14] F. J. Hingston, R. J. Atkinson, A. M. Posner and J. P. Quirk, *Nature*, **275**, 1459 (1967); id. *Trans. 9th Int. Cong. Soil Sci.*, **1**, 669 (1968).

[15] G. H. Giles, D. Smith and A. Huitson, *J. Colloid Interface Sci.*, **47**, 755 (1974).

[16] D. Muljadi, A. M. Posner and J. P. Quirk, *J. Soil Sci.*, **17**, 238 (1966).

[17] R. C. Weast, *CRC Handbook of Chemistry and Physics*, CRC Press, Inc., Florida (1983), p. D76.

[18] G. H. Bolt, In: G. H. Bolt and M. G. M. Bruggenwer (ed.) Soil Chemistry. B. Physico-Chemical Models, p. 27; Elsevier Scientific Publishing Company Amsterdam (1979).

RESUMO

Adsorção de molibdato por minerais de argila – II – montmorilonite e ilite

Estudou-se a adsorção de molibdato por montmorilonite e ilite a 25°C e a 40°C em meio de cloreto de sódio 0.01 M. Testou-se a influência do pH na adsorção tendo-se verificado um máximo a pH = 3.8 para a montmorilonite e a pH = 4.0 para a ilite. Ambos os minerais de argila adsorvem menos molibdato a 40°C do que a 25°C. As isotérmicas de adsorção ajustam-se bem à equação de Langmuir para os dois adsorventes e temperaturas. Os recobrimentos totais são respectivamente 1.98 e 1.80 mg Mo por grama de montmorilonite a 25°C e 40°C respectivamente; os correspondentes valores para a ilite são 0.424 e 0.270 mg Mo por grama de adsorvente.

Para concentrações de equilíbrio inferiores a 0.2μg Mo cm⁻³ para a montmorilonite e a 3μg Mo cm⁻³ para a ilite as isotérmicas de adsorção confundem-se com rectas podendo o equilíbrio ser tratato como um problema de partição e caracterizado por um coeficiente de distribuição Kd, igual a $(15.3 \pm 1.6) \times 10^2$ cm³ g⁻¹ para a montmorilonite e igual a (5.9 ± 0.2) cm³ g⁻¹ para a ilite. Apresentam-se estimativas dos valores da energia livre, entalpia e entropia de adsorção para os dois minerais de argila bem como para a caulinite.

M. JOAQUINA S. A. AMARAL TRIGO
M. ISABEL M. R. ESTEVES BARBEDO
Centro de Investigação em Química da Universidade do Porto.
Faculdade de Ciências do Porto
4000 Porto
PORTUGAL

NEW APPROACH TO THE USE OF 2-CHLOROETHYL GROUP AS CARBOXYL PROTECTION IN PEPTIDE SYNTHESIS (*)

The synthesis of six new fully protected dipeptides 2-chloroethyl esters and a new method for the removal of the C-protection by the action of the sulphide anion are described.

A number of compounds of biological and synthetic interest containing the carboxyl group often have to be suitably C-protected during synthesis procedures. The most representative example of this is verified in the field of peptide synthesis.

The carboxyl protection has been achieved mainly through esterification and there is a wide range of ester groups which can be cleaved under very diversified hydrolytic conditions [2, 3].

2-Haloethyl ester groups, mono or polysubstituted, have been used as they allow both solvolysis removal and reductive elimination. In principle, the most attractive of these groups would be the 2-chloroethyl ester, but being rather stable its removal has been described, lately, only for the corresponding benzoate, although achieved by a variety of reagents:

a) The binucleophiles trithiocarbonate ion [4] and ethanedithiolate ion [5].
b) The supernucleophile cobalt(I) phthalocyanine ion [6, 7].
c) The hydrogen selenide ion [8] and the hydrogen telluride ion [9].
d) The vitamin B_{12} derivatives as catalysts for the reductive elimination [10].

The 2-chloroethyl group has had little application in peptide synthesis as it is inert towards the deblocking reagents commonly used in this field.

However, 2-chloroethyl esters of some aminoacids and peptides were used as intermediates in the synthesis of other C-protected derivatives such as 2-(4-methylphenylthio)ethyl esters [11] and 2-iodoethyl or choline esters [12].

HO and WONG [13] described an interesting procedure for the deprotection of 4-chlorobutyl and 5-chloropentyl esters of simple carboxyl acids by the action of the bidentate nucleophile sulphide anion. The reaction proceeds by nucleophilic substitution of the chloride ion, followed by intramolecular substitution. This prompted us to investigate similar removing conditions with the 2-chloroethyl

ester group used as carboxyl protection in peptide synthesis. For this purpose the 2-chloroethyl esters of glycine and L-leucine (as hydrochlorides) were coupled with N-benzyloxycarbonyl, N-t-butyloxycarbonyl and N-trityl glycines, by the N,N'-dicyclohexylcarbodi-imide procedure, giving the six new fully protected dipeptides XHNCH$_2$CO–HNCHRCOOCH$_2$CH$_2$Cl; (R = H, CH$_2$CH(CH$_3$)$_2$; X = Z, Boc, Trt). The 2-chloroethyl ester group could be selectively removed from all these peptides by the action of sodium sulphide in aqueous acetonitrile with reflux for one hour. The N-protected dipeptides were isolated in 42 to 75% yields. The N-t-butyloxycarbonyl and the N-trityl groups were also selectively removed from the fully protected dipeptides under acidic conditions, by the action of hydrogen chloride in acetic acid and in ethanol, respectively, and 72 to 85% yields were obtained.

EXPERIMENTAL

The purity of all compounds was confirmed by t.l.c. on kieselgel 60 F$_{254}$, usually in the four systems n-butanol-acetic acid-water (4 : 1 : 5), benzene-methanol (5 : 1), chloroform-ethylacetate-methanol (95:3:5) and chloroform-methanol (9 : 1). The compounds were revealed by the (NH$_4$)$_2$SO$_4$ – H$_2$SO$_4$ method [14]. Evaporations and concentrations were all carried out under reduced pressure with a rotary evaporator. Optical rotations were measured with a Bellingham and Stanley Pepol 66 polarimeter. N.m.r. spectra were recorded by Dr. J. A. B. Baptista at 33°C with a Perkin Elmer R32 90 MHz spectrometer. The microanalyses were carried out by Dr. Ilse Beetz (Kronach, Germany).

Glycine 2-chloroethyl ester hydrochloride and L-*leucine 2-chloroethyl ester hydrochoride* were both prepared by direct esterification of the aminoacids [11].
According to the procedures described in the literature N-*benzyloxycarbonylglycine*

[15], N-*t-butyloxycarbonylglycine* [16] and N-*tritylglycine* [17 a] were prepared.
General Procedure for the Synthesis of 2-Chloroethyl Esters of N-Protected Dipeptides:
To a solution of N-protected aminoacid (0,025 mol) in dry dichloromethane (55 ml), cooled to -10°C and stirred, was added *N,N'*-dicyclohexylcarbodi-imide (0.025 mol). The aminoacid chloroethyl ester hydrochloride (0.025 mol) and triethylamine (0.025 mol) were added. The mixture was kept at 0°C for 4 hours and at room temperature for 3 to 4 days. The precipitated *N,N'*-dicyclohexylurea was filtered off and the filtrate was washed [saturated aqueous sodium chloride, aqueous 5% citric acid (with the exception of the Boc-derivatives), aqueous 1$\underline{M}$-sodium hydrogen carbonate and saturated aqueous sodium chloride], dried (MgSO$_4$) and evaporated. The residue was dissolved in acetone and kept at 0°C for 24 hours. After filtration the solvent was removed and, when possible, the fully protected peptide was crystallised. The following dipeptides were prepared in this way:

N-*Benzyloxycarbonylglycylglycine 2-chloroethyl ester,* 74% yield, m. p. 110°C (from ethanol), δ(DMSO-d$_6$), 3.60-3.83 (4 H, complex, CH$_2$Cl and NCH$_2$CO), 4.23-4.45 (2 H, t, COOCH$_2$), 5.03 (2 H, s, PhCH$_2$), 7.20-7.50 (6H, complex, Ph and NH), 8.05-8.30 (1 H, t, NH) (Found: C, 51.4; H, 5.3; Cl, 10.6; N, 8.5. C$_{14}$H$_{17}$ClN$_2$O$_5$ requires C, 51.2; H, 5.2; Cl, 10.8; N, 8.5%).
N-*t-Butyloxycarbonylglycylglycine 2-chloroethyl ester,* 50% yield, m. p. 70-72°C (from ethyl ether), δ (CDCl$_3$) 1.45 (9 H, s, Bu^t), 3.58-3.77 (2 H, t, CH$_2$Cl), 3.77-3.95 (2 H, d, NCH$_2$CO), 4.03-4.18 (2 H, d, NCH$_2$COO), 4.32-4.50 (2H, t, COOCH$_2$), 5.28-5.53 (1H, t, NH), 6.80-7.05 (1 H, t, NH). (Found: C, 44.7; H, 6.3; Cl, 11.9; N, 8.9. C$_{11}$H$_{19}$Cl N$_2$O$_5$ requires C, 4.48; H, 6.5; Cl, 12.0; N, 9.5%).
N-*Tritylglycylglycine 2-chloroethyl ester,* 70% yield, m. p. 144-145°C (from ethanol), δ (DMSO-d$_6$) 2.65-2.90 (2 H, d , NCH$_2$CO), 3.70-3.90 (2 H, t, CH$_2$Cl), 3.9-4.05 (2 H, d , NCH$_2$COO), 4.25-4.45 (2 H, t, COOCH$_2$),

6.90-7.60 (16 H, complex, Ph and NH), 8.30-8.60 (1 H, t, NH). (Found: C, 69.2; H, 5.8; Cl, 7.4; N, 6.4.$C_{25}H_{25}ClN_2O_3$ requires C, 68.7; H, 5.8; Cl, 8.1; N, 6.4%).

N-*Benzyloxycarbonylglycyl-L-leucine 2-chloroethyl ester*, 58% yield, an oil, δ(CDCl$_3$) 0.80-1.10 (6 H, d , CH$_3$), 1.15-1.90 (3 H, complex, CH$_2$CH), 3.50-3.75 (2 H, t, CH$_2$Cl), 3.75-4.00 (2 H, d, NCH$_2$CO), 4.20-4.45 (2 H, t , COOCH$_2$), 4.50-4.80 (2 H, complex, NCH), 5.10 (2 H, s, CH$_2$Ph), 5.55-5.80 (1H, t , NH), 6.60-6.80 (1 H, d, NH), 7.30 (5 H, s, Ph).

N-*t-Butyloxycarbonylglycyl-L-leucine 2-chloroethyl ester*, 72% yield, an oil, δ (CDCl$_3$) 0.97-1.10 (6 H, d, CH$_3$), 1.40-1.90 (12H, complex, Bu^t and CH$_2$CH), 3.58-3.75 (2H, t, CH$_2$Cl), 3.75-3.90 (2 H, d, NCH$_2$CO), 4.28-4.50 (2H, t, COOCH$_2$), 5.35-5.55 (1 H, t , NH), 6.70-6.95 (1 H, d, NH).

N-*Tritylglycyl-L-leucine 2-chloroethyl ester*, 75% yield, an oil δ (CDCl$_3$) 0.90-1.10 (6 H, d, CH$_3$), 1.50-1.85 (3 H, complex, CH$_2$CH), 2.95 (2 H, s, NCH$_2$CO), 3.50-3.85 (2H, t, CH$_2$Cl), 4.20-4.45 (2 H, t, COOCH$_2$), 4.50-6.90 (1H, complex, NCH), 6.60-7.00 (1 H, d, NH), 7.00-7.50 (15, complex, Ph), 7.50-7.90 (1 H, t, NH).

Removal of N-Protecting Groups from the Dipeptides Esters.

a) N-*t-Butyloxycarbonyl group*

N-t-Butyloxycarbonylglycylglycine 2-chloroethyl ester (0.45g;0.0015mol) was dissolved in a solution of 1$\underline{M}$-HC1 in acetic acid (8,5ml) The reaction mixture was stirred for 20 minutes at room temperature and by addition of ethyl ether a white solid precipitated. After cooling, the product was filtered off and recrystallised from ethanol, giving the pure *glycylglycine 2-chloroethyl ester hydrochloride*, (0.30g;85%), m.p. 183-185°C, δ(DMSO-d$_6$) 3.10-3.50 (2H, broad, NCH$_2$CO), 3.75-3.90 (2H, t, CH$_2$Cl), 3.90-4.10 (2H, d, NCH$_2$CO), 4.25-4.50 (2H, t, COOCH$_2$), 8.10-8.65 (3H, broad, $\overset{+}{N}H_3$), 8.90-9.20(1H, t, NH) (Found: C,31.3; H,5.2; Cl,30.8; N,12.2. $C_6H_{12}Cl_2N_2O_3$ requires C,31.2; H,5.2; Cl,30.7; N, 12.1%).

Similarly, the *glycyl-L-leucine 2-chloroethyl ester hydrochoride* was prepared, 72% yield,

m.p. 167-168°C, $[\alpha]_D^{20}$ – 37.4° (c 0.5 in MeOH), δ(DMSO-d$_6$) 0.75-1.10 (6H, complex, CH$_3$), 1.40-1.85 (3H, complex, CH$_2$CH), 3.10-3.60 (2H, complex, NCH$_2$CO), 3.70-4.00 (2H, t, CH$_2$Cl), 4.15-4.60 (3H, complex, NCH and COOCH$_2$), 8.00-8.60 (3H, broad, $\overset{+}{N}H_3$), 8.90-9.10 (1H, d, NH). (Found: C,42.0; H,7.0; Cl,24.3; N,9.7. $C_{10}H_{20}Cl_2N_2O_3$ requires C,41.8; H,7.0; Cl,24.7; N,9.8%).

b) N-*Trityl group.*

N-Tritylglycylglycine 2-chloroethyl ester (0.44g; 0.001 mol) in ethanol (5ml) and 1.5$\underline{M}$-ethanolic HCl (2.8ml) were heated at 60°C for 3 minutes. Concentration to half volume and precipitation with ether gave a solid. This, after recrystallisation from ethanol, gave glycylglycine 2-chloroethyl ester hydrochloride (0.18g; 78%), m.p. and mixed m.p. 183-185°C. Similarly, the glycyl-L-leucine 2-chloroethyl ester hydrochloride was obtained, 79% yield, m.p. and mixed m. p. 167-168°C.

Removal of the 2-Chloroethyl Ester Group.

General Procedure: A mixture of the fully protected dipeptide (0.005 mol) and sodium sulphide nonahydrate (0.006mol) in 10 ml of aqueous acetonitrile (2:3) was refluxed for 1 hour with stirring. The reaction mixture was cooled and, after addition of water (30ml), extracted with diethyl ether. The aqueous layer was mixed with ethyl acetate, titrated with aqueous 2$\underline{M}$-HCl at pH3 with stirring, separated from the organic solvent and washed several times with ethyl acetate. The combined organic extracts were dried (MgSO$_4$) and evaporated do dryness to yield the N-protected dipeptide which was further recrystallised from a suitable solvent.

From the corresponding fully protected dipeptides 2-chloroethyl esters, using the described method for the ester removal, the following N-protected dipeptides were prepared:

N-Benzyloxycarbonylglycylglycine, 75% yield, m.p. 175-178°C (from ethanol) (lit.[18], m.p. 177-178°C).

N-t-Butyloxycarbonylglycylglycine, 50% yield, m.p. 135-136°C (from ethyl acetate), δ(DMSO-d_6) 1.20-1.50 (9H, s, Bu^t), 3.45-3.68 (2H, d, NCH$_2$CO), 3.68-3.88 (2H, d, CH$_2$COO), 6.70-7.00 (1H, tripleto, NH), 7.85-8.10 (1H, t, NH). (Found: C,46.0; H,6.8; N,12.0. C$_9$H$_{16}$N$_2$O$_5$ requires C,46.5; H,7.0; N,12.1%).

N-Tritylglycylglycine, 70% yield, m.p. 178-180°C (from ethanol) (lit. [17b], 174-177°C).

N-Benzyloxycarbonylglycyl-L-leucine, 55% yield, m.p. 100-101°C, $[\alpha]_D^{23}$ − 9.7°(c 2 in EtOH) (lit.[19], m.p. 100-101°C; $[\alpha]_D^{25}$ − 9.5°(c 5 in EtOH). N-t-Butyloxycarbonylglycyl-L-leucine, 68% yield, m.p. 135-137°C (from ethyl acetate), $[\alpha]_D^{22}$ − 15.6° (c 0.5 in MeOH), δ(DMSO-d_6) 0.70-1.05 (6H, d, CH$_3$), 1.35-1.80 (3H, complex, CH$_2$CH), 3.55-3.80 (2H, d, NCH$_2$CO), 4.05-4.50 (1H, complex NCH), 4.90-5.10 (2H, s, PhCH$_2$), 7.15-7.50 (6H, complex, Ph and NH), 7.80-8.05 (1H, d, NH) (Found: C,54.2; H,8.4; N,9.8. C$_{13}$H$_{24}$N$_2$O$_5$ requires C,54.2; H,8.4; N,9.7%).

N-Tritylglycyl-L-leucine, 42% yield, m.p.73-83°C (from ethyl acetate/light petroleum ether), $[\alpha]_D^{22}$− 4.0° (c 0.2 in MeOH) (lit.[20], m.p. 75-85°C).

ACKNOWLEDGEMENT

REFERENCES

[1] M.J.S. A. AMARAL TRIGO, M. I. M. R. E. BARBEDO, «Peptides 1982», eds. K. Bláha and P. Malon, Walter de Gruyter, Berlin, 1983, p. 133.
[2] T. W. GREENE, «Protective Groups in Organic Synthesis», John Wiley & Sons, New York, 1981, p. 152.
[3] E. HASLAM, Tetrahedron, 36, 2409 (1980).
[4] T.-L. HO, Synthesis, 715 (1974).
[5] T.-L. HO, Synthesis, 510 (1975).
[6] H. ECKERT, I. UGI, Angew. Chem. Intl. Edn, 15, 681 (1976)
[7] H. ECKERT, I. LAGERLUND, I. UGI, Tetrahedron, 33, 2243 (1977).
[8] T.-L. HO, Synth. Commun., 8, 301 (1978).
[9] J. CHEN, X.-J. ZHOU, Synth. Commun., 17, 161 (1987).
[10] R. SCHEFFOLD, E. AMBLE, Angew. Chem. Intl. Edn., 19, 629 (1980).
[11] A. W. MILLER, C. J. M. STIRLING, J. Chem. Soc. (C), 2612 (1968).
[12] H. KUNZ, M. BUCHHOLZ, Chem. Ber., 112, 2145 (1979).
[13] T.-L. HO, C. M. WONG, Synth. Commun., 4, 307 (1974).
[14] T. ZIMINSKI, E. BOROWSKI, J. Chromatog., 23, 480 (1966).
[15] M. BERGMANN, L. ZERVAS, Chem. Ber., 65, 1192 (1932).
[16] E. SCHNABEL, Annalen, 702, 188 (1967).
[17] F. O. S. P. SERRÃO, «Síntese de Péptidos Assimétricos, Protegidos, da L-Cistina., Porto, 1960, a) p. 159; b) p. 185.
[18] J. A. MACLAREN, Austral. J. Chem., 11, 360 (1958).
[19] R. W. YOUNG, K. H. WOOD, R. J. JOYCE, G. W. ANDERSON, J. Am. Chem. Soc., 78, 2126 (1956).
[20] F. CHILLEMI, Gazz. Chim. Ital., 93, 1079 (1963).

RESUMO

Novo estudo para o uso do grupo 2-cloroetilo como protecção em síntese peptídica

Neste trabalho descreve-se a síntese de seis novos ésteres 2-cloroetílicos de dipéptidos N-protegidos e um novo método para remover a C-protecção, utilizando o anião sulfureto.

C. F. G. C. GERALDES
M. T. BARROS
M. I. SILVA
Chemistry Department
University of Coimbra
3000 Coimbra
PORTUGAL

C. D. MAYCOCK
Chemistry Department
Faculty of Sciences
University of Lisb. .
1200 Lisbon
PORTUGAL

STUDIES OF SOME β-KETODITHIOLANES AND β-KETODITHIANES BY PROTON AND 13C NMR

Several β-keto-1,3-dithiolanes and one β-keto-1,3-dithiane were synthesized and characterized by proton and carbon-13 NMR spectroscopy. It was found that there is no general correlation between the preferred directions of enolization of the parent assymetric β-dicarbonyl compounds and the regioselectivity of protection of the carbonyl groups by formation of the 1,3-dithiolane (dithiane) rings. This indicates that steric effects due to the substituents next to the carbonyl groups are more important than electronic effects in determining the point of attack of the bulky nucleophilic dithiolate agent.

INTRODUCTION

The cyclic thioacetal compounds of the β-keto-1,3-dithiolane and β-keto-1,3-dithiane families are very interesting intermediates in organic synthesis, as they can originate effectively regioselective reactions at the free carbonyl function. The protected carbonyl group can later be regenerated using the appropriate hydrolytic methods [1, 2].

In this work, the β-ketodithiolane compounds **1-5**, **7** and **8**, as well as the β-ketodithiane compound **6** (see Fig. 1), were synthesized and characterized using proton and 13C nuclear magnetic resonance (NMR) spectroscopy. The existence of a correlation between the preferential direction of enolization of assymetric β-diketones and the preferred protection of one of their carbonyl groups by dithiols was also investigated. This was done by comparing the yields of regioisomers in the synthesis of β-ketodithiolanes and β-ketodithianes with the populations of species in the enol-enol tautomeric equilibrium present in solutions of the corresponding parent assymetric β-diketones, which were previously obtained using proton, 13C and 17O NMR spectroscopy [3].

EXPERIMENTAL

The β-ketodithiolane compouds **1**, **2**, **3**, **4**, **5** and **7**, and the β-ketodithiane **6**, which are cyclic thioacetals, were synthesized from the corresponding β-diketones [4, 5] by reacting them with ethane-dithiol-1,2 (dithiolanes) or with propanedithiol-1,3 (dithiane **6**), as shown in the following equation:

n= 2 or 3

n = 1 or 2
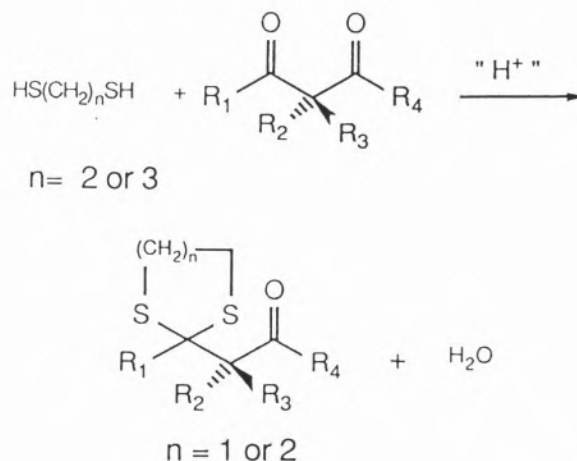
1. $R_1 = CH_3$; $R_2 = R_3 = H$; $R_4 = CH_3$
   1-[2-methyl-2-(1,3-dithiolanyl)]-propanone
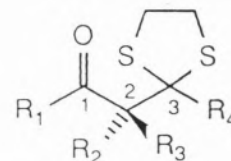
2. $R_1 = CF_3$; $R_2 = R_3 = H$; $R_4 = CH_3$
   1-[2-methyl-2-(1,3-dithiolanyl)]-3,3,3-trifluoro-propanone

3. $R_1 = C_6H_5$; $R_2 = R_3 = H$; $R_4 = CH_3$
   1-[2-methyl-2-(1,3-dithiolanyl)]-acetophenone

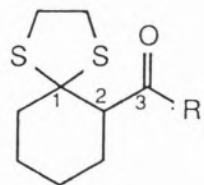4. $R_1 = C_2H_5$; $R_2 = R_3 = H$; $R_4 = CH_3$
   1-[2-methyl-2-(1,3-dithiolanyl)]-2-butanone

5. $R_1 = COOC_2H_5$; $R_2 = R_3 = H$; $R_4 = CH_3$
   ethyl 2-oxo-3-[2-methyl-2-(1,3-dithiolanyl)]-propanoate

6. $R_1 = R_4 = CH_3$
   1-[2-methyl-2-(1,3-dithianyl)]-propanone
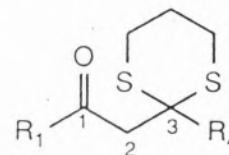
7. $R_1 = CH_3$
   6-acethyl-1,4-dithio-spiro-[4,5]-decane

8. $R_1 = R_4 = CH_3$
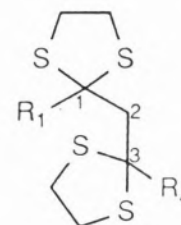   1-1-di-[2-methyl-2-(1,3-dithiolanyl)]-methane

Figure 1

Chemical structures, IUPAC names and numbering scheme adopted for the carbon atoms of the backbone nuclei for NMR assignment purposes (this is not a IUPAC numbering scheme) of the β-ketodithiolanes and β-ketodithianes studied

Compound **8** was also synthesized through protection of both carbonyl carbons. The condensation reaction is carried out in solution of ZnCl$_2$/HCl in ether or in the presence of the diethyletherate adduct of boron trifluoride, $BF_3(C_2H_5)_2O$, both reactions taking place initially in the absence of water [6]. Table 3 summarizes the yields of synthesis as well as some physical data and results of microanalysis for the compounds which were synthetised for the first time in this work, as well as key references for the other compounds already described in the literature.

0.1 M solutions of these compounds were prepared in CDCl$_3$ (99.8% D), from Stohler Isotope Chemicals.
All NMR measurements were carried out at room temperature on a Varian XL-200 spectrometer equipped with Fourier transformation using the deuterium resonance of CDCl$_3$ as an internal lock. Proton spectra were obtained at 200.053 MHz and broadband proton decoupled ^{13}C spectra were obtained at 50.053 MHz. All the proton and ^{13}C chemical shifts were relative to TMS, which was used as an internal reference. The precision of the mea-

sured chemical shift values was ± 0.01 ppm for ^{1}H and ± 0.05 ppm for ^{13}C. Spectral assignments were carried out using comparisons with the literature values for similar compounds [4, 7], by performing homonuclear proton decoupling experiments or by recording proton-coupled or off-resonance proton-decoupled ^{13}C spectra.

RESULTS AND DISCUSSION

The β-ketodithiolane and β-ketodithiane compounds **1** to **8** were studied using proton and ^{13}C NMR spectroscopy. The corresponding chemical shift values are presented in Tables 1 and 2, respectively. In the cases of

compounds **1**, **3** and **6**, previously studied by proton NMR [4, 7], the proton chemical shifts obtained were in close agreement with literature values. The resonances of the bridge groups, -SCH$_2$CH$_2$S- and -SCH$_2$CH$_2$CH$_2$S-, of the 1,3-dithiolanes and the 1,3-dithianes, respectively, are of importance in the diagnosis of these compounds. These resonances also depend on the conformation of the rings present in the compounds. The conformational properties of the five or six-membered rings of the dithiolanes and the dithianes, respectively, have been previously studied by proton NMR [5, 8-11]. The 1,3-dithiolane ring is very flexible and exists in a rapid equilibrium, in the NMR time scale, between C_2 half-chair (I) and C_1 envelope (II) conforma-

Table 1

Proton chemical shift values, (ppm), of β-ketodithiolanes and β-ketodithianes in CDCl$_3$ solutions

Compound	Central Part			R$_1$						R$_4$
	CH$_{(3)}$	SCH$_2$	CH$_2$	CH$_3$	CH$_2$	OCH$_2$	CH$_{(2,6)}$	CH$_{(3,5)}$	CH$_{(4')}$	CH$_3$
1	3.17	3.30	—	2.15	—	—	—	—	—	1.81
2	3.47	3.34	—	—	—	—	—	—	—	1.91
3	3.78	3.34	—	—	—	—	7.97	7.47	7.55	1.96
4	3.17	3.32	—	1.06	2.45	—	—	—	—	1.86
5	2.90	3.40	—	1.92	—	4.32	—	—	—	1.92
6	3.09	2.90	1.99	2.26	—	—	—	—	—	1.75
7	3.12 [a]	3.24	—	2.23	—	—	—	—	—	—
		3.21								
8	2.88	3.32	—	1.90	—	—	—	—	—	1.90

[a] Non-equivalent

Table 2

^{13}C chemical shifts, δ(ppm), of β-ketodithiolanes and b-ketodithianes in CDCl$_3$ solutions

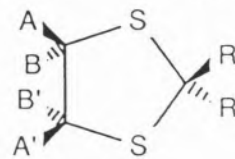| Compound	Central Part					R$_1$									R$_4$
	C$_{(1)}$	C$_{(2)}$	C$_{(3)}$	SCH$_2$	CH$_2$	CH$_3$	CH$_2$	CF$_3$	OCH$_2$	C$_{(1')}$	C$_{(2,6)}$	C$_{(3,5)}$	C$_{(4')}$	CO	CH$_3$
1	204.5	57.8	61.5	38.8	—	30.4	—	—	—	—	—	—	—	—	31.6
2	188.2	52.4	60.2	41.2	—	—	—	115.4	—	—	—	—	—	—	31.5
3	195.8	53.2	62.2	38.5	—	—	—	—	—	135.5	127.3	126.9	132.8	—	31.5
4	207.6	56.8	67.2	39.3	—	31.4	—	—	61.7	—	—	—	—	—	36.4
5	191.5	51.7	61.5	39.9	—	31.0	—	—	53.6	—	—	—	—	158.8	31.3
6	204.4	52.7	45.5	26.5	24.4	27.9	—	—	—	—	—	—	—	—	32.1
7	209.9	60.6	68.4	38.2	—	—	—	—	—	—	—	—	—	—	30.6
				3.21											
8	65.7	58.2	65.7	39.2	—	33.4	—	—	—	—	—	—	—	—	33.4

[a] Non-equivalent

tions [8]. Its $C_{(4)}$ and $C_{(5)}$ protons form an AA'BB' spin system consisting of two pairs of diastereotopic nuclei (III). The $C_{(4)}$ and $C_{(5)}$ methylene protons of the 2,2-assymmetrically

the carbon-13 satellites of the singlet resonance [12].

The literature reports and the present results show that there is a certain degree of selecti-
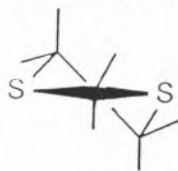
I
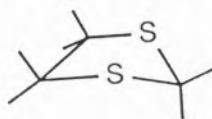
II

III

disubstituted 1,3-dithiolanes are, however, isochronous in all cases of flexible molecules except in compound **7**, which has a locked structure. Therefore, in the former cases, those methylene protons simplify to a singlet resonance, whereas in **7** they keep their AA'BB' complex pattern. The ^{13}C spectra also give a single resonances for the two cases, respectively. In the 1,3-dithiane **6**, the six-membered ring adopts a chair conformation [9] with the bulky substituent possibly occupying the equatorial position. A thorough study of the conformation of these cycles by NMR would require the measurement of vicinal coupling constants between the ring methylene protons, which would be possible either by direct observation at very low temperatures or indirectly at room temperature from

vity in the reaction of the carbonyl group in assymmetric β-dicarbonyl compounds when they are protected using the synthetic method described in the experimental section. Table 3 compares the isomer ratios of β-ketodithiolanes (dithianes) obtained from assymmetric β-dicarbonyl compounds (diketones and keto esters) and the equilibrium constant K for the enol-enol equilibrium present in CDCl$_3$ solution of those β-dicarbonyl compounds, obtained using ^{13}C NMR spectroscopy [3]. The preferential direction of enolization of the parent dicarbonyls, described by the value of K, was obtained by comparison of the ^{13}C chemical shifts of their two carbonyl compounds with model shift values for those nuclei in the two enol forms possible, using a method which has been described previously in the literature

Table 3

Comparison of the yields and isomer ratios obtained in the synthesis of the β-ketodithiolanes (dithianes) studied with the equilibrium constants K for the enol forms in the corresponding β-dicarbonyl compounds

Compound	R_1	R_4	Yield (%)	K	Isomer ratio	Characterization
1	CH$_3$	CH$_3$	95[a]	1.00	—	ref. 7
2	CF$_3$	CH$_3$	87	1.38 ± 0.05	19 : 1	b.q. 120°C/0.1mm; Found S, 27.81; calc. S, 27.85
3	C$_6$H5	CH$_3$	94	1.21 ± 0.09	19 : 1	ref. 7
4	C$_2$H$_5$	CH$_3$	82	[c]	4 : 1	b.q. 160°C/15mm; Found C, 50.79; H, 7.49; S, 33.95; Calc. C, 50.49; H, 7.41; S, 33.69
5	COOC$_2$H$_5$	CH$_3$	80	1.95 ± 0.10	19 : 1	ref. 5
6[b]	CH$_3$	CH$_3$	92	1.00	—	ref. 4
7			76	0.67 ± 0.04	9 : 1	b.q. 120°C/0.07mm; Found C, 55.70; H, 7.31; S, 29.63; Calc. C, 55.51; H, 7.45; S, 29.64
IV	CH$_3$	OC$_2$H$_3$	89	>>1	—	ref. 7

[a] The secondary product obtained is the compound with both carbonyl groups protected;   [b] β-Ketodithiane compound;   [c] Not studied

[13] for compound 3. The values of K obtained for the compounds studied in reference 3, and listed in Table 3, correspond to an application of that method to the compounds listed. A more complete description of that method and the results obtained will be published soon [3]. The constant K is defined in such a way that a value of $K > 1$ means that the carbonyl group closest to the R_1 substituent is preferentially enolized. This comparison shows that there is not a a general correlation between the carbonyl group which enolizes preferentially and the group which is preferentially protected. In fact, while in the linear β-diketones and in the β-ketoester corresponding to IV, the group which is preferentially protected is the one which enolizes to a lesser extent, in the rigid β-diketone corresponding to **7** the preferentially protected group is also the most enolized one. The results obtained therefore indicate that the substituent groups of the β-dicarbonyl compounds affect the point of nucleophilic attack by the bulky dithiolane dianion mainly through stereochemical effects.

CONCLUSION

The synthesis of various β-keto-1,3-dithiolane compounds and of one dithiane analog allowed their characterization by NMR spectroscopy. The five and six-membered rings are quite flexible, generally simplifying the expected spectra.

It was found that preferred directions of enolization of assymmetric β-dicarbonyl compounds do not generally correlate with preferred protection of carbonyl groups in those compounds by formation of 1,3-dithiolane (dithiane) rings, indicating that stereochemical, rather than electronic effects, determine the attack of the bulky dithiolate nucleophile.

REFERENCES

[1] D. SEEBACH, N. R. JONES and E. J. COREY, *J. Org. Chem.*, **33**, 300 (1968).
[2] B. T. GROBEL and D. SEEBACH, *Synthesis*, 357 (1977).
[3] C. F. G. C. GERALDES, M. T. BARROS, C. D. MAYCOCK and M. I. SILVA, *J. Mol. Struct.*, to be published.
[4] I. STAHL, B. SCHRAMM, R. MANSKE and J. GOSSELCK, *Liebigs Ann. Chem.*, 1158 (1982).
[5] I. STAHL, R. MANSKE and J. GOSSELCK, *Chem. Ber.*, **223**, 800 (1980).
[6] P. J. BARRY and B. M. CRAIG, *Can. J. Chem.*, **33**, 716 (1955).
[7] L. A. FEDOROV, M. S. ZHUKOV, N. Y. KORSAKOVA, Y. M. DEDKOV and A. N. ERMATOV, *Izv. Akad. Nauk. SSSR, Ser. Kheim*, 1763 (1984).
[8] L. A. STERNSON, D. A. COVIELLO and R. S. EGAN, *J. Am. Chem. Soc.*, **93**, 6529 (1971).
[9] E. L. ELIEL and R. O. HUTCHINS, *J. Am. Chem. Soc.*, **91**, 2703 (1969).
[10] J. GELAN and M. ANTEUNIS, *Bull. Soc. Chim. Belg.*, **78**, 599 (1969).
[11] E. L. ELIEL, V. S. RAO and F. G. RIDDELL, *J. Am. Chem. Soc.*, **98**, 3583 (1976).
[12] N. SHEPPARD and J. J. TURNER, *Proc. Roy. Soc., Ser. A*, **252**, 566 (1959).
[13] A. A. KOLTSOV, YU. A. IGNATEV, V. V. KOPEIKIN and E. F. PANARIN, *Zh. Org. Khim.*, **12**, 1982 (1976).

RESUMO

Estudos RMN de β-ceto-1,3-ditiolanos e β-ceto-1,3-ditanos

Sintetizaram-se vários β-ceto-1,3-ditiolanos e um β-ceto-1,3-ditiano, tendo sido caracterizados por RMN de protão e de 13C. Verificou-se não haver qualquer correlação geral entre a direcção preferencial de enolização dos compostos β-dicarbonílicos assimétricos parentes e a regioselectividade da protecção dos grupos carbonílicos devido à formação dos anéis 1,3-ditiolano (ditiano). Este facto indica que os efeitos estereoquímicos dos substituintes próximos dos grupos carbonilo são mais importantes do que os efeitos electrónicos no que respeita à definição do ponto de ataque do agente nucleofílico volumoso que é o ditiolato.

EDMUNDO J. S. GOMES DE AZEVEDO
Centro de Química Estrutural, Compexo I
Instituto Superior Técnico
1096 Lisboa
PORTUGAL

JOHN M. PRAUSNITZ
Department of Chemical Engineering
University of California
Berkeley CA 94720
USA

PARTIAL MOLAR VOLUMES OF NAPHTHALENE DILUTE IN SUPERCRITICAL FLUID SOLVENTS[*]

Supercritical-fluid extraction is a separation technique with much potential for a variety of industries.

To design and operate a supercritical-fluid extraction process, it is important to understand the behavior of solutes dilute in solvents at conditions close to the solvent's critical point.

In this work, we use Chueh's modification of the Redlich-Kwong equation of state to calculate the pressure dependence of the partial molar volumes of naphthalene infinitely dilute in carbon dioxide (isotherms between -3.15°C and 67°C) and in ethene (isotherms between 0°C and 60°C). These calculations were performed using a binary interaction parameter k_{12} determined from solubility data.

As the solvent's critical point is approached, the solute's partial molar volumes become very large but negative with a sharp minimum at temperatures close to the solvent's critical.

Calculated results compare well with available experimental data. In the critical region the partial molar volume is highly sensitive to temperature and pressure. Therefore, the fugacity coefficient of the solute changes dramatically with small changes in operating conditions. It is this dramatic change which leads to the unique advantages of supercritical-fluid-extraction process.

INTRODUCTION

Much attention has been given to separation processes using a supercritical fluid (SCF) for extraction. In this separation technique, a fluid at temperatures and pressures slightly exceeding those at its critical point is used to extract a solute (solid or liquid) from a solution.

Compared with conventional extraction methods, SCF extraction is advantageous for energy savings, and for economic recovery of the solvent. Further, a supercritical fluid is often more useful than a liquid solvent because of higher diffusity, lower density and lower viscosity of the supercritical fluid when compared with those of typical liquid solvents. Carbon dioxide is a popular SCF extractant. It fulfills many of the characteristics for an advantageous extraction agent: good extracting power, non-toxic, chemical stability, inexpensive, readily available and a conveniently low critical temperature (31.1°C).

Several industrial processes using compressed gases for material separation are suggested in the literature (for a review see Paulaitis *et al.* [1]). They include the separation of organic chemicals from water, caffeine from coffee, extraction of hops, spices, tobacco, and extraction of volatile materials from coal and other heavy fossil fuels. While only a few of these applications are as yet used in industry, there is good reason to believe that their number may increase in the near future.

Since the understanding of the behavior of solutes dilute in supercritical fluids is essential for design and operation of SCF extraction equipment, we discuss here the calculation of partial molar volumes of naphthalene infinitely dilute in the supercritical solvents, carbon dioxide and ethene. The partial molar volume is a key quantity for determining optimum operating conditions because it determines the rate at which the fugacity coefficient (and hence the solubility) changes with pressure.

THERMODYNAMIC ANALYSIS

To describe the solubility of a solid in a super-critical fluid, we assume that the solid phase is pure and incompressible.

With these assumptions, it can be shown [2] that at temperature T and pressure P the solubility of a solid (component 2) in a SCF (component 1) is given by

$$y_2 = \frac{P_2^{sat}}{P} \left\{ \frac{\phi_2^{sat}}{\phi_2} \exp\left[\frac{v_2^s}{RT} (P-P_2^{sat}) \right] \right\} \quad (1)$$

where P_2^{sat} is the sublimation pressure of the pure solid, ϕ_2^{sat} is the fugacity coefficient at P_2^{sat}, and the exponential term is the Poynting correction for the fugacity of pure solid, all at system temperature T.

It is the pressure dependence of ϕ_2 which is primarily responsible for the variation of y_2 with pressure. At low pressures, the term set in brackets in Eq. (1) is not far removed from unity. In that case, $y_2 = P_2^{sat}/P$ which is the ideal solubility of solid 2 in the gas phase. At high pressures, the term in brackets is larger, often very much larger, than unity.

The pressure dependence of fugacity coefficient ϕ_2 can be evaluated from

$$\left(\frac{\partial \ln\phi_2}{\partial P} \right)_{T,y} = \frac{\bar{v}_2}{RT} - \frac{1}{P} \quad (2)$$

where $\bar{v}_2$ is the partial molar volume of the solute in the fluid phase.

At high pressures, if $\bar{v}_2$ is negative, $(\partial \ln\phi_2 / \partial P)_T$ may be large and negative. If we raise P, we obtain lower ϕ_2; then y_2 must rise because the fugacity of the pure solid is approximately constant and, at equilibrium,

$$\text{constant} \approx f_2^s = f_2^G = \phi_2 \, y_2 \, P \quad (3)$$

One convenient way to calculate ϕ_2 is from an equation of state. In this work we use Chueh's modification [3] of the Redlich-Kwong equation of state. From this equation we obtain [2] for ϕ_2,

$$\ln\phi_2 = \ln \frac{v}{v-b} + \frac{b_2}{v-b} - \frac{2\sum_i y_i a_{i2}}{RT^{1.5}b} \ln \frac{v+b}{v} +$$

$$+ \frac{ab_2}{RT^{1.5}b^2} \left[\ln \frac{v+b}{v} - \frac{b}{v+b} \right] - \ln \frac{Pv}{RT} \quad (4)$$

For the mixture, parameters a and b are given by the usual mixing rules,

$$a = \sum_i \sum_j y_i \, y_j \, a_{ij} \qquad b = \sum_i y_i b_i \quad (5)$$

For the pure components, a and b are calculated from

$$a_i = \frac{\Omega_{a_i} \, R^2 \, T_{c_i}^{2.5}}{P_{c_i}} \qquad b_i = \frac{\Omega_{b_i} \, R \, T_{c_i}}{P_{c_i}} \quad (6)$$

where Ω_{a_i} and Ω_{b_i} are dimensionless constants obtained from saturated vapor data.

We evaluate the cross term a_{12} in Eq. (5) from

$$a_{12} = (\Omega_{a_1} + \Omega_{a_2}) \, R^2 T_{c_{12}}^{2.5} / 2 \, P_{c_{12}} \quad (7)$$

with

$$P_{c_{12}} = z_{c_{12}} \, RT_{c_{12}}/v_{c_{12}} \quad (8)$$

$$v_{c_{12}} = \frac{1}{8} (v_{c_1}^{1/3} + v_{c_2}^{1/3})^3 \quad (9)$$

$$z_{c_{12}} = 0.291 - 0.08 \left(\frac{\omega_1 + \omega_2}{2} \right) \quad (10)$$

and

$$T_{c_{12}} = (T_{c_1} T_{c_2})^{1/2} \, (1 - k_{12}) \quad (11)$$

In these equations, subscript c refers to the critical property, ω_i is the acentric factor for component i and k_{12} is the binary interaction parameter.

Partial molar volumes were also calculated from the Redlich-Kwong equation, through the thermodynamic relation

$$\bar{v}_2 = - \frac{\left(\frac{\partial P}{\partial n_2} \right)_{T, V, n_1}}{\left(\frac{\partial P}{\partial V} \right)_{T, n}} \quad (12)$$

where V is the total volume of the mixture containing n_1 moles of component 1, etc.

Since the solubility of the solute in the gas phase is small, we consider the solute infinitely dilute in the supercritical fluid phase. In that case, $\bar{v}_2^\infty$, the partial molar volume of solute at infinite dilution, is defined by

$$\bar{v}_2^\infty = \lim_{n_2 \to o} \left(\frac{\partial V}{\partial n_2} \right)_{P, T, n_1} \quad (13)$$

We obtain $\bar{v}_2^\infty$ by calculating the derivatives in Eq. (12) from Redlich-Kwong equation. The result is

$$\bar{v}_2^\infty = \frac{\dfrac{RT}{v-b}\left(1 + \dfrac{b_2}{v-b}\right) - \dfrac{2a_{12} - \dfrac{ab_2}{v+b}}{v(v+b)T^{0.5}}}{\dfrac{RT}{(v-b)^2} - \dfrac{a}{T^{0.5}}\left\{\dfrac{2v+b}{v^2(v+b)^2}\right\}} \quad (14)$$

At infinite dilution, a, b, and v are the corresponding values for the pure solvent.

RESULTS

Using solubility data for naphthalene in CO_2 at 35°C [4, 5] and in ethene at 25°C [5, 6] we used Eq. (1), together with Eqs. (4)-(11) to obtain interaction parameter k_{12}.

Data for pure components were taken from IUPAC Tables [7] (CO_2 and C_2H_4) and from reference 8 (naphthalene).

Figure 1 compares experimental with calculated solubilities of naphthalene in supercritical ethene at 25°C.

With $k_{12} = 0$, agreement is good only at low pressures where the gas phase is almost ideal. In the range of pressures studied, calculated solubilities of naphthalene in C_2H_4 agree with experimental data using $k_{12} = -0.0182$, even at higher temperatures as shown in Fig. 2.
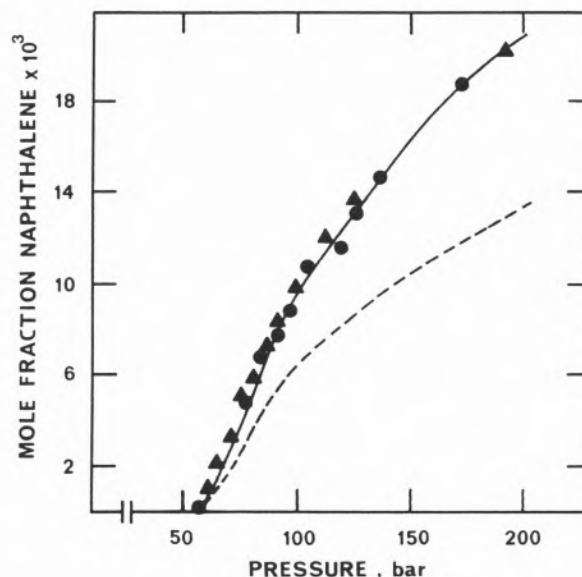

Figure 1

Experimental (▲ , ● from ref. 5,6) and calculated solubilities for naphthalene in supercritical ethene at 25°C. Calculations from Redlich-Kwong equation of state with $k_{12} = 0$ (broken line) and $k_{12} = -0.0182$ (full line)
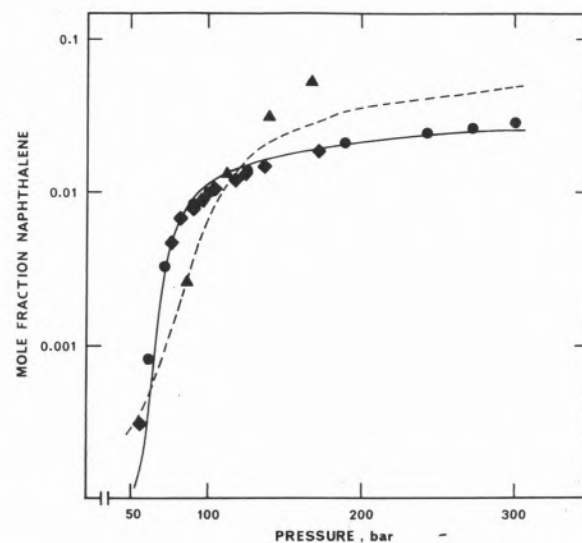

Figure 2

Experimental (● at 25°C, ref. 5; ▲ at 50°C, ◆ at 25°C from ref. 6) and calculated solubilities (with $k_{12} = -0.0182$) for solid naphthalene in supercritical ethene at 25°C (full line) and at 50°C (broken line)

Similar results were obtained for the solubility of naphthalene in supercritical CO_2. Figure 3 compares calculated solubilities

104

(using k_{12} = 0.0626) with experimental data at 35°C.

Using Eq. (14) with k_{12} obtained from solubility data, we calculated $\bar{v}_2^\infty$ as a function of pressure and temperature. Figure 4 shows isotherms (between 0°C and 60°C) of calculated partial molar volumes as a function of pressure for naphthalene infinitely dilute in ethene.

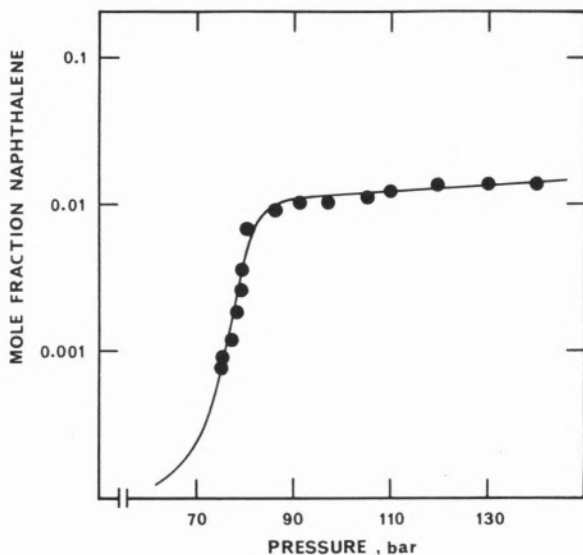

Figure 3

Experimental [4,5] and calculated solubilities (with k_{12} = 0.0626) for solid naphthalene in supercritical carbon dioxide at 35°C

Figure 5 shows similar isotherms (between –3.15°C and 67°C) for naphthalene in CO_2.

As shown in Figs. 4 and 5, at low pressures the partial molar volumes of the solute are small and positive. As pressure increases, $\bar{v}_2^\infty$ decreases strongly until a minimum is observed. At higher pressures, $\bar{v}_2^\infty$ increases and eventually become positive again. At conditions of pressure and temperature where the solvent is supercritical, a sharp minimum is observed. This minimum shifts to higher pressures as the temperature rises; the same trend is observed [9] for similar curves showing the dependence of solubility maxima on pressure and temperature.
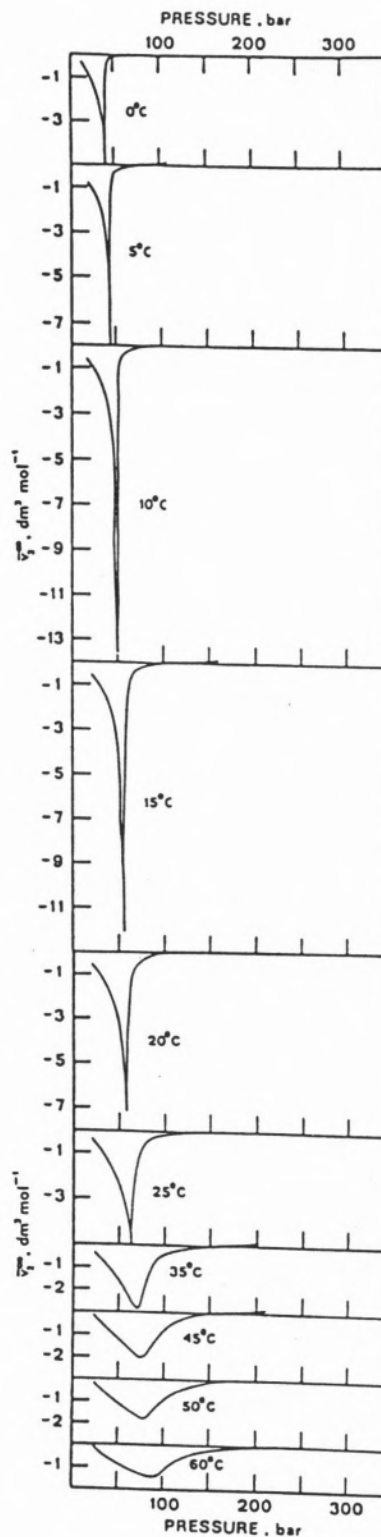

Figure 4

Calculated partial molar volumes of naphthalene infinitely dilute in ethene. Values of $\bar{v}_2^\infty$ are large and negative at temperatures close to the ethene's critical (t_c = 9.5°C)

mental chromatographic data [10] for naph-thalene in supercritical carbon dioxide. Agreement is good. The data indicate that $\bar{v}_2^\infty$ may attain negative infinity when approaching the critical point of the solvent. Results shown in Fig. 6 also confirm the strong correlation observed between $\bar{v}_2^\infty$ and the isothermal compressibility of the pure solvent [10].
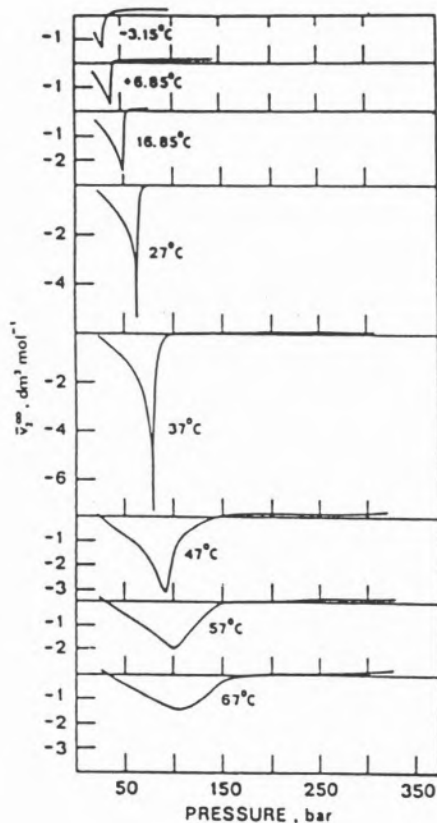
Note that the sharp minima indicate values for $\bar{v}_2^\infty$ which are not only negative but very much larger than the volume of pure condensed naphthalene.
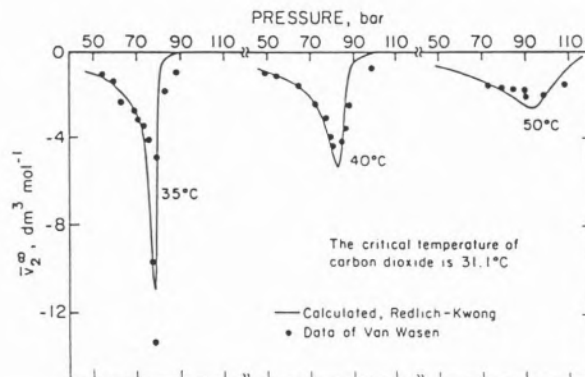

Figure 5

Calculated partial volumes of naphthalene infinitely dilute in carbon dioxide ($t_c = 31.1°C$)

Figure 6

Comparison of calculated partial molar volumes of naphthalene at infinite dilution in supercritical carbon dioxide with experimental chromatographic data [10]. (Prausnitz / Lichtenthaler / Gomes de Azevedo, MOLECULAR THERMODYNAMICS OF FLUID-PHASE EQUILIBRIA, 2/E, p. 464, 1986. Reproduced by permission of Prentice-Hall, Inc., Englewood Cliffs, N. J.)

In addition we point out that an analytic equation of state, such as the Redlich-Kwong we used in this work, cannot describe the behavior of systems very near the critical state. For this reason, Figs. 4 and 5 do not include any calculations at temperatures very near the critical region of the pure solvents.

Figure 6 shows three isotherms which compare $\bar{v}_2^\infty$ calculated from Eq. (14) with experi-mental chromatographic data [10] for naph-

This particular behavior of the solute's partial molar volumes has also been observed for other solute properties. Similar unusual effects are reported for excess enthalpies, apparent molar heat capacities and solubilities of solutes in mixtures near the solvent's critical point [11].

Addition of small quantities of solute to the near-critical solvent acts like a «condensing agent» which is responsible for the large negative partial molar volumes.

As shown, a simple equation of state like the Redlich-Kwong equation (with a binary interaction parameter obtained from other experimental data) is able to predict unusually large and negative partial molar volumes and their sensitivity to small changes in pressure when the solvent is near its critical state.

Very low fugacity coefficients lead to solubilities much larger than those calculated by as-

suming ideal behavior. Large negative molar volumes tell us that a small decrease in pressure can dramatically reduce the solubility. It is precisely this feature which makes SCF extraction attractive because it permits simple and economic solvent recovery.

ACKNOWLEDGMENT

REFERENCES

[1] M. E. PAULAITIS, V. J. KRUKONIS, R. T. KURNIK, R. L. REID, Rev. Chem. Eng., I(2), 179 (1983).
[2] J. M. PRAUSNITZ, R. N. LICHTENTHALER, E. G. AZEVEDO, Molecular Thermodynamics of Fluid-Phase Equilibria, 1986, Prentice-Hall (Englewood Cliffs).
[3] P. L. CHUEH, J. M. PRAUSNITZ, Ind. Eng. Chem. Fund., 6, 492 (1967).
[4] M. McHUGH, M. E. PAULAITIS, J. Chem. Eng. Data, 25, 326 (1980).
[5] Y. V. TSEKHANSKAYA, M. B. IOMTEV, E. V. MUSHKINA, Russ. J. Phys. Chem., 38, 1173 (1964).
[6] K. P. JOHNSTON, C. A. ECKERT, A. I. Ch. E. Journal, 27, 773 (1981).
[7] IUPAC, International Thermodynamic Tables of the Fluid State, Pergamon Press (Oxford).
[8] J. M. PRAUSNITZ, NBS Technical Note. 316, July, 1965.
[9] R. T. KURNIK, R. C. REID, A. I. Ch. E. Journal, 27, 861 (1981).
[10] U. VAN WASEN, G. M. SCHNEIDER, J. Phys. Chem., 84, 229 (1980).
[11] R. F. CHANG. G. MORRISON, J. M. H. LEVELT-SENGERS, J. Phys. Chem., 88, 3389 (1984).

RESUMO

Volumes parciais molares de naftaleno em solventes supercríticos

A extracção supercrítica é uma técnica de separação com grandes possibilidades de aplicação em várias indústrias.

No projecto e na operação de processos envolvendo a extracção supercrítica é importante conhecer o comportamento de solutos diluídos em solventes em condições próximas do ponto crítico do solvente.

Neste trabalho utilizou-se a modificação de Chueh da equação de estado de Redlich-Kwong para calcular a dependência com a pressão dos volumes parciais molares do naftaleno infinitamente diluído em dióxido de carbono (isotérmicas entre -3.15ºC e 67ºC) e em eteno (isotérmicas entre 0ºC e 60ºC). Estes cálculos foram efectuados usando um parâmetro de interacção binária k_{12} determinado a partir de dados de solubilidade.

À medida que se aproxima o ponto crítico do solvente, os volumes parciais molares do soluto tornam-se muito grandes e negativos, com um mínimo acentuado para temperaturas próximas da temperatura crítica do solvente.

Os resultados calculados estão em boa concordância com os resultados experimentais existentes.

Na região crítica, o volume parcial molar é muito sensível à temperatura e à pressão. Por isso, o coeficiente de fugacidade do soluto varia acentuadamente com pequenas alterações nas condições de operação. É esta variação apreciável que conduz às vantagens particulares dos processos de extracção supercrítica.

NOTATION

a	constant in Redlich-Kwong equation of state
b	constant in Redlich-Kwong equation of state
f	fugacity, bar (1 bar = 10^5 Pa)
k	deviation from geometric mean
n	number of moles
P	pressure, bar
R	gas constant, bar cm^3 mol^{-1}K^{-1}
T	temperature, K
t	temperature, ºC
v	molar volume, cm^3 mol^{-1}
V	total volume, cm^3
x	liquid phase mole fraction
y	gas phase mole fraction
z	compressibility factor
ϕ	fugacity coefficient
ω	acentric factor
Ω	dimensionless constant in Redlich-Kwong equation of state

Subscripts

1, 2, i, j	components
c	critical property

Superscripts

G	gas phase property
sat	evaluated at saturation
s	solid phase property
–	partial molar property
∞	infinite dilution property
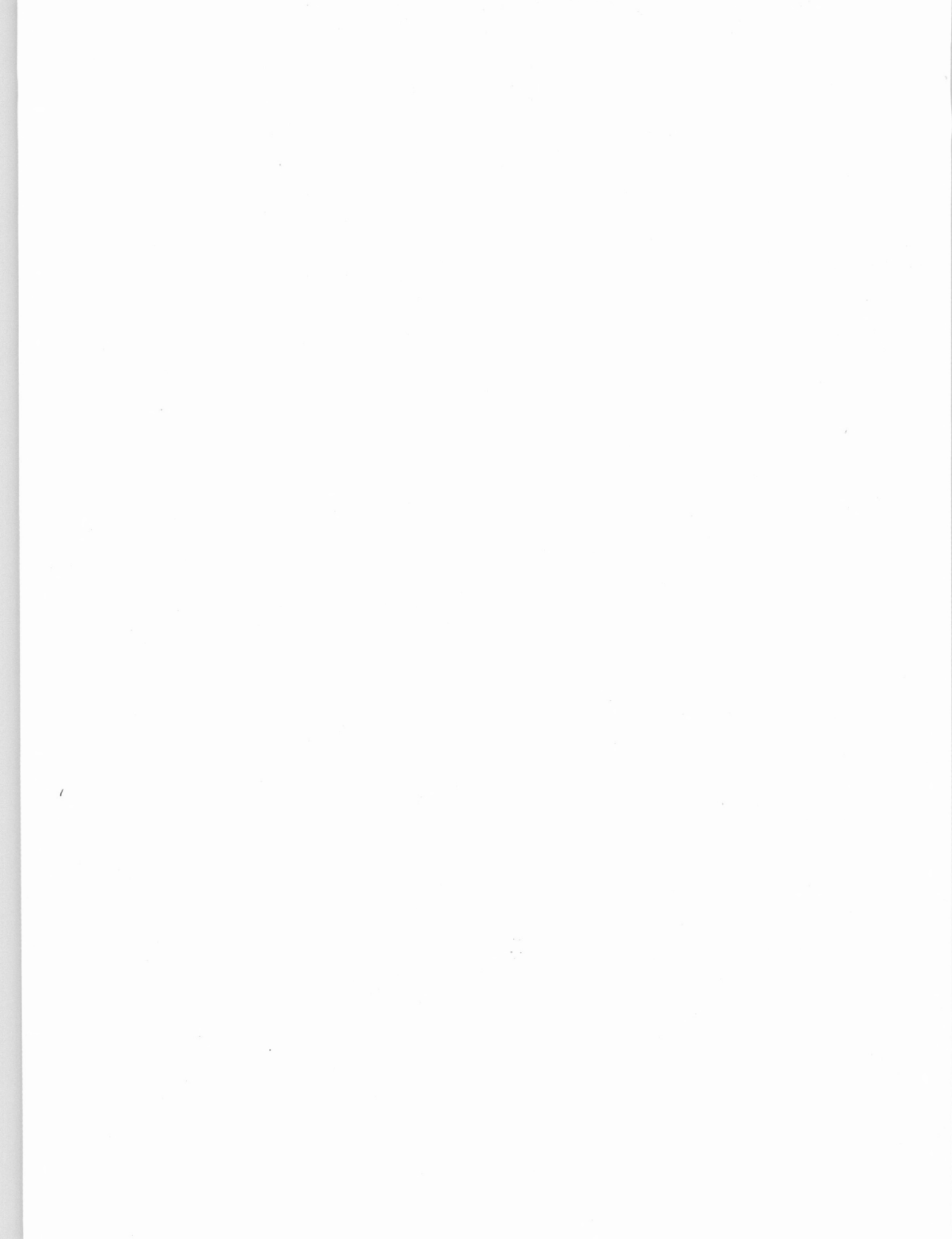
INSTRUCTIONS FOR AUTHORS

1. The **Revista Portuguesa de Química** accepts for publication original papers, research notes and review articles.

2. All manuscripts will be sent to referees for assessment.

3. Manuscripts should be written either in Portuguese or English.

4. Three complete copies of the manuscript should be submitted to one of the Editors. The manuscript should be typed on only one side of the paper with double spacing throughout the text, tables, figure legends, footnotes, and list of references, and with a margin of not less than 4 cm on the left-hand side of each page. The title page should carry the title of the paper, the authors' names, the name and address of the laboratory where the work was done, the name and address of the person to whom proofs should be sent, and a short resuming title for printing at the head of each right-and printed page. An abstract, both in Portuguese and English, in not more than about 300 words should be included; it should be typed on a separate page. A list of figure legends, begining on a new page, should be included. Finally, a list of references in numerical sequence, also begining on a new page, should be included. References should be given in the *current* style of *Chemical Abstracts,* particular care being taken always to give authors' initials.
Research notes should be brief, no more than five typed pages, and need no abstract.

5. Authors are strongly advised to adhere to international conventions in the choice of symbols, units and notation.
A few non-SI units are acceptable without definition; these include Å, cm⁻¹, eV and u (unified atomic mass unit). Atomic units are also acceptable provided they are stated explicitly as in the IUPAC recommendations (*Pure and Applied Chemistry*, 1978, **50**, 75). In general, however, non-SI units should be avoided, but in the rare cases where this is particularly inconvenient the non-SI units should be defined once in each paper.
When numerical values of a physical quantity are tabulated, the expression placed at the head of the comumn should be a pure number. For example, a table of entropies could have as a heading $S/(JK^{-1} mol^{-1})$. Similarly, the axis labels for graphs should also be pure numbers, such as the quotient of the symbols for the physical quantity and the symbol for the unit used. Manuscripts which do not conform to these conventions will be edited appropriately and in some cases may be returned to the authors for editing, after they have been accepted.

6. There are no page charges for the journal. Offprints may be ordered from the editors at the proof stage.